Universitat Autònoma de Barcelona

Encapsulation of Inorganic Payloads into Carbon Nanotubes with Potential Application in Therapy and Diagnosis

Markus Martinčić

Universitat Autònoma de Barcelona

Encapsulation of Inorganic Payloads into Carbon Nanotubes with Potential Application in Therapy and Diagnosis

Markus Martinčić

Doctoral Thesis

Tesi Doctoral

Programa de Ciència dels Materials

Director: Dr. Gerard Tobias Rossell

Tutor: Dr. José Peral Pérez

Departament de Química

Facultat de Ciències

2017


ICMAB
INSTITUT DE CIÈNCIA DE MATERIALS DE BARCELONA
EXCELENCIA
SEVERO
OCHOA
CSIC
CONSEJO SUPERIOR DE INVESTIGACIONES CIENTÍFICAS

This dissertation is presented for graduation as Doctor by Markus Martinčić. To this effect, Dr. Gerard Tobias Rossell (PhD supervisor, ICMAB-CSIC) and Dr. José Peral Pérez (tutor, UAB) sign this certificate.

Dr. Gerard Tobias Rossell

Dr. José Peral Pérez

Markus Martinčić

Bellaterra, 31/05/2017

“Once you have eliminated the impossible, whatever remains, however improbable, must be the truth.”

Leonard Nimoy

Acknowledgments

My time spent at ICMAB was very bumpy, like a ride without a seatbelt! However, I had some people around that were trying to hold me during that trip, although they were in the same beltless ride. I'd like to start by thanking Dr. Gerard Tobias for the guidance and support given through the three years of my Thesis, and Dr. José Peral Pérez for accepting being the tutor of this Thesis.

The first person next to me, Magdalena Kierkowicz, helped me a lot, I know I would have been flying out the window if it weren't for her... Thanks for listening, for helping me out whenever you could, for the investigation we did together, for your friendship and support. Simo, Dr. Mohamed Aklalouch, thanks for the friendship during the research period. Thanks for understanding, although I knew you had your own bumpy ride, thanks for listening and helping. Dr. Judith Oró-Solé, Roberta Ceravola and Marixa Arnedillo, thanks for trying to fix the bumpy car, for the supporting analysis performed at ICMAB. Dr. Belén Ballesteros, Elzbieta Pach and Marcos Rosado for the electronic microscopy that was covering the whole roadside. Mar Estelles, a big thank for the TGA and BET support, and your valuable advices.

Sharing a car can be quite stressful, therefore, people from the office, thank you a lot for sharing it in a peaceful way, including Davide Blasi, Wenjie Qian, Alessandro Sorrenti, Marta Riba, Maria Aguado, Cristina Oliveras, Laura López, Marcos Paradinas and Magdalena Kierkowicz. People I worked with, supervised by me during their stay, including Dr. Robert Feldman and Dr. Cinzia Spinato. People from the group, namely Dr. Adem Guven, Dr. Jorge Pérez, Dr. Laura Cabana, Dr. Dejan Kepić, Dr. Stefania Sandoval and once again, the one and only Magdalenka. People from Manchester, under the supervision of Prof. Kostas Kostarelos, especially Dr. Sandra Vranić for the help and support during my stay in the UK.

People from the project, thanks for the given map of the trip ahead and thanks for accepting all of my samples. Dr. Jean-Claude Saccavini and Dr. Robert Feldman, thank you for the irradiation experiments. Prof. Benjamin G. Davis, Dr. Christopher Serpell, Sonia De Munari and Reida

Rutte from Oxford, thanks for accepting my samples and for the very efficient work you did over there. Prof. Khuloud Al-Jamal, Dr. Rebecca Klippstein and Maxime Burgognon, thank you for your biological contribution. Prof. Maurizio Prato, Prof. Tatiana Da Ros and Agnieszka Gajewska, Dr. Alberto Bianco, Dr. Cecilia Menard-Moyon, Dr. Aritz Perez and Dr. Cinzia Spinato, all of you, I'm grateful mostly for the functionalization, but also for the other studies performed as well. Last, but not least, I'd like to thank Dr. Martin Kalbac and Ana Santidrian for the Raman studies. Anne Marie Forney, I'm happy that you got married and that you are happy there in the States, but at the same time sad that we did not finish the bumpy road trip together. Nevertheless, it was a pleasure collaborating with you.

To Prof. Dubravka Matkovic Čalogović, Dr. Biserka Prugovečki, Prof. Ernest Meštrović, Prof. Nenad Judas, Denis Besic, Milka Dajak and Andelka Zrakic Potkonjak, I would like to thank for the scientific assistance over the course of years, prior to my PhD, and the guidance provided during that time. Without that I wouldn't be standing here today.

And finally, thanks to my mom and family, for being ever so proud and encouraging me all the way until the very end. There is a long list of friends, colleagues and better halves that I could list here, such as Goran, Đivo, Tea, Ivan, Luka, Maja, Alberto, Adri, Fernando, David, Laura, Ana-Maria, Teo, Ivan, Luka and many, many more, to whom I'm really grateful and I wish you all manage to achieve your designated goals in your life!

This Thesis has been developed within the framework of the European project RADDEL "Nanocapsules for Targeted Delivery of Radioactivity" (https://projects.icmab.es/raddel). It has received funding from the People Programme (Marie Curie Actions) of the European Union's Seventh Framework Programme under REA grant agreement n^{o} 290023.

Abstract

Carbon nanotubes present a relatively novel group of materials with potential application in different scientific fields. The scope of this Thesis is to benefit from their inner cavities to encapsulate biomedically relevant payloads. Carbon nanotubes allow the confinement of selected materials within their walls, preventing their leakage and, as a consequence, undesired effects of such materials to the surrounding media. This makes filled carbon nanotubes very elegant vectors for the diagnosis and therapy of diseases.

The process used to purify samples of carbon nanotubes proved to be a valuable asset, not only in the reduction of impurities which might cause cytotoxicity, but also for shortening the length of nanotubes. Thermogravimetric analysis is a widely-used technique in evaluating the purity of carbon nanotube samples. The role of different parameters that control the analysis has been investigated to assure that the most appropriate and representative results are obtained. The purification process has also been readjusted to assure the presence of the lowest amount of catalyst possible in the carbon nanotube samples with the employed purification strategy. We have also introduced a simple UV-Vis spectrophotometric assertion of the catalyst content in samples of nanotubes in a precise and reliable manner.

The preparation of dry samarium(III) chloride from samarium(III) oxide was investigated, together with the nanotube filling-ability of the prepared material, of interest for the development of radiotracers. Bulk filling of carbon nanotubes results in samples that contain a large amount of external, non-encapsulated material, which can compromise the performance of the material in the biological context. We have developed a protocol to monitor the removal of the non-encapsulated material by means of UV-Vis, which in turn allows improving the washing procedure.

The usage of multi-walled carbon nanotubes has some benefits over their single-walled counterparts, due to the presence of a bigger cavity which can host more material. The spontaneous closure of the tips of multi-walled carbon nanotubes by thermal annealing was investigated at different temperatures, along with the encapsulation of different

materials. The prepared filled multi-walled samples were tested in-vitro to assess cytotoxicity and cellular uptake of the developed nanosystems.

Resumen

Los nanotubos de carbono representan un grupo de materiales relativamente nuevo con potencial aplicación en diferentes áreas científicas. Esta tesis se centra en beneficiarse de sus cavidades internas para encapsular compuestos biomédicamente relevantes. Los nanotubos de carbono permiten el confinamiento de materiales en su interior impidiendo su fuga y, en consecuencia, reduciendo los efectos secundarios, no deseados, de estos materiales en el medio circundante. Esto hace que los nanotubos de carbono sean unos vectores elegantes para el diagnóstico y tratamiento de enfermedades.

Se ha demostrado que el proceso utilizado para purificar muestras de nanotubos de carbono permite no sólo la reducción de impurezas, que podrían causar citotoxicidad, sino también acortar la longitud de los nanotubos. Teniendo en cuenta que el análisis termogravimétrico es una técnica ampliamente utilizada para evaluar la pureza de muestras de nanotubos de carbono, se ha investigado la influencia que tienen diferentes parámetros que controlan este análisis para asegurar que los resultados obtenidos son lo más precisos y representativos posible. El proceso de purificación también ha sido reajustado para minimizar la cantidad de catalizador en muestras de nanotubos de carbono. También hemos desarrollado un protocolo que permite determinar el contenido de catalizador en muestras de nanotubos de carbono mediante espectroscopía ultravioleta-visible de una manera precisa y fiable.

Se ha investigado la preparación de cloruro de samario(III) anhidro a partir de óxido de samario(III), así como la capacidad que ofrece el material preparado para el llenado de nanotubos de carbono, ya que éste tiene interés para el desarrollo de radiotrazadores. El proceso de llenado de nanotubos de carbono resulta en muestras que contienen grandes cantidades de material externo, no encapsulado, lo cual puede comprometer el rendimiento del material en el contexto biológico. Hemos desarrollado un protocolo para monitorizar la eliminación del material no encapsulado a través de espectroscopía de ultravioleta-visible, que a la vez permite mejorar el procedimiento de lavado.

El uso de nanotubos de carbono multicapa tiene algunos beneficios sobre sus homólogos monocapa debido a la presencia de una cavidad interna más grande que puede contener más material. Se ha investigado el cierre espontáneo de las puntas de nanotubos de carbono multicapa a través de su calentamiento térmico a diferentes temperaturas, así como la encapsulación de distintos materiales en el mismo rango de temperaturas. Finalmente, distintas muestras de nanotubos de carbono multicapa llenos han sido examinadas in-vitro con el fin de evaluar su citotoxicidad y la captación celular de los nanosistemas desarrollados.

Structure of the Thesis

This Thesis is presented as a compendium of published articles, according to the regulations established by the Universitat Autònoma de Barcelona (UAB). For that reason, paper format was used throughout the whole Thesis, for all reported results. There are two groups of articles: original works as first author, that are part of the Thesis and have been approved by the UAB Commission prior to the submission of this dissertation, and original co-authored work. This work has given rise to many collaborations that resulted in published articles presented in the second group. Published articles are:

1) articles as first author presented to the PhD UAB Commission

Article 1. *Synthesis of Dry $SmCl_3$ from Sm_2O_3. Implications for the Encapsulation of Samarium Compounds into Carbon Nanotubes*, Markus Martincic, Carlos Frontera, Elzbieta Pach, Belen Ballesteros, Gerard Tobias, *Polyhedron*, **2016**, 116, 116. This work is presented in section 3.2.1.

Article 2. *Quantitative Monitoring of the Removal of Non-Encapsulated Material External to Filled Carbon Nanotube Samples*, Markus Martincic, Elzbieta Pach, Belen Ballesteros, Gerard Tobias, *Phys Chem Chem Phys*, **2015**, 17, 31662. This work is presented in section 3.2.2.

2) articles as contributing author

Article 3. *Carbon Nanotubes Allow Capture of Krypton, Barium and Lead for Multichannel Biological X-ray Fluorescence Imaging*, Christopher Serpell, Reida Rutte, Kalotina Geraki, Elzbieta Pach, Markus Martincic, Magdalena Kierkowicz, Sonia De Munari, Kim Wals, Ritu Raj, Belen Ballesteros, Gerard Tobias, Daniel Anthony, Benjamin Davis, *Nat Commun*, **2016**, 7, 13118.

Article 4. *Design of Antibody-Functionalized Carbon Nanotubes Filled with Radioactivable Metals Towards a Targeted Anticancer Therapy*, Cinzia Spinato, AritzPerez Ruiz de Garibay, Magdalena Kierkowicz, Elzbieta Pach, Markus Martincic, Rebecca Klippstein, Maxime Bourgognon, Julie Tzu-Wen Wang, Cecilia Menard-Moyon, Khuloud T.

Al-Jamal, Belen Ballesteros, Gerard Tobias, Alberto Bianco, *Nanoscale*, **2016**, 8, 12626.

Article 5. *Evaluation of the Immunological Profile of Antibody-functionalized Metal-Filled Single-walled Carbon Nanocapsules for Targeted Radiotherapy*, Aritz Perez Ruiz de Garibay, Cinzia Spinato, Rebecca Klippstein, Maxime Bourgognon, Markus Martincic, Elzbieta Pach, Belen Ballesteros, Cecilia Menard-Moyon, Khuloud T. Al-Jamal, Gerard Tobias, Alberto Bianco, *Sci Rep*, **2017**, 7, 42605.

Table of Contents

List of Figures

List of Tables

1. INTRODUCTION

1.1. Carbon Nanomaterials

Carbon comes in different forms in nature, including those of diamond and graphite, but also as fullerenes, carbon nanotubes and graphene. Each one of these materials is entirely made out of carbon atoms and because of that, they possess extraordinary properties that scientist can exploit for different usage depending on the necessity. Interestingly enough, diamond is one of the hardest materials known to man, while graphite is the complete opposite of that, all thanks to their unique intrinsic properties.

Graphene has attracted the scientific community ever since the report of Geim and Novoselov in 2004.[1] Graphene remains as one of the most interesting and promising material scientist are working with. It can be seen as a fundamental building block for other graphitic nanomaterials.[2] By rolling sheets of graphene we get carbon nanotubes, by stacking them, graphite and by wrapping them up, fullerenes (Fig. 1). Graphene can be defined as a single hexagonal sheet of carbon atoms and can be viewed as a two-dimensional material. Having one sheet of carbon atoms is idealistic, that being the reason of the material coming in two (bi-) or more (multi-) layers of those stacked sheets due to the attraction between them. The hybridized sp^2 bonding and the two-dimensional aspect of the material gives rise to interesting mechanical, thermal and electrical properties. Both Young's modulus of 1.0 ± 0.1 TPa and a breaking strength of 42 Nm^{-1} make it one of the strongest materials up to date.[3] It is also a great conductor and has a high in-plane thermal conductivity of between 2000 and 4000 $Wm^{-1}K^{-1}$.[4-5]

On the other hand, fullerenes were reported back in 1985[6]. They come in different ball-like shapes which include spheres and ellipsoids, where the most famous one comes in the shape of a C_{60} ball (buckministerfullerene). Unlike graphene, fullerenes can have

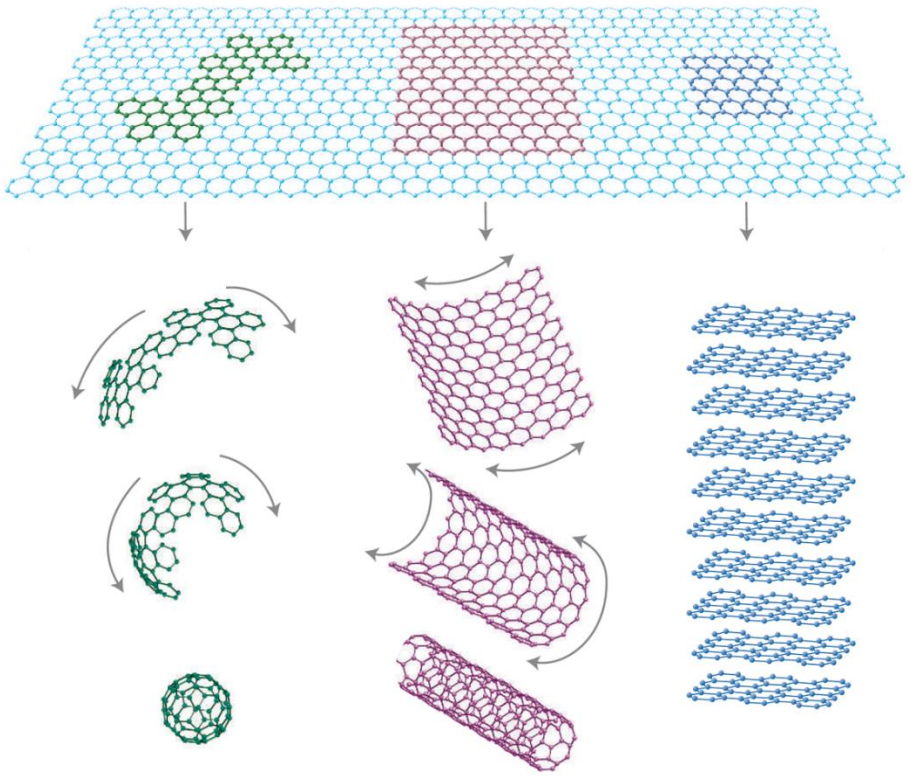

Figure 1. Graphene as mother of all graphitic forms; as a 2D material, it can be rolled-up into a 1D carbon nanotube, wrapped-up into a 0D fullerene or stacked together into a 3D graphite form.[2]

additional pentagonal or even heptagonal rings in their structure. Carbon nanotubes (CNTs) can also be seen as tubular or cylindrical fullerenes, and for that reason some sources are classifying them as fullerenes. Come to think of it, both have an interior which can be used to host other atoms or molecules, being the major difference that fullerenes have smaller cavities, while nanotubes have bigger ones. This implies that more material can fit inside carbon nanotubes than in fullerenes, which is of particular interest for this Thesis. However, nanotubes have the special property of having closed or opened ends, which, if used wisely, can be beneficial in their applications.

As discussed, carbon nanotubes consist of concentric layers of rolled graphene sheets, and depending on the number of those layers, we distinguish between single-walled (one layer, SWCNT) and multi-walled

(several layers, MWCNT) carbon nanotubes (Fig. 2) with diameter dimensions, typically between 0.4 - 2.0 nm and 2 - 100 nm respectively.[7] The production of those materials includes mostly arc-discharge, chemical vapor deposition or laser ablation methods among others, that result in the production of nanotubes varying in lengths (usually in microns), number of layers and diameters, but also in impurity levels.[8] Typically, metal catalysts are being used for the production of nanotubes, which results in their introduction in the sample, seen as impurities which, in order to control the behavior of nanotubes in general, have to be removed prior to their application.[9] Apart from catalytic impurities, additional graphitic particles, which can in turn be surrounding metal catalyst, are being produced, making the removal of metal particles even more difficult, together with amorphous carbon and small fullerenes. Different purification techniques have been developed throughout the years, allowing an effective and targeted removal of these impurities, to achieve high quality nanotube samples.[9]

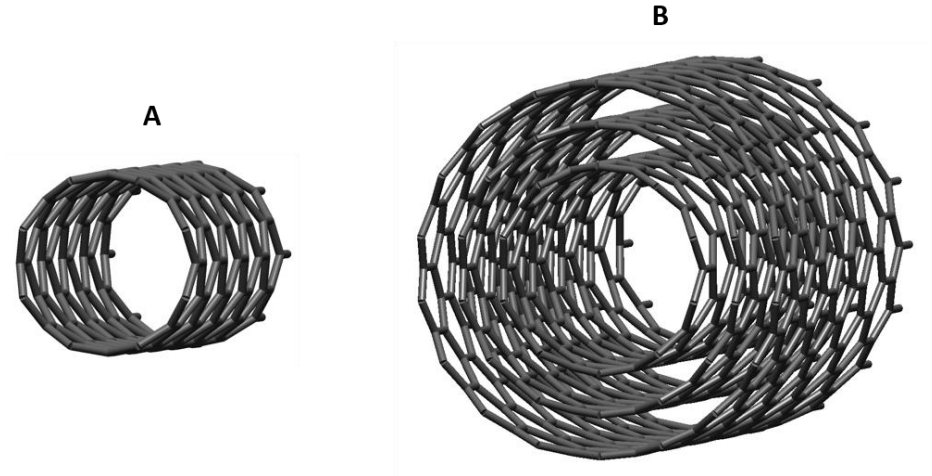

Figure 2. Carbon nanotubes; a single-walled (A) and a multi-walled (B) carbon nanotube.

There are several methods that allow the synthesis of carbon nanotubes, arc-discharge, laser ablation and chemical vapor deposition being the most widely employed ones. Arc-discharge implies the use of direct current along two graphite electrodes in an inert gas atmosphere that prevents their oxidation.[8] This allows the deposition of single-

walled (only when using metal catalyst on anode) or multi-walled nanotubes in the system, as soot or layered on an electrode.

Laser ablation entails the usage of a high-power laser which can vaporize carbon from a graphite source, which can also contain metal catalyst, under an inert gas flow.[8] The created gas phase is transferred into a lower temperature chamber where it condenses, forming single-walled or multi-walled nanotubes, depending on the catalyst content of the graphite source, on a copper-cooled collector.

Chemical vapor deposition typically implies the usage of a carbon-containing gas precursor which is then decomposed using a plasma source.[8] The created carbon diffused in the catalyst-coated substrate gives rise to single-walled or multi-walled carbon nanotubes, depending on the size of the catalyst employed. Unlike the other two high temperature methods, chemical vapor deposition is a medium temperature method that allows better control over the synthesis of carbon nanotubes.

Although multi-walled carbon nanotubes were observed in the arc discharge soot when producing fullerenes by Sumio Iijima in 1991[10], and later in 1993[11] in the case of single-walled carbon nanotubes by using transition-metal catalyst, there is a long history of existence of carbon nanotubes predating these two events, making it difficult to give credit to whoever discovered them in the first place. Already in 1889 the possibility of forming carbon filaments from the thermal decomposition of methane was reported[12], followed by two other papers in 1889 and 1890.[13] The problem lies in the microscopic limitations of that time that made the confirmation of carbon nanotubes growth impossible. In Russia in 1952 a paper was published showing hollow graphitic carbon filaments as the first TEM evidence of the existence of multi-walled carbon nanotubes of 50 nm in diameter.[14] Concentric and bamboo structures of carbon nanotubes were already reported in 1958[15], but it was debated in the seventies with the TEM resolution improvement over time.[16] In 1960 the friction properties of carbon nanotubes due to rolling sheets of graphene was reported showing clear TEM evidence of

a rolled nanotube.[17] This was followed by a similar report in 1971.[18] In 1976 Oberlin et al., and Endo in his Thesis, presented a TEM image of a tubular structure resembling a single-walled carbon nanotube, although it is more likely to be a multi-walled carbon nanotube of 5 nm in diameter.[13, 19] Due to low magnification, fringes were not observed and it is difficult to assess the number of walls present, although the first double-walled carbon nanotube ever imaged is not out of question.

Noteworthy is the natural occurrence of carbon nanotubes all around us, since fullerene-like nanocrystals and multi-walled carbon nanotubes were observed in samples of ancient ice (Fig. 3) obtained from an ice core in the Greenland ice cap (roughly 10000 years old).[20] The same was observed indoors, by using water heaters, furnaces and household appliances powered by natural gas.[21-22] Multi-walled carbon nanotubes were observed in propane or natural gas from typical kitchen stoves.[21] In the outdoor, airborne particulate matter was collected in El Paso in Texas and Houston, consisting of 15% of carbonaceous aggregates, including multi-walled carbon nanotubes.[22] It is believed that fuel-gas combustion generated multi-walled carbon nanotubes are produced from automobiles, power plant, wood burning, industrial processes and diesel-powered vehicles such as buses and trucks.[23] TEM images of a sample of Damascus sabre steel, from the seventeenth century, may suggest the existence of carbon nanotubes and cementite nanowires that had previously been filled in carbon nanotubes during the production of such steels.[24] Finally, in 2001, after the collapse of the World Trade Center, many reported adverse health effects, mostly lung diseases.[25] A dense cloud dust containing pollutants covered the surrounding area, and over 60000 people were exposed. The findings of carbon nanotubes in digested lung tissue in four of seven patients

suggest that nanotubes may have contributed to lung disease development.

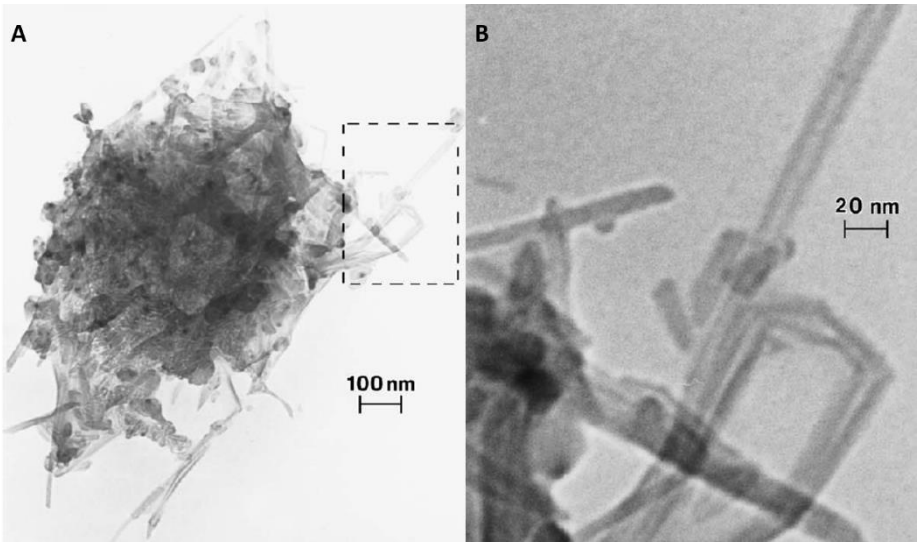

Figure 3. Bright-field TEM image of a carbon nanotube aggregate; the aggregate (A) and a magnified portion of the aggregate (B) showing individual tubes in a sample of ancient ice.[20]

There is a global concern on carbon nanotube toxicity. As we will discuss in the following sections, to exploit the potential of carbon nanotubes as vectors for diagnosis and therapy of diseases, it is necessary to use purified samples of short and well dispersed nanotubes, which have been reported as biocompatible.

1.2. Properties of Carbon Nanotubes

The materials of interest for this Thesis are carbon nanotubes, together with the staggering properties that come with them. When it comes to mechanical properties, the strength of carbon nanotubes is attributed to the sp^2 bonds between carbon atoms.[26] The average value of Young's modulus for multi-walled nanotubes was found to go up to 1.8 TPa, while for single-walled was 1.25 TPa.[27-28] The stiffness of other materials can be enhanced by adding nanotubes as additives and many composites have been created in this way.[29]

Optical properties of carbon nanotubes can also be used advantageously. For instance, the emission range of carbon nanotubes (800 - 2000 nm for single-walled nanotubes) covers the biological tissue transparency window, making them ideal for imaging in biological media.[30] Unlike metallic nanotubes, upon photoexcitation, semiconducting carbon nanotubes emit near infrared light. The fluorescence and photoluminescence of nanotubes can be used for biomedical applications in photoacoustic imaging or photothermal therapy.[31] Electroluminescence was also observed in nanotubes.[32] Optical absorption is widely used to assess the quality of carbon nanotube samples.[33] Raman spectroscopy is, for instance, widely used for studying the structure of carbon nanotubes as minimal sample preparation is required. The Raman spectra of carbon nanotubes has three very distinctive areas. Radial breathing mode (RBM) is associated to the radial contraction/expansion of carbon nanotubes and falls in the region below 400 cm^{-1}.[34] This area is useful for estimating diameters of single-walled carbon nanotubes.[35] The D-band falls around 1340 cm^{-1}, and is associated to sp^2 carbon such as defects present in the nanotube structure, while G band can be found around 1580 cm^{-1}, and

corresponds to planar vibrations of carbon atoms.[36] The ratio between the intensities of G and D bands is typically used for quality assertions of the material.

Outstanding thermal properties of carbon nanotubes are once again attributed to the core properties of the sp^2 lattice. The high thermal conductivity makes nanotubes ideal for thermal management devices. The observed thermal conductivity exceeds 3000 Wm^{-1} K^{-1} in the case of single-walled carbon nanotubes.[37] High current density (up to 109 A/cm^2), ballistic transport along the tube (low resistance), thermal conductivity and mechanical strength make carbon nanotubes an ideal material for building electronic components.[38-39]

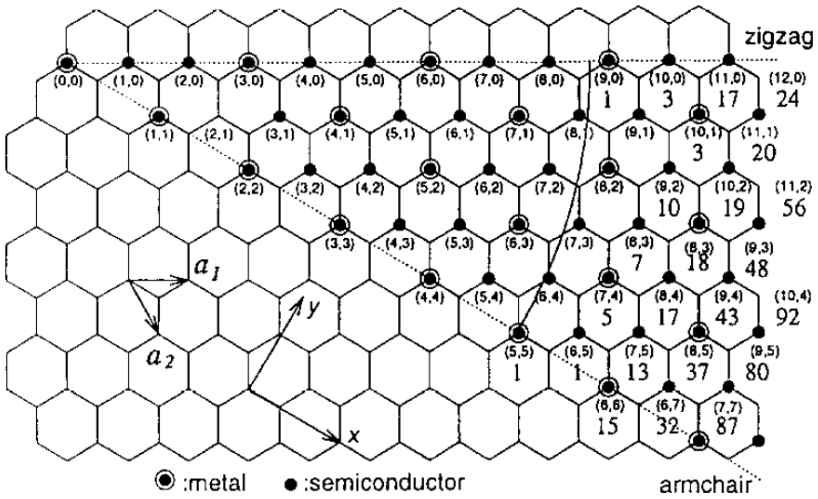

Figure 4. Schematic representation of a graphene sheet; the pair of integers inside the brackets (n, m) are specifying the chiral vector C_h of the carbon nanotube resulting upon rolling-up the graphene sheet.[40]

The structure of single-walled carbon nanotubes (Fig. 4) can be described with a chiral vector C_h, which is defined by $C_h = na_1 + ma_2$ where n and m are integers that define the chiral vector, representing a possible tube structure, while a_1 and a_2 are the unit vectors of the hexagonal graphene lattice.[40] Depending on the chiral angle and n and m values, nanotubes exhibit semiconducting ($n - m \neq 3q$, with band gap) or metallic ($n - m = 3q$) behavior, where q is an integer. Also, we make

a distinction between armchair (n = m ≠ 0, θ = 30°), zig-zag (n = 0, m ≠ 0, θ = 0°) and chiral (n ≠ m ≠ 0) nanotubes. The chiral vector, together with the diameter, has a direct effect on the electronic properties of nanotubes. Taking into account the mentioned properties of carbon nanotubes, other applications of nanotubes can be expected in the near future, including neural regeneration[41], optoelectronic[42] and sensors[43] to name some. Several reviews have already been published on this topic.[44]

From the wide range of applications, we will focus on the use of filled carbon nanotubes for therapy and diagnosis. We will focus on carbon nanotubes with the size that allows celluar penetration, and exploit the availability of the inner cavity for the shielding and delivery of selected payloads. The outer wall thus remains available for decoration which makes carbon nanotubes ideal candidates for biomedical applications (discussion in section 1.4.). Decoration of the external wall can be used for targeting purposes (discussion in section 1.3.1.) and to increase the dispersability and biocompatibility of the system, making the whole construct bio-friendly.

1.3. Filled Carbon Nanotubes

1.3.1. Decoration of Carbon Nanotubes

The nature of carbon nanotubes allows their modification (addition of guest molecules), which can result in altering their properties. This can have a direct effect on the application of such materials. Since carbon nanotubes are cylindrical, we can distinguish between the inner and the external wall of those nanotubes, i.e. the surface located inside or outside of them correspondingly. With this in mind, we can extricate two kinds of modifications, namely exohedral and endohedral, depending on the wall in question.[45] Exohedrally functionalized carbon nanotubes have guest molecules attached to their outer walls, and this can be achieved either through covalent[46] or non-covalent[47-48] functionalization (Fig. 5). A bond can be formed between nanotubes and molecules of interest, allowing their permanent attachment on the outer wall, or electrostatic interactions that can be used to stack guest molecules on top of nanotubes, like using for instance π-π interactions in a removable fashion[49], although highly stable π-interactions have also been reported.[50] In contrast, endohedral functionalization takes profit of the internal space, cavities of nanotubes, which can host guest molecules, and here we are talking about the filling of nanotubes (Fig. 5) which is the focus of this Thesis. When filling nanotubes, the external wall remains unchanged, leaving space for additional exohedral functionalization if needed. The combination of the two functionalization approaches can lead to interesting controlled applications of these materials in different fields, especially for the development of smart biomedical systems.

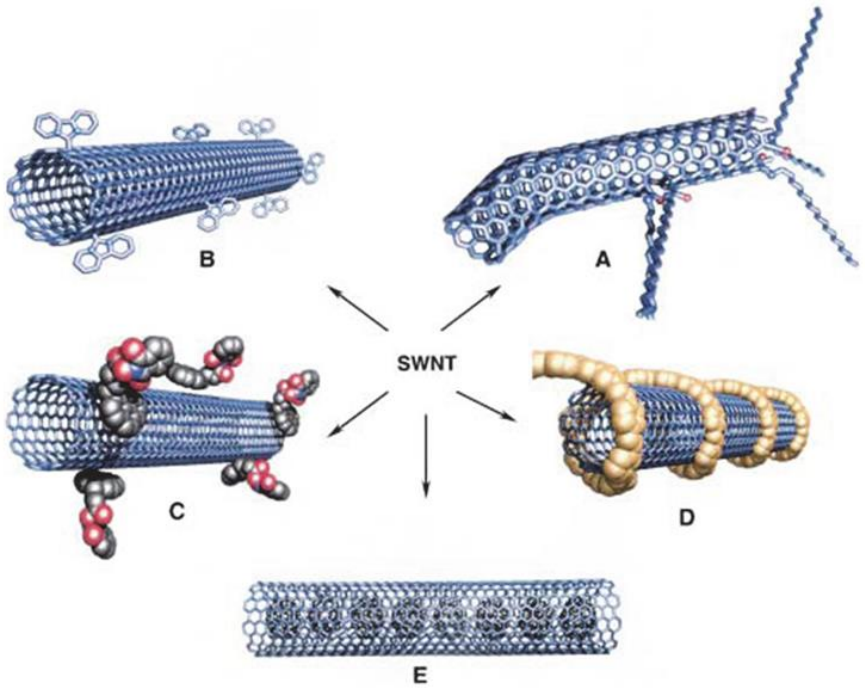

Figure 5. A decorated single-walled carbon nanotube (SWNT), in different ways; (A) and (B) exohedral covalent functionalization of defect-group and sidewall respectively; (C) and (D) exohedral non-covalent functionalization via π-π stacking and wrapping respectively; (E) endohedral functionalization/filling.[45]

1.3.2. Filling of Carbon Nanotubes

After the report on carbon nanotubes by Iijima[10], scientists speculated on the exploitation of their interior cavity. Until now, different methods have been developed which can successfully be used for filling of a variety of materials.[51] After discovering the in-situ filling of fullerene molecules inside carbon nanotubes[52], scientist began to explore the possibility of filling nanotubes during their production. The filling resembled peapods, hence their name. This kind of filling has been used for inorganic materials as well, including palladium nanoparticles[53] and iron.[54] The drawbacks here are that the process typically results in low filling yields and the inadequate temperature range in which most organic materials, and some inorganic, decompose. Filling of carbon

nanotubes using a post-synthesis approach has been widely employed. Sublimation filling consists of filling by converting a solid into a gas phase, which can then enter inside the nanotubes, followed by the recrystallization within. This method is very efficient and clean, but, from a practical point of view, can be used only for materials with a relatively low sublimation point. Fullerenes and a variety of organic materials have successfully been filled using sublimation filling.[55] Solution filling on the other hand uses a concentrated solution of a material that, by mixing with nanotubes, can be filled inside nanotubes. This is fairly straightforward and the use of high temperatures is avoided. However, the efficiency of this method is low and solvent molecules can also be found trapped inside nanotubes. Different solvents can be used, including organic solvents, water or even acids, keeping in mind that they can sometimes alter the structure of nanotubes during the filling. Different materials have been filled within nanotubes by solution filling, from metals to organic molecules.[56-57] Finally, the last method is molten-phase (melt) filling that consists in converting the material of interest from a solid to a liquid phase that can subsequently enter inside the cavities of nanotubes by capillary forces. This method proved to be more efficient than solution filling, especially for inorganic salts, as there are no solvent molecules involved and higher filling yields can be achieved, compared to solution filling. Like every method discussed, this one has some drawbacks as well, as the material has to melt, be thermally stable once molten and cannot react with carbon nanotubes. This method is widely used, and many materials have been successfully filled, from metals to inorganic salts.[58-59]

It is well known that as-produced carbon nanotubes in general come with closed ends.[60] Opening of those ends is essential to allow the passage of the material inside the nanotubes. For this purpose, different opening strategies have been already developed, which in some cases also result in the removal of impurities from the sample at the same time.[61] Actually, as already mentioned, the purification of as-produced carbon nanotubes is important for the use of these systems

as nanovectors. In this sense, oxidative treatments, magnetic treatments, ultrasonication, thermal treatments and filtration take profit of different properties of such impurities, and result in samples with lowered impurity levels, which mostly include carbonaceous materials and catalyst particles. This is particularly important for the biological environment, seeing that such impurities can lead to adverse effects.[62] The use of oxidative treatments in general leads to samples of opened-ended carbon nanotubes. The most used method in our lab is thermal annealing in a mild-oxidative environment, using steam[63-64], as the oxidative properties of water provide the right conditions for the removal of carbon impurities, opening of the tips, and also for the shortening of the nanotubes. This is followed by a treatment with hydrochloric acid that leads to the removal of the exposed catalyst particles.

A huge variety of different materials have been successfully encapsulated inside both single and multi-walled carbon nanotubes. These include metals[54] and alloys[65], different fullerenes[52], inorganic salts[57], organic molecules[66], organometallic compounds[67], gases[68] and solvent[69] molecules. As discussed earlier, not all filling methods are suitable for every compound, a proper experimental design is required for a successful encapsulation of the payload of interest. For instance, a metal can have a high melting point, an even higher sublimation point and likeliness to be insoluble in certain solvents, while on the other hand organic molecules are prone to decomposition by thermal annealing and unwanted interactions with the walls of nanotubes can occur, especially when dealing with molecules with aromatic rings.[70] Another important property to consider is the surface tension of the liquid to be filled. It has been predicted, following Young-Laplace's equation, that a liquid with a surface tension below 200 mN/m should spontaneously enter inside of the cavity.[71-73] This has been proven for different materials.[74] When dealing with higher surface tension, adequate pressure difference at the interface ought to be used. All these aspects have to be kept in mind when trying to encapsulate payloads inside carbon nanotubes. Once the compound is successfully

encapsulated, the material remaining external to the carbon nanotubes needs to be removed if a clean sample is required, which sometimes is not straightforward. If the ends of carbon nanotubes remain opened after the filling experiment, there is a high probability for the filled compound to escape from the interior of the nanotubes while removing the outer, non-encapsulated material. However, this is not the case when good sealing of the ends is provided, allowing a selective removal of the non-encapsulated material.[75] Different strategies have been developed over the years that allow closing the ends of filled carbon nanotubes. Thermal annealing in vacuum, above the melting point of the encapsulate, allows the filling and spontaneous closure of the ends upon cooling down, provided the sample has been annealed above 700 °C.[75-76] This is the most frequently used method in our laboratory for the filling of single-walled carbon nanotubes with inorganic payloads (Fig. 6), as it is forthright and exhibits high filling yields.

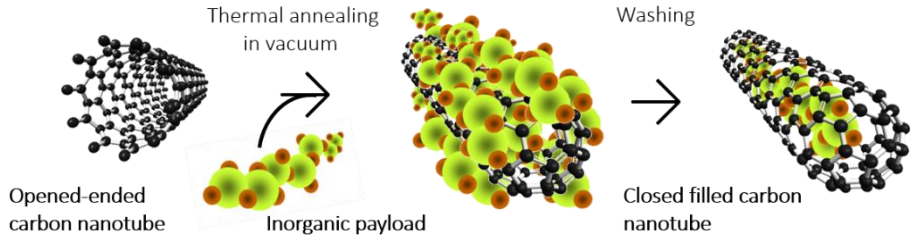

Figure 6. Schematic representation of the melt filling process of opened-ended carbon nanotubes with inorganic payloads.

1.3.3. Applications of Filled Carbon Nanotubes

There are numerous applications of empty carbon nanotubes[77-78], but these can be widened even more by including filled nanotubes. The inner cavity of carbon nanotubes can be exploited as a porous system through which molecules in gas or liquid phase can pass through, making them act as nanomembranes.[79] It has been shown that different gas molecules can pass through single-walled carbon nanotube membranes.[80-81] Although not really in the jurisdiction of filled nanotubes, these theoretical works showed that carbon nanotubes can act like nano-cylinders that allow molecules to pass through the inner cavity due to the inner potential energy surface. H_2, He, N_2, O_2, Ar, CO_2 and different hydrocarbon gases, from CH_4 to C_4H_8 were also diffused through aligned double and multi-walled carbon nanotubes.[82] Apart from gas molecules, polystyrene particles, 60 and 100 nm (± 10 nm) in diameter, were transported through nanotube membranes, with diameters of 150 nm.[83] Soon after, the transport of N_2 and $Ru(NH_3)_6^+$ in solution through aligned multi-walled carbon nanotubes was achieved.[84] Membranes with functionalized carbon nanotube tips with biotin showed a 15 times lower $Ru(NH_3)_6^+$ flux when bounded with streptavidin, demonstrating the possibility to gate molecular transport through carbon nanotube cores for future chemical separations and sensing.

Different gaseous species, together with gold colloids and $Ru^{2+}(bipyr)_3$, were used to estimate the diameter size of double-walled carbon nanotubes.[82] The average diameter size of these nanotubes was between 1.3 - 2 nm, estimated due to exclusion of gold nanoparticles of 2 nm. Molecular dynamics simulations showed that carbon nanotube membranes can be used for desalination via reverse osmosis.[85] Sun et al. first showed that polar molecules, such as water, can enter the non-polar interior of a nanotube using multi-walled carbon nanotubes with an inner diameter of 150 nm.[83] Both Holt et al.[82] and Majumder et al.

showed that carbon nanotubes have long slip-planes and that flow rates through the inner cavity were 4 to 5 orders of magnitude faster than conventional fluid flow predictions.[86] Nanotubes used for the study were multi-walled carbon nanotubes, while fluids included water, ethanol, iso-propanol, hexane and decane.

In addition to membranes, nanotubes can be used as nanosensors as well, based on the ability to alter certain properties of the encapsulated material. One of such materials is the semimetal mercury telluride that, after being encapsulated in single-walled carbon nanotubes, changes its structure to a graphene-like crystallographic form that becomes semiconducting.[87] PbI_2 as a semiconductor is a useful X-ray and γ-ray contrast agent, with a large band gap (between 2.2 - 2.6 eV) due to polytypism that is forbidden once the material in confined within single or double-walled carbon nanotubes.[88] Other materials that change their structure upon being filled in nanotubes include CoI_2[89], BaI_2[90] and CrO_x.[91] Metal-coated[92-93], metal capped[94-96] and metal filled[97-98] carbon nanotubes have all been used for magnetic force microscopy.

Another application of the interior of carbon nanotubes is its use as a nano-reactor. Both catalyst (Rh) and fluids (CO and H_2) synergistically confined within multi-walled carbon nanotubes can be used in the creation of ethanol with a formation rate higher than the one of the reaction carried out with Rh nanoparticles outside of nanotubes.[99] Fe-Pt or Pt-Ru nanoclusters inside carbon nanotubes can be used in electrocatalysis of methanol oxidation and oxygen reduction for fuel cell purposes and gas phase catalysis of hydrocarbon decomposition.[100] Single-walled carbon nanotubes were also used as nanotube-diameter dependent nanoreactors for aromatic halogenation reactions where both selectivity and kinetics were improved.[101] A recyclable nano-reactor was proposed.

The first demonstration of an application of filled single-walled carbon nanotubes was that of a CrO_x@SWCNTs that can be used in building electrodes for supercapacitor devices with enhanced charging speed.[102] This is possible thanks to Faradaic reactions occurring between CrO_x

nanocrystals and the acidic electrolyte. A good cycling performance and high rate capability was achieved for Fe_2O_3 nanoparticles filled carbon nanotubes.[103] Those filled nanotubes were used as anode material in a lithium-ion battery. The smallest phase-change material was synthesized by filling GeTe in single-walled carbon nanotubes.[104] Amorphous to crystalline changes were observed under the influence of electron-beam irradiation, making this material suitable for non-volatile memory devices.

Peapods can be used as solar cells since they have the active medium and electrode naturally integrated where fullerenes in peapods can act as active electron-hole producing medium.[105] The band gap of the semiconducting tubes was reduced to 0.1 eV by encapsulating metallofullerenes in single-walled carbon nanotubes that act as charge donors.[106] Also, due to the donor/acceptor behavior of metallofullerenes, peapods-based transistors showed conduction for both polarities of the gate bias, while C_{60}-peapod-based transistors showed a unipolar p-type behavior.[107] C_{60} peapods showed a single-electron transistor behavior.[108] At room temperature, a p-type conductance was observed. At lower temperatures, 1.8 K, the positive bias showed random oscillations depending on the gate potential, attributed to the presence of fullerenes in the interior of carbon nanotubes. This can be explained by the creation of quantum dots between fullerenes separated by empty tube segments, where the transport in the nanotube is performed through the quantum dots in the form of single electrons.[106]

The well-defined periodicity of fullerenes encapsulated in carbon nanotubes can also serve as photonic crystals.[109] Due to the dielectrical properties and periodicity of fullerenes, an optical gap of 7 nm was observed. This means that soft X-rays with the same wavelength could be trapped inside peapods, thus enabling the creation of a soft X-ray laser in the future.

A slow progress is being made in the area of using filled carbon nanotubes containing endofullerenes in single spin devices[110-111] for

future solid state quantum computers.[112] Quantum computing was already demonstrated on a 7-qubit system using NMR.[113] Herneit suggested preparing a linear chain of spin qubits for quantum computing using fullerenes.[114] Later, it has been proposed to use N@C_{60} endofullerenes[115], where nitrogen is decoupled by the fullerene cage and the application of this molecule for such purposes has been demonstrated.[116] The concept of fullerenes moving relatively easy inside a nanotube by a rapid shuttling between different bit values has also been proposed.[117] Charging fullerenes with K atoms[118] or encapsulating $C_{59}N$ azafullerenes[119-120] would enable electrostatic control and thus the driving force for the memory switch.

The most promising applications of filled carbon nanotubes are those for biomedical purposes, which include therapy and diagnosis and thus will be reviewed in the next section.

1.4. Applications of Filled Carbon Nanotubes in the Biomedical Field

1.4.1. Biocompatibility and On-Demand Release

There are many publications dealing with successful biomedical imaging, diagnosis and therapy mediated by carbon nanotubes which show promising results for future translation into clinic.

The first problem that needs to be addressed is the possible toxicity of carbon nanotubes in the biological context. The lack of toxicity enhances biocompatibility and vice versa. Biocompatibility of a nanomaterial in cells and organisms implies absence of acute inflammatory responses, absence of deposition of the material in the body, absence of intoxication from possible metabolites from the material and absence of adverse reactions such as apoptosis and necrosis of cells during the interaction of the material, in this case nanotubes, with the biological milieu.[31, 121] Indeed, early reports on pristine nanotubes showed toxicity, but that was later attributed to their size and impurity content.[62, 122] Obviously, the longer the nanotubes, the more toxic they are. This was addressed for the first time by Poland et al., as nanotubes that are over 20 µm showed asbestos-like behavior.[62, 123] To enhance biocompatibility and reduce toxicity implies a proper shortening and purification method that will render nanotubes short (typically below 500 nm) and free of catalyst. In addition to the length, catalyst particles, such as iron and nickel, can also induce toxicity in cells, as shown in the case of human epidermal

keratinocytes.[124-125] Exohedral decoration of nanotubes, especially with bio-friendly materials, will make nanotubes even more biocompatible. It has been shown that the asbestos-like behavior of long multi-walled nanotubes can be diminished by a simple functionalization of the outer wall of nanotubes.[122]

Although exohedrally modified nanotubes decorated with bio-active compounds are commonly examined and different studies have been published[126], the main drawback of this approach is the possible detachment and interaction of the bio-active compound with the biological milieu upon administration. Alternatively, the endohedral approach ensures the encapsulation and protection of the chosen bio-active payload, while the external walls remains available and can be functionalized for biocompatibility or targeting purposes.[31] Unlike the exohedral method, where active molecules are attached to the exterior of carbon nanotubes, this approach allows a more controlled release of drug molecules. Another big advantage over the exohedral approach is that, once filled, nanotubes provide shielding to the encapsulated payload from oxidation or degradation and unwanted interactions or even reactions of the cargo with the biological milieu.[31]

Improved biocompatibility and specific targeting can be achieved by means of functionalization of the external walls.[127] For instance, specific antibodies, folic acid and peptides can all be used for targeting purposes and delivery of the cargo to specific types of cells.[128-129] For drug delivery purposes, it is crucial to have contact of drug molecules with the specific receptors, and for that reason drug molecules must leave the interior of the nanotubes when reaching the target. Maximum performance is achieved when no release of drug molecules is present prior to reaching the designated destination. For that aim, different release methods have been developed making drug delivery systems even smarter.

An efficient triggered release of the encapsulated payload is essential in improving drug delivery systems. It is possible to release the

encapsulated material using current density[130-132], voltage[133] or by changing the local environment[134] of the nanotube. Fullerenes can be used to close the opened-ended single-walled carbon nanotubes[133, 135] and they can be removed using dichloromethane[135], toluene/ethanol[136] or dichlorobenzene.[137] A smart pH-dependent system for releasing dimethylamino-functionalized fullerenes has been developed.[134] A similar system has also been developed where the capping agents are silica nanospheres that can be removed with 1,4-dithiothreitol or by heating.[138] Other approaches include wrapping filled nanotubes with surfactants where the release is achieved by radiofrequencies[139], or by using polymers for wrapping and current for releasing of the material[140]. Depending on the nature of the molecule, simple heating or a magnetic field can expel the filled material[141] or the environmental pH can trigger the release of the drug molecule.[71, 142] Optical heating[143] or pulsed NIR irradiation[144] may also serve the same purpose.

1.4.2. Filled Carbon Nanotubes for Therapy

Different studies involving filled carbon nanotubes with bio-active compounds are predating this Thesis. Both single and multi-walled carbon nanotubes were tested in a test-tube, in-vitro, in-vivo or as a molecular dynamics simulation showing promising results towards the future application of these systems therapeutically.

Gene therapy can greatly benefit from filled carbon nanotubes, as the insertion of both RNA[145] and DNA[146-150] in carbon nanotubes has been observed and confirmed. Protein encapsulation into carbon nanotubes[151] is also of peculiar interest, since there are protein drugs already available on the market. For the biomedical significance, SmtA as a bacterial metallothionein[152], HRIP[153-154], as an HIV replication inhibitor peptide and Zadaxine[155], that is being used for treating hepatitis B, have all been encapsulated within carbon nanotubes in different molecular dynamics simulations.

Anticancer drugs are the most studied group of drugs, as there are theoretical, test-tube in-vitro and in-vivo studies already existing. Cisplatin, carboplatin and even oxaliplatin have all been encapsulated into carbon nanotubes. Theoretical studies[156-158] show the capability of cisplatin encapsulation in and release from carbon nanotubes, while the test-tube[159], in-vitro[139, 160-162] and in-vivo[163] experiments confirm the encapsulation, release and improved therapeutic efficacy compared to the free drug alone. Carboplatin[164] and oxaliplatin[165] activity has been tested in-vitro as less toxic analogues of cisplatin where cytotoxicity of the novel system is also observed. Another platinum prodrug has also been tested in conjugation with carbon nanotubes on cell lines[166-167] and mice models.[163] Pt(IV) is reduced to its cytotoxic Pt(II) form and released from carbon nanotubes showing potential mitochondrial damage that leads to cell apoptosis. Other anticancer drugs include temozolomide[168], paclitaxel[169-170] and doxorubicin[170-171] on which

theoretical carbon nanotube encapsulation studies were performed. Alteramine[135] showed a possible triggered release from carbon nanotubes by using methylene chloride. Irinotecan[142] was released from carbon nanotubes by lowering the pH. Paclitaxel, in combination with C6-ceramide[141], showed an increased cell toxicity compared to free drug usage. Theoretical encapsulation studies[172-174] and an in-vivo study[175] were performed on gemcitabine. Molecular dynamics simulations with the focus on encapsulation were separately performed on different drug molecules.[143, 147, 176-179] Finally, both in-situ and in-vitro studies were also performed on different drug molecules.[140, 180-181]

Aside from carbon nanotubes filled with drug molecules, and although less explored, other filling materials can also be employed for therapeutic applications as well.[31] For instance, it has been shown that iron-filled carbon nanotubes can be used for inducing hyperthermia, which in return results in cytotoxicity.[182]

1.4.2. Filled Carbon Nanotubes for Biomedical Imaging and Diagnosis

Apart from the therapeutical benefit, filled carbon nanotubes have also been exploited for diagnostic purposes and, in some cases, both at the same time. The release of the confined material in this case is generally not needed, and the carbon shell provides shielding from potential damage to the biological surrounding.

Biomedical imaging with filled carbon nanotubes is particularly interesting as nanotube systems can be robust and versatile by means of both external and internal functionalization. Filled iodine materials can be used in different ways. Micro-CT (Micro computed tomography) images of iodine filled carbon nanotubes were acquired showing increased opaque contrast compared to empty nanotubes.[183] Radioactive iodine-125 can also be encapsulated in nanotubes[184-185] and used for imaging with potential for therapeutic treatment purposes. Wilson's group managed to encapsulate astatine-211[186], a short lived α-radionuclide, bismuth[187] for CT, which showed brighter contrast in CT images, and dysprosium and gadolinium salts that were used as MR (Magnetic resonance) contrast agents. The same group used nitroxide radicals as T_1 and T_2 weighted contrast agents showing contrast enhancements in-situ in both cases.[188] A great deal of attention is given to the so called gadonanotubes (gadolinium filled carbon nanotubes) for future diagnostic applications. Gadonanotubes used for magnetic resonance imaging (MRI) showed in-situ[189-193], in-vitro[190, 193-194] and in-vivo[194-198] enhanced performance compared to commercially available MRI contrast agents. Dual PET (Positron emission tomography) and MRI imaging can be achieved by using gadolinium and copper-64 filled carbon nanotubes in-vivo.[198]

Metal-filled nanotubes, in particular ferromagnetic materials[199-200], are interesting from the imaging and therapeutic point of view. In-vivo[201-

[202] and in-vitro[182, 202-203] studies showed efficient T_2 weighted contrast signal. Hyperthermia treatment with the same material was also efficient on cell lines, as selective cytotoxicity was observed.[182] Carbon nanotubes filled with iron(III) oxide conjugated with quantum dots were used for imaging and mapping of cancer cells, and targeted treatment in-vitro showing that magnetically guided drug delivery of doxorubicin can cause cell death.[204] Recently, we have shown that filled nanotubes can be used for X-ray fluorescence imaging of cells.[205] Filled nanotubes exohedrally decorated with targeting peptides were observed in different cellular compartments (Fig. 7).

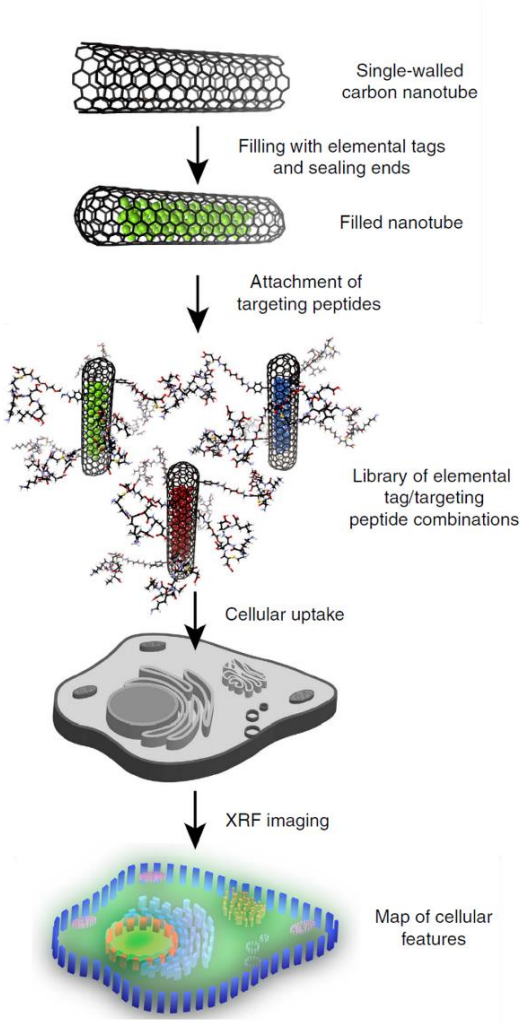

Figure 7. Experimental design for XRF imaging of cellular organelles.[205]

2. OBJECTIVES

2.1. Objectives

The aim of this Thesis is to provide support for future applications of filled carbon nanotubes, with the primarily focus on nanomedicine.

The main objective of this Thesis is to prepare samples of carbon nanotubes filled with radioactivable metals of high purity suitable for both biomedical imaging and therapy. To achieve this, the first step in the synthesis of filled carbon nanotubes is the purification process. With this Thesis, we are trying to give insights on the purification process and how to achieve the lowest amount of impurities possible for both single and multi-walled carbon nanotubes. Special emphasis is devoted to the decrease of catalyst content which could interact with the biological milieu, leading to undesirable side-effects. To get reliable results, the second aim of the Thesis is to optimize and study the effect of different parameters used for thermogravimetric analysis of carbon nanotubes. This technique is widely employed for the characterization of carbon nanotubes and will benefit from this study. We also aim to explore an additional, cheap, fast and reliable UV-Vis analysis method for the evaluation of the catalyst content in carbon nanotube samples.

The second step in the synthesis is the filling of opened-ended nanotubes. The aim here is to synthesize dry samarium(III) chloride from samarium(III) oxide for the purpose of filling carbon nanotubes with samarium in a high yield. Once filled, the ends of carbon nanotubes need to be closed to allow the selective removal of the non-encapsulated samarium compounds, external to the walls of carbon nanotubes. In this context, we will explore the ability of closing the ends of multi-walled carbon nanotubes by thermal annealing, as this material has proven to be more biocompatible than single-walled nanotubes, and it also has bigger cavities which potentially should allow a large amount of material to be confined in their interior.

The last synthetic step is the removal of the external, non-encapsulated compounds from the samples of filled carbon nanotubes. We will investigate and optimize the removal efficacy of the non-encapsulated material under different conditions. This study has the goal of developing a protocol that allows a fast washing evaluation, which is essential when dealing with radioactive materials.

Finally, after the synthesis, we delve into in-vitro studies of filled multi-walled nanotubes in two cell line models: breast cancer for therapeutical evaluations, and bronchial cells for exposure evaluations. This is a crucial step towards future in-vivo biomedical applications of filled carbon nanotubes for both therapy and diagnosis.

Here is a comprehensive list of the specific objectives of this Thesis:

- optimization of the TGA parameters for carbon nanotube samples
- purification of carbon nanotubes with special emphasis on the removal of catalytic nanoparticles
- development of a protocol for the evaluation of catalyst content in carbon nanotube samples by UV-Vis spectroscopy
- fill carbon nanotubes with samarium in a high yield
- optimization and monitoring of the washing protocol for the non-encapsulated material external to filled carbon nanotubes
- investigation of the end-closure of multi-walled carbon nanotubes by thermal annealing
- in-vitro cytotoxicity and intake studies of empty and filled multi-walled carbon nanotubes, on epithelial breast cancer and healthy bronchial cell lines

3. RESULTS AND DISCUSSION

3.1. Assessment of the Purification Degree of Carbon Nanotube Samples

3.1.1. Thermogravimetric Analysis of the Inorganic Impurities Present in Carbon Nanotube Samples

3.1.1.1. Introduction

During the synthesis of carbon nanotubes, different impurities are introduced in the sample, which possibly include catalyst residue, graphitic particles, which can also be coating the catalyst, amorphous carbon and fullerenes.[9] Different impurities can compromise the properties and quality of the sample. A variety of techniques can be employed for the analysis of CNTs, including electron microscopy, inductively coupled plasma (ICP), UV-Vis spectroscopy, infrared and Raman spectroscopy, which give different information on the local morphology and structure of the sample, elemental content, optical properties, functionalization and nanotube integrity respectively. One of the most basic, but also most widely used analytical technique for CNTs is thermogravimetric analysis (TGA).[206] It has the capability of assessing physical and chemical changes of materials, including thermal stability, combustion or reaction temperature of the material. The analysis can be performed using different gases, depending on the type of analysis planned, including air, argon, nitrogen, helium, oxygen, carbon dioxide, or reaction gases. When performing TGA on CNTs under air, usually the weight loss corresponds to the oxidation of carbon into

carbon dioxide, and the resulting residue to metal oxide from the catalyst employed in the CNT synthesis.[9] By using inert gases for the TGA of the same material, the weight loss can be attributed to removal of functional groups, thus allowing the assignment of the level of functionalization of the material.[207] Apart from the gas employed, there are several parameters that control the TGA, including the gas flow rate, the heating rate and the mass of the sample employed. In this chapter, we get insights on the role that the experimental TGA parameters have on the obtained data, and suggest the optimal conditions to obtain reliable data. Furthermore, we show the importance of reporting the employed parameters for the TGA in order to allow data comparison between different analyses. The role of these parameters on the thermal analysis of different materials has been previously investigated[208-209], but to the best of our knowledge, there are no reports on their influence on CNT samples.

3.1.1.1. Experimental

CVD synthesized single-walled carbon nanotubes (SWCNTs), provided by Thomas Swan Co. Ltd., were grinded, using a high-polished agate mortar, with pestle and placed in an opened-ended silica tube. Around 200 mg of SWCNTs were used per purification. The purification was performed in a tubular furnace in an argon and steam flow at 900 °C for 4 hours, in order to remove carbonaceous impurities.[63-64, 210] This was followed by an acid treatment on the sample at 110 °C overnight by using 200 mL of 6 M hydrochloric acid (Panreac) in order to dissolve the exposed catalyst. Samples were collected by filtration and washed with water until the pH of the filtrate was neutral.

Thermogravimetric analyses were performed using a TA instrument TGA Q5000-IR. 10 mL/min balance flow in nitrogen was used for all samples, while the combustion of samples was done in air by using different parameters: CNT sample masses between 1 and 20 mg, gas

flow rates between 5 and 200 mL/min and heating rates between 1 and 50 °C/min. The samples were analyzed in high temperature 100 µL platinum pans, with an Inconel handle that prevents the fusion of the platinum hook and pan during the analysis. All TGA curves were analyzed using TA Universal Analysis program and OriginPro.

Scanning Electron Microscope (SEM) QUANTA FEI 200 FEG-ESEM and Transmission Electron Microscope (TEM) 120 KV JEOL 1210 were used for visualization and analysis of the TGA residue with Energy Dispersive X-ray Spectroscopy (EDS) for elemental composition and Electron Diffraction (ED) mode for determining the cell parameters and space groups of the crystals. Samples for TEM, SEM, EDS and ED analyses have been prepared by dispersing the TGA residue by sonication in pure ethanol (Panreac), and placing a few drops onto a lacey copper grid. Samples for Raman measurements were prepared by dispersing the sample in isopropanol (Panreac) using the same ultrasonic bath, placing a few drops of the liquid onto a glass plate, and slowly evaporating the solvent at 85 °C. Raman measurements were performed on a Lab Ram HR 800 Raman Jobin Yvon spectrometer, samples were measured between 100 and 2000 cm^{-1} using a 20 mW He-Ne laser (632 nm). Elemental Analysis (EA) of CNTs was performed at the Universitat de Barcelona on two replicas (around 1 mg per analysis), on an elemental analyzer EA 1108 Instrument, by adding vanadium(V) oxide and tin to ease the combustion, and using sulfanilamide as a pattern. Superconducting Quantum Interference Device (SQUID) Quantum design MPMS XL-7T was used at 10 K (liquid nitrogen) under external DC magnetic field. Hysteresis loops were taken in the range between -50 000 to +50 000 Oe to monitor the catalyst content. Samples for SQUID were placed in a gelatin capsule (about 6 mg per sample) and fixed with non-magnetic glass wool to avoid sample movement during the measurement.

3.1.1.3. Results and Discussion

We started by determining the composition of the sample. To do this, we performed TGA of the as-received (raw) CNTs under flowing air, and analyzed the solid residue remaining on the pan after the complete combustion of the carbonaceous species. The inorganic residue composition shows the presence of iron and oxygen by EDS on SEM (Fig. 8), revealing the presence of an iron oxide, as a result from the oxidation of iron (catalyst) during the TGA. The crystalline structure of the iron oxide can be determined by ED on TEM (Fig. 9). Both monocrystal and polycrystalline diffractogram patterns correspond to iron(III) oxide, hematite. EDS and ED confirm the absence of other iron compounds such as iron carbide and also other species such as alumina, which has for instance been found in samples of MWCNTs.[211]

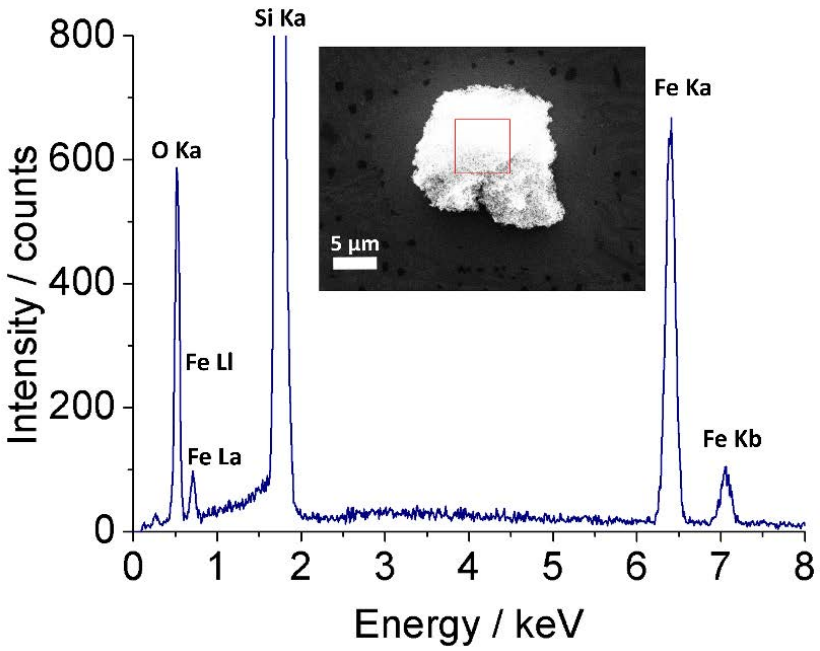

Figure 8. EDS analysis and SEM image (inset) of the collected residue after TGA under flowing air of as-received (raw) SWCNTs confirming the presence of iron and oxygen; silicon is present in the sample holder; the red square on the SEM image shows the area of acquisition of the spectra.

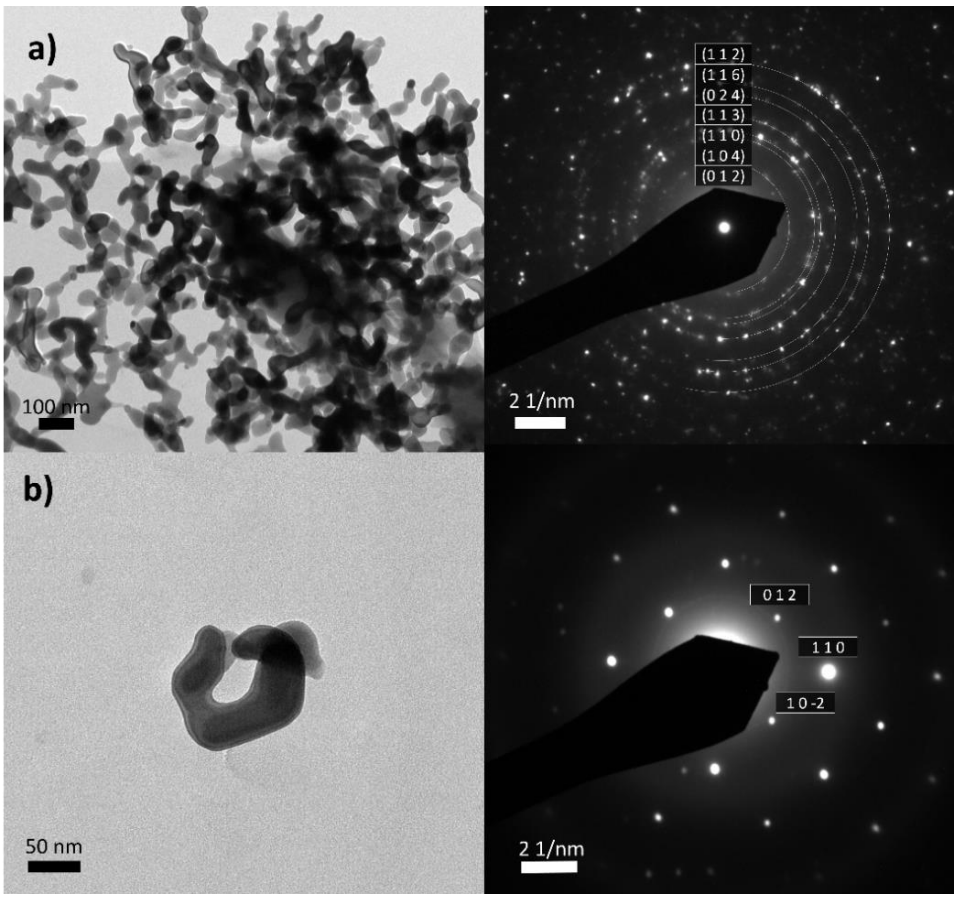

Figure 9. Analysis of the collected residue after TGA under flowing air of as-received (raw) SWCNTs; TEM image and ED of polycrystalline (a) and monocrystalline (b) areas. Indexed patterns are in agreement with the presence of α-Fe_2O_3.

The oxidation temperature of a sample can be defined in many ways by analyzing the TGA curve. We present four different temperatures used to describe the oxidation process (Fig. 10): weight loss onset temperature (T_{onset}) and weight loss "offset" temperature (T_{offset}), which give a temperature range in which oxidation occurs; temperature at 50% of weight loss (T_{50}) and temperature of the maximum in the weight loss rate (T_0=dm/dT). The width of the derivative thermogravimetric (DWC) peak can be used as an indicator of material purity, where a narrower peak corresponds to cleaner material. Finally, we will also refer to the surface area underneath the peak of the derivative curve

(A) versus time. It is important to note that comparison between surface areas cannot be employed to different heating rates since the area is also time dependent.

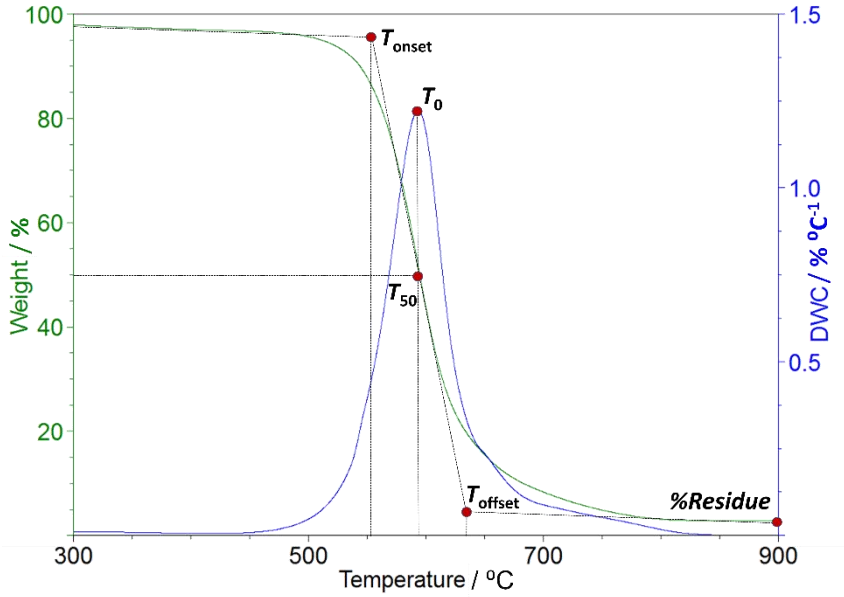

Figure 10. TGA curve of raw carbon nanotubes under flowing air. Different temperatures can be used to describe the combustion of the sample (weight loss onset temperature - T_{onset}, temperature on the maximum at the weight loss rate - T_0, temperature at 50% of weight loss - T_{50}, weight loss "offset" temperature T_{offset}) and final inorganic residue (%Residue) attributed to iron(III) oxide.

TGA was performed on purified and non-purified, raw material, with the same pretreatment, which consisted of allowing the sample to stabilize at room temperature for 20 minutes, followed by a heating rate of 10 °C/min, up to 120 °C and holding the temperature for 20 minutes under an air flow of 20 mL/min. For statistical purposes, we analyzed 5 samples using typically employed values of mass, gas flow rate and heating rate, namely 5 mg, 25 mL/min and 10 °C/min respectively. This allowed us to determine a statistical range for the amount of catalyst and combustion temperature that will be included as an error bar in subsequent analyses.

Let us start by analyzing the influence that the mass of the sample employed for the TGA has on the obtained data. By changing the mass of sample to 1, 2, 5, 10, 15 and 20 mg, while keeping the heating rate constant at 10 °C/min, up to 900 °C, and gas flow rate constant at 25 mL/min, we observed changes in the TGA curves in terms of combustion temperatures and catalyst content (Fig. 11). The higher the mass of the sample, the more time is needed to completely combust the sample. The catalyst content is also being altered. The catalyst content for 2 mg, 5 mg and 10 mg of CNTs is similar and within the statistical error (Fig. 11). Figure 11D clearly shows an increase in the T_0, T_{50} and T_{offset} temperatures with the sample mass increase, while T_{onset} remains relatively similar. This suggests that the combustion of the sample starts at the same time irrespective of the sample mass, while the ending point increases with the mass, due to the increased time needed to combust the sample. Also, the surface area below the derivative curve (Fig. 11E) shows that all investigated sample masses fall within the predetermined statistical area, except for 1 mg, which is due to the low volume of the sample, and a shorter time needed to complete its combustion.

Gas flow rates are also affecting the TGA output data obtained for CNTs. 5, 10, 25, 50, 100, 150 and 200 mL/min were employed keeping the mass of the sample constant at around 5 mg and the heating rate constant at 10 °C/min (Fig. 12). As it can be seen in the TGA (Fig. 12A) curves, it takes longer time to complete the oxidation of the sample when employing low flow rates (5 mL/min and 10 mL/min). One possible explanation for the change in the aspect of the curve is the lack of oxygen supply necessary to oxidize carbon at low flow rates, making the combustion temperature higher, which can be seen by the wider DWC peak (Fig. 12B), while fast flows of air result in faster oxidation. Whereas, T_{onset} remains practically constant, suggesting that the change in the gas flow rate does not affect the commencement of the oxidation, T_0, T_{50} and T_{offset} are shifted to higher temperatures at low flow rated (5 mL/min and 10 mL/min). With low flow rates of air, oxygen

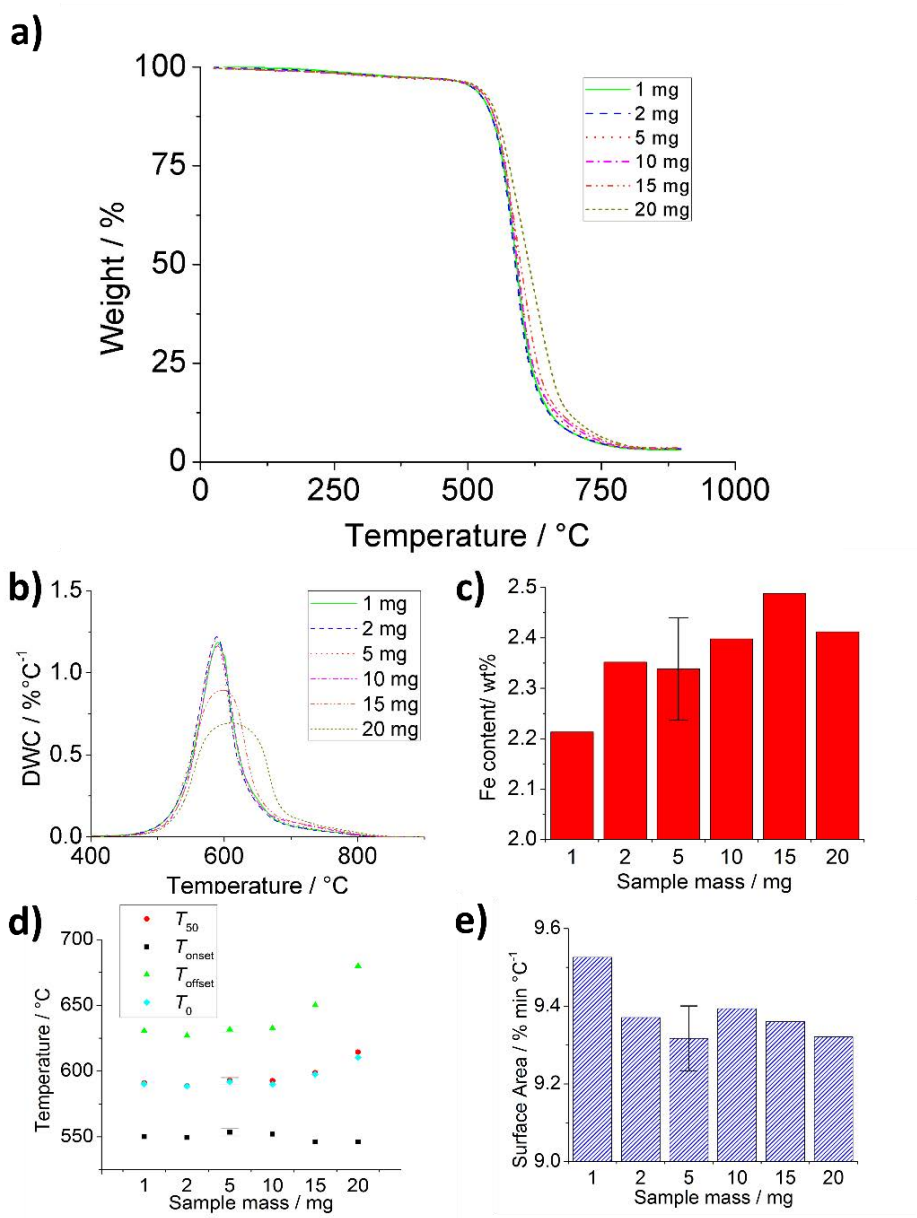

Figure 11. The role of sample mass on the TGA data; TGA curve (a) and calculated first derivative curves (b) of non-purified nanotubes analyzed by changing the mass of the sample, while keeping other parameters constant - gas flow of 25 mL/min and heating rate 10 °C/min; iron catalyst content (c) calculated from the residue leftovers after the analysis corresponding to iron(III) oxide, different temperatures (d) related to sample oxidation estimated from (a) and (b), and surface area under the derivative curve versus time (e).

flow is decreased and more time is needed for the complete combustion of the sample, resulting in higher combustion temperatures. No significant change in the surface area was observed (Fig. 12E). In terms of catalyst content, when using gas flows between 25 and 100 mL/min, the obtained residue is similar, while other flows employed for the analyses fall outside the predetermined statistical range values (Fig. 12C). The apparent increase of catalyst content with gas flow is probably due to the constant gas exchange which might lower the local temperature nearby the sample holder, leaving the sample partially unoxidized. Another possibility can be that the flow of air slightly pushes the platinum pan up, interfering with the TGA output data.

The most dramatic change in terms of curve aspect was detected when changing the heating rate to 1, 5, 10, 15, 20 and 50 °C/min (Fig. 13). For this set of experiments, the sample mass was kept constant at around 5 mg, and gas flow rate was kept constant at 25 mL/min. Higher heating rates resulted in higher combustion temperatures. As the speed of heating increases, the sample combustion is delayed due to the incapability of the system to heat the whole sample at a given temperature; i.e. the furnace increases from a given temperature A to B before the whole sample of nanotubes has reached the temperature. As a consequence, at high heating rates the real temperature of the sample is lower than the temperature of the furnace. This was clearly observed when using the highest heating rate (50 °C/min). Not only did the combustion process start later, but even at 900 °C the combustion was not completely finished yet; a black residue was collected in the platinum pan at the end of the analysis, indicating the presence of CNTs. In this case only, we expanded the heating range up to 1000 °C to assure the complete combustion of the sample (Fig. 13). In agreement, Figure 13D reveals the increase of all defined temperatures, T_0, T_{50}, T_{onset} and T_{offset} with the increase of the heating rate. Obviously, time plays a key role with this parameter, as more time is needed for sample combustion with lower heating rates and vice versa. This is clearly shown in Figure

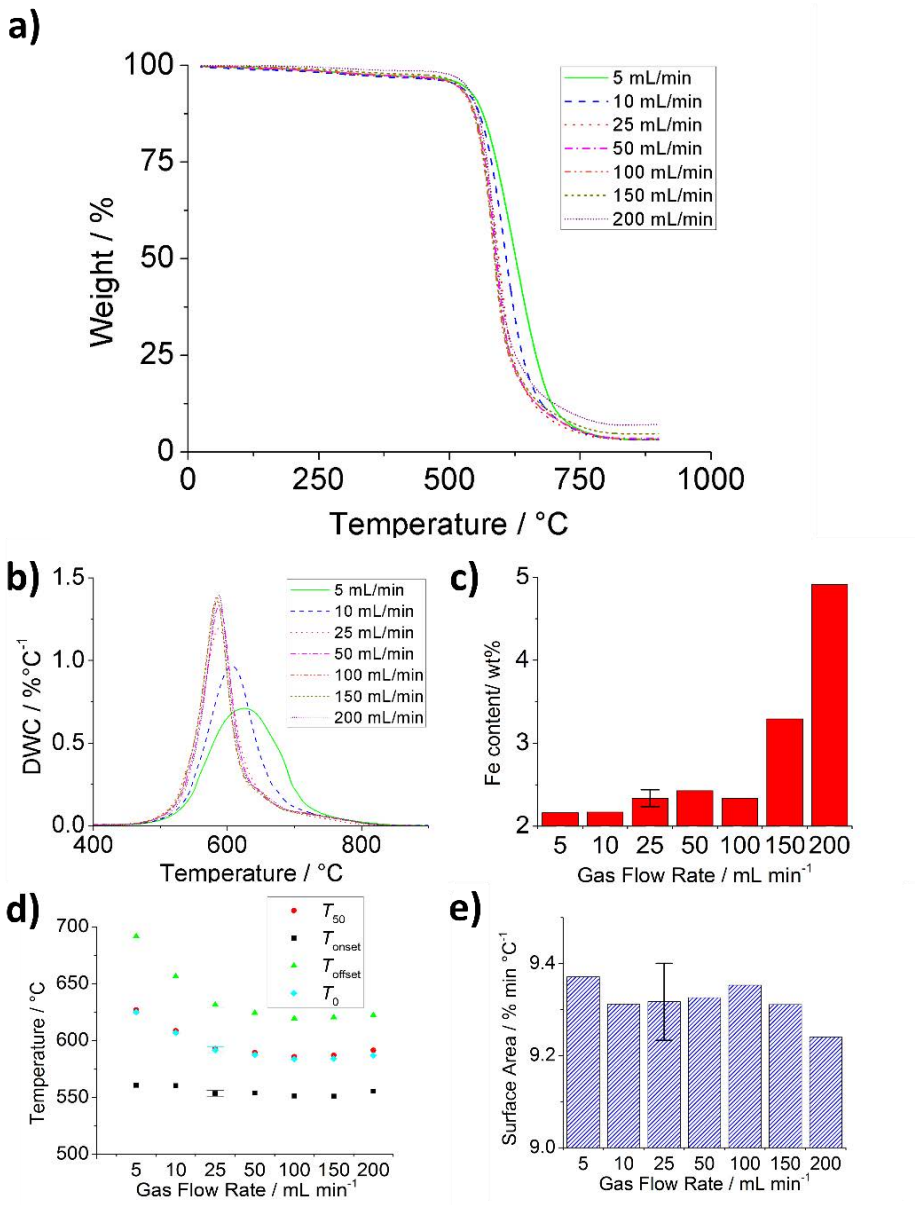

Figure 12. The role of gas flow on the TGA data; TGA curve (a) and calculated first derivative curves (b) of non-purified nanotubes analyzed by changing the gas flow rate, while keeping other parameters constant - sample mass of 5 mg and heating rate 10 °C/min; iron catalyst content (c) calculated from the residue leftovers after the analysis corresponding to iron(III) oxide, different temperatures (d) related to sample oxidation estimated from (a) and (b), and surface area under the derivative curve versus time (e).

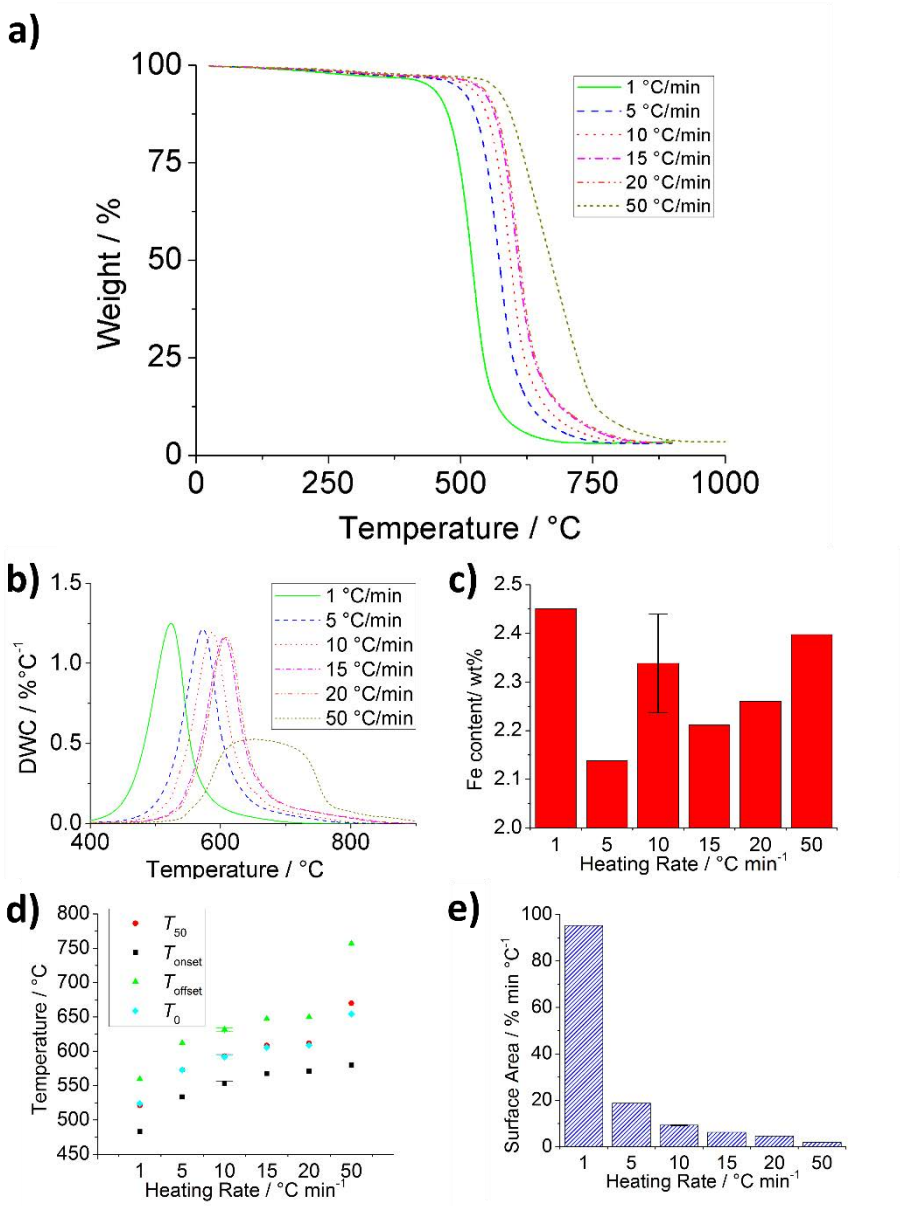

Figure 13. The role of heating rate on the TGA data; TGA curve (a) and calculated first derivative curves (b) of non-purified nanotubes analyzed by changing the heating rate, while keeping other parameters constant - sample mass of 5 mg and gas flow rate of 25 mL/min; iron catalyst content (c) calculated from the residue leftovers after the analysis corresponding to iron(III) oxide, different temperatures (d) related to sample oxidation estimated from (a) and (b), and surface area under the derivative curve versus time (e).

13E, where the time-dependent surface area is decreasing with the increase of the heating rate, which implies shorter analysis times. The catalyst content for most samples remained within the statistical setting (Fig. 13C).

With the analyses performed so far, we suggest using the following suitable parameters when performing TGA on carbon nanotubes:

- sample mass between 2 and 10 mg
- gas flow rate between 25 and 100 mL/min
- heating rate of 10 °C/min

When comparing data of a given set of samples, we advise using the same TGA parameters and detail them when presenting the data.

To complete the study and to stress out the importance of keeping the TGA parameters constant when analyzing different samples, here we present few possible outcomes when different TGA analysis parameters are used for purified and as-received (raw) material. Initially the TGA of both as received and purified SWCNTs was performed using the optimized conditions, namely 5 mg of sample, 25 mL/min of air flow and a heating rate of 10 °C/min. Both TGA and DWC curves of purified and as-received material are shown in Figure 14A. The catalyst content of pristine SWCNTs determined by TGA is being decreased by the purification process[63]. Furthermore, due to the removal of amorphous carbon and the more defective nanotubes from the sample, higher energy requirements are necessary for carbon combustion, leading to an improved stability of purified SWCNTs compared to the pristine one. The surface area of the derived weight change peak is slightly increased (9.75 ± 0.166 % min C^{-1}, *N*=4) for purified material compared to raw SWCNTs (9.32 ± 0.084 % min C^{-1}, *N*=4).

To provide evidence on the indirect observations made from the TGA of raw and purified SWCNTs we analyzed both samples by Raman spectroscopy. Raman spectroscopy gives insight into the structure of

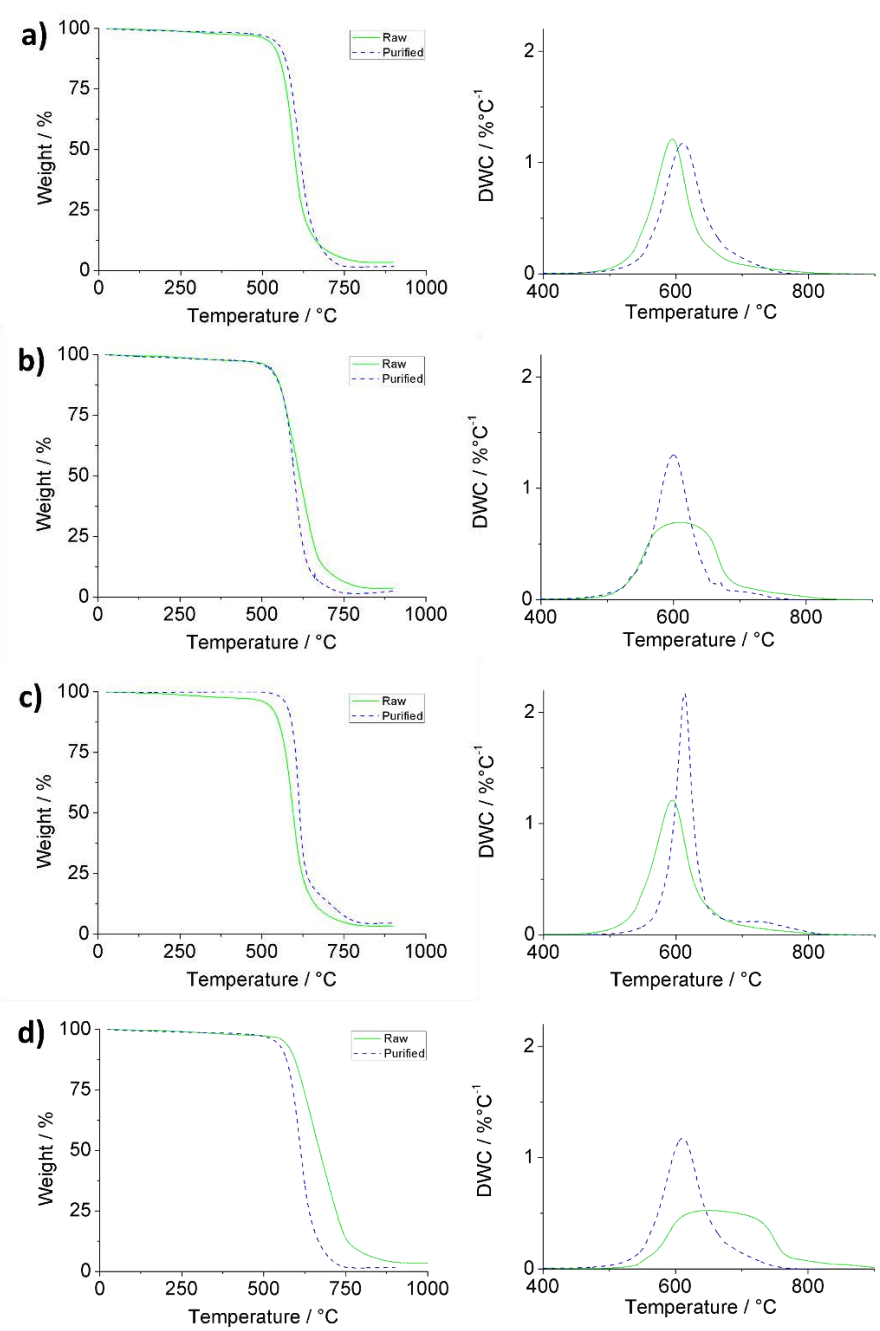

Figure 14. TGA curves and first derivative curves of purified and raw carbon nanotubes; correct (a) and inversed (b, c, d) relationship obtained by changing the sample mass, 1 mg for purified vs 20 mg for raw SWCNTs (b), gas flow rate, 200 mL/min for purified vs 25 mL/min for raw SWCNTs (c) and heating rate, 10 °C/min for purified vs 50 °C/min for raw SWCNTs (d). The rest of parameters are kept constant to the values employed for (a), namely 5 mg of sample, 25 mL/min gas flow rate and 10 °C/min heating rate.

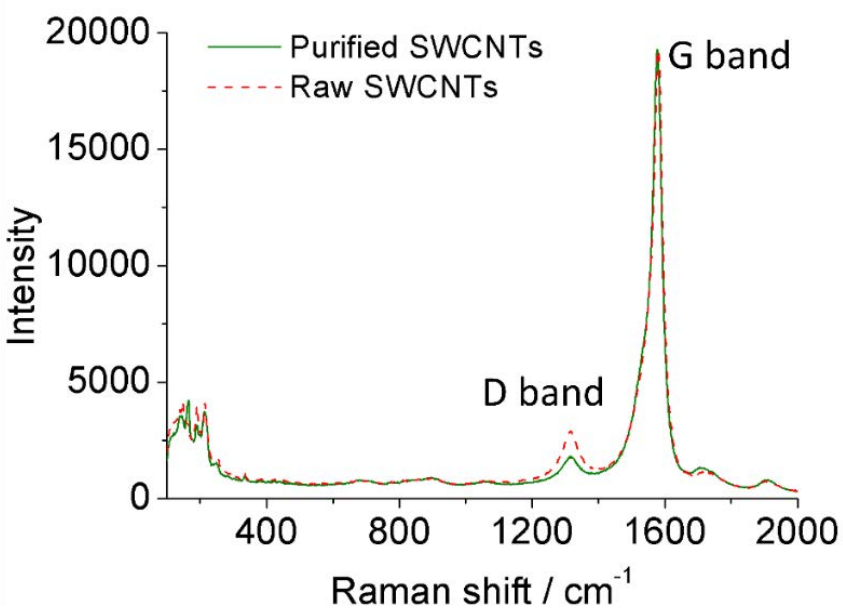

Figure 15. Normalized Raman spectra of both raw and 4 hours steam purified (followed by an HCl wash) SWCNTs; D band present at around 1350 and G band around 1570 cm-1.

carbon nanotubes. Whereas the D band at around 1350 cm^{-1} is attributed to the presence of sp^3 carbon atoms and requires a defect for its activation, the G peak (around 1570 cm^{-1}) corresponds to the E_{2g} photon at the Brillouin zone center. The I_D/I_G ratio is therefore employed to assess the quality of the CNTs. The more defective the material, or the higher the amount of amorphous carbon, the bigger the I_D/I_G ratio.[212] After employing four hours of steam purification on carbon nanotubes, followed by an HCl treatment, the I_D/I_G ratio decreased from 13.7 ± 0.4 to 9.8 ± 1.6 (N=4), confirming the structural benefit from purification. The decrease of the D band has been previously attributed to the removal of amorphous carbon and the more defective nanotubes from the sample.[63] Catalyst content can be precisely monitored by SQUID, since it is a very sensitive technique used for magnetic materials.[63, 213] In agreement with TGA, we observed a decrease of catalyst content after purification, starting from 3.1 emu/g (1.4 wt% of Fe) for the raw material, down to 1.1 emu/g (0.5 wt% of Fe) after the steam and HCl purification. The removal of metal catalyst should result in a relative increase of the carbon content. EA reveals

that the carbon content increased from 91.4% for raw material to 96.9% after the employed purification.

Next, from the three different TGA parameters under investigation (mass, flow rate and heating rate), we modified one of them for the analysis of raw and purified SWCNTs, while keeping the other two constant (Fig. 14B, C, D). As we can clearly see, the real relationship between non-purified (raw) and purified material can be compromised, thus leading to draw false conclusions when comparing them. For instance, when using 1 mg of purified SWCNTs and 20 mg of pristine SWCNTs for the TGA (gas flow 25 mL/min and heating rate 10 °C/min), an inverse relationship is observed in terms of temperature of combustion (Fig. 14B). The same effect has been observed when employing a heating rate of 10 °C/min for purified SWCNTs and 50 °C/min for raw SWCNTs (sample mass 5 mg, gas flow 25 mL/min) showed in Fig. 14D. When using a higher flow rate for purified CNTs, 200 mL/min, than for raw CNTs, 25 mL/min (sample mass 5 mg, heating rate 10 °C/min), the determined catalyst content turns out to be higher (3.1 wt%) compared to the catalyst content of pristine CNTs (2.3 wt%), when in reality it is much lower (Fig. 14C). The inverse amount of catalyst content between purified and raw material would also lead to draw false conclusions, since the catalyst content is supposed to drop after purification, as shown by SQUID data.

3.1.1.4. Conclusion

As the number of papers on carbon nanotubes continuously increases, for the sake of data comparison, parameters used for the analysis ought to be stated. That being said, the best correlation between different samples can be achieved by using the same, or at least similar, analysis parameters. The reported study, that assess the best parameters for TGA on the stability and purity of single-walled carbon nanotubes, can be extrapolated not only to other carbonaceous materials, such as graphene, multi-walled carbon nanotubes, graphite or diamond, but also to other inorganic, organic or composite materials as well. Single-walled carbon nanotubes showed some notable differences in the TGA curve by employing different parameters of analysis. The most profound differences can be seen when applying different heating rates. When using the most extreme conditions employed in this study, i.e. 20 mg of sample, 5 mL/min of gas flow and/or 50 °C/min heating rate, the DWC peak becomes wider and the assessment of the sample purity can be compromised. The nature of thermal analyses performed on carbon nanotubes makes it difficult to give a straightforward answer to at which temperature do carbon nanotubes burn. For the single-walled carbon nanotubes employed in this study, we observed a wide range of combustion temperatures between 480 and 770 °C, depending on the parameters used. This can be at least partially overcome by using always the same analysis parameters. From the performed study, we suggest to employ a sample mass between 2 and 10 mg, a gas flow rate between 25 and 100 mL/min and a heating rate of 10 °C/min for the TGA of carbon nanotubes.

3.1.2. UV-Vis Evaluation of the Metal Content in Multi-Step Steam Purified Carbon Nanotube Samples

3.1.2.1. Introduction

The nature of the production of carbon nanotubes implies the inevitable introduction of impurities, as discussed earlier. This refers to amorphous carbon, graphite nanoparticles, fullerenes, metal catalyst particles and other inorganic impurities. In turn, the metal catalyst can be surrounded by graphitic shells. To fully exploit the potential of CNTs, these impurities have to be removed and many different methods have already been developed.[9, 214] Our focus has been in the efficient removal of such impurities, without damaging the structure of the carbon nanotubes, while avoiding the introduction of unwanted functional groups at the same time. Since pristine nanotubes come with closed ends, and short nanotubes are desirable for biomedical applications, we chose an established steam purification and shortening treatment that leads to samples of opened-ended nanotubes.[64] The mild oxidizing environment that steam offers is efficient in removing the amorphous carbon and graphitic particles which might be coating the catalytic nanoparticles present in the sample. After the steam treatment, the catalytic nanoparticles free of the protecting graphitic surrounding can be easily dissolved with a hydrochloric acid wash.[63] As mentioned, steam treatment also opens the ends of the nanotubes, which is of particular interest to allow their subsequent filling with the selected payload, and shortens their length. The larger the time of the steam treatment, the shorter the length of the resulting nanotubes.[215] Being a mild oxidizing agent, the use of steam minimizes the introduction of functional groups or structural defects in the carbon nanotube backbone.

There are several parameters that control the purification protocol, including heating or cooling ramp, annealing temperature or time of steam treatment that can lead to different outcomes in terms of sample purity. By adjusting those parameters, it is possible to achieve a low amount of catalyst content, which is of particular interest for biomedicine. The quantity of catalyst present in the samples can be determined by different techniques, being TGA, ICP, SQUID the most commony emplyed.[214] Here we discuss the use of UV-Vis spectroscopy which, unlike other techniques used for this purpose, is a fast, reliable, easily accessible and affordable technique for many laboratories. A similar study that employs ferroin complexes has been published recently.[216] The authors found that measuring the iron content directly from samples of carbon nanotubes proved not to be as efficient as measuring the amount of iron in the ash, probably due to some leftovers of entrapped iron in graphitic shells.

3.1.2.2. Experimental

Around 200 mg of CVD synthesized single-walled carbon nanotubes (SWCNTs), provided by Thomas Swan Co. Ltd., were grinded with a pestle in a highly-polished mortar, placed in an opened-ended silica tube employed as sample holder, which was then positioned at the center of a tubular furnace. Argon flux together with a steam flux at 900 °C for 4 hours was employed in order to remove carbonaceous impurities. [63-64, 210] This was followed by acid treatment of the sample at 110 °C overnight by using 200 mL of 6 M hydrochloric acid (Panreac) in order to dissolve the exposed catalyst. Samples were washed with water until the pH of the filtrate was neutral, and dried at around 80 °C overnight. A combination of multiple purifications was performed on single-walled carbon nanotubes by repeating the steam (for a selected amount of time) and acid treatments several times. The steam treatments were repeated up to six times for one hour, up to 3 times

for two hours, up to 2 times for three hours, and a control of 6 hours of continuous steam treatment was also included for comparison. An acid treatment was performed in between each steam purification to remove the exposed metal catalyst.

TGA analysis of CNTs was carried out on a NETZCH-STA 449 F1 Jupiter instrument, where about 5 mg of sample was burned under flowing air. The TGA parameters optimized in the previous study were employed for the analyses: 25 mL/min gas flow and 10 °C/min heating ramp up to 900 °C. This results in the complete oxidation of carbon from the sample, leaving the oxidized iron as the analyzable residue. After the analysis by TGA, the oxidized catalyst was completely dissolved in 50 mL of concentrated HCl (Panreac) for the UV-Vis analysis which was carried out using a Cary 5.0 UV-Vis double beam spectrophotometer with 10-mm optical path quartz cells. Samples dispersed in isopropanol (Panreac) by sonication were used for Raman measurements, by placing a few drops of the dispersed material onto a glass plate, and slowly evaporating the liquid at about 85 °C. The Raman spectra were acquired on a Lab Ram HR 800 Raman Jobin Yvon spectrometer, between 100 and 2000 cm^{-1} by using a 20 mW He-Ne laser (632 nm). For Superconducting Quantum Interference Device (SQUID) measurements, nanotubes were placed into a gelatin capsule (around 6 mg per sample) and fixed with glass wool to avoid sample movement during the measurement, which was performed on a Quantum design MPMS XL-7T at 10 K (in liquid nitrogen) under an external DC magnetic field. The catalyst content was monitored between -50 000 to +50 000 Oe.

For the quantitative determination of the catalyst content by UV-Vis, we constructed a calibration curve by dissolving Fe_2O_3 in concentrated HCl and preparing five different concentrations in the range between 0.2 and 1 µmol dm^{-3}. For the analysis of iron content in samples of CNTs, each residue after the TGA analysis was dissolved in a small amount of concentrated HCl in a 25 mL flask by sonication, after which the flask was filled with HCl up to the mark. The concentration of samples was

calculated by fitting the observed absorbance at 243 nm to the linear equation determined from the calibration curve.

3.1.2.3. Results and Discussion

The employed purification of carbon nanotubes consists of two steps: 1) annealing of carbon nanotubes in an inert atmosphere (Ar) in the presence of a mild oxidizing agent (H_2O) that can oxidize carbonaceous material and 2) acid treatment (HCl) under reflux for 6 hours. The first step results in the loss of material due to the oxidation of carbon in the sample. This includes amorphous carbon, graphitic particles which can be coating catalytic nanoparticles, and the more reactive carbon nanotubes (ends, defects). After the steam treatment, the catalytic particles that are no longer surrounded by graphitic shells, can be removed by an acid treatment with HCl. The dissolution of the catalytic iron nanoparticles can be seen by the appearance of a yellow color in the acidic solution. The dissolved metal catalyst can be then easily separated by filtration, leaving the solid CNTs on top of the membrane.

As seen in section 3.1.1., the composition of the oxidized catalyst collected after the TGA proved to be hematite, whose nature allows its dissolution by HCl. Direct steam purification of carbon nanotubes for a given amount of time results in samples with different amounts of catalyst content (Fig. 16A). Initially, we tested up to 6 hours (annealing) of steam treatment on as-received (raw) single-walled carbon nanotubes, followed by an acid treatment. The lowest amount of catalyst for this direct purification protocol was observed after three hours of steam treatment (1.1 wt% Fe) as determined by TGA (Fig. 16A).

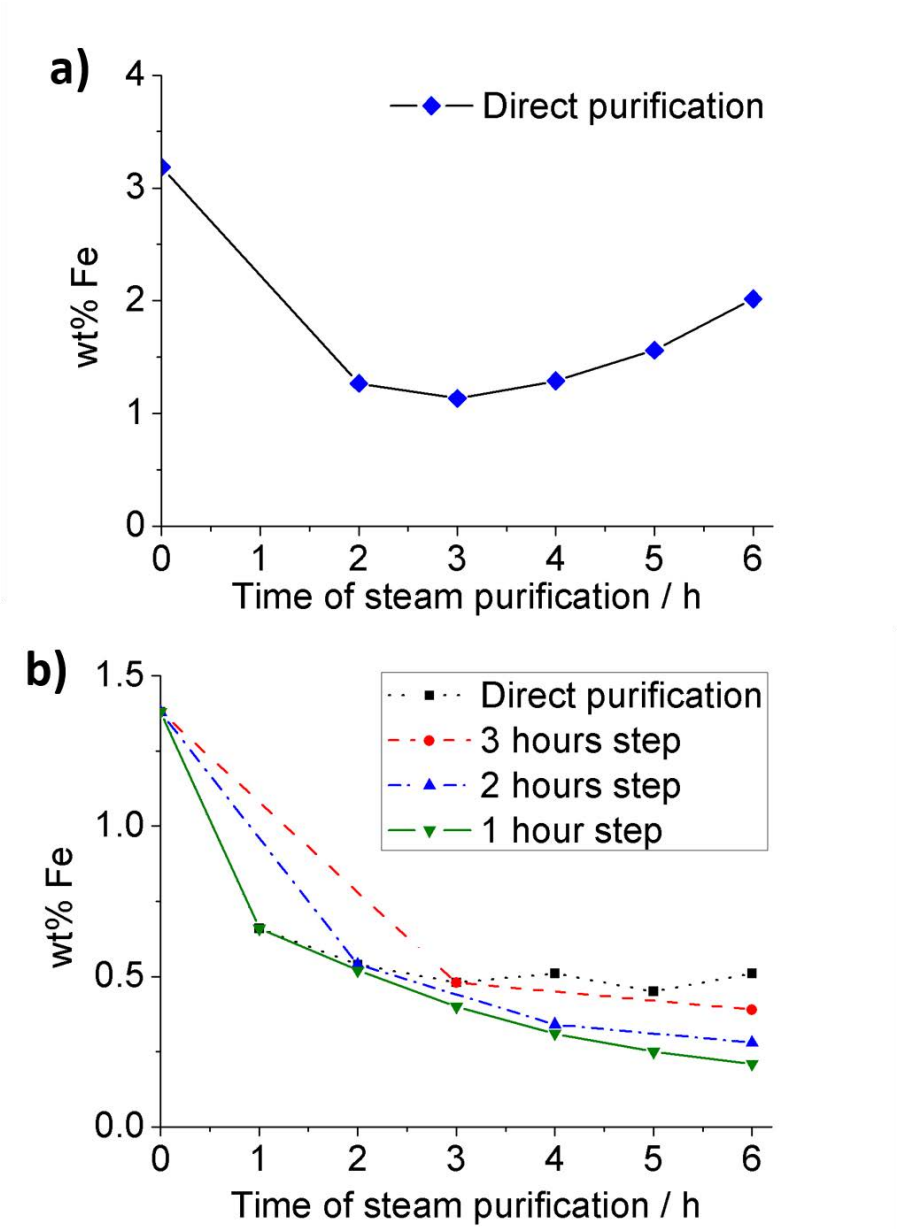

Figure 16. Iron catalyst content present in samples of carbon nanotubes purified with steam for different times (after HCl wash) determined by TGA of raw (0 hours) and steam purified carbon nanotubes where the steam purification was performed only once for the given amount of time (a) and iron catalyst content determined by SQUID of raw (0 hours) and steam purified carbon nanotubes where the steam purification was performed only once for the given time (direct purification) or multiple times (1, 2 or 3 hours step), always reaching 6 hours of steam treatment in total (b). Note that two different batches of carbon nanotubes were used for (a) and (b).

The amount of iron present in the samples can be determined from the TGA residue, by stoichiometric conversion, since iron gets oxidized to iron(III) oxide by the TGA under flowing air. After reaching the minimum amount of catalyst content, there is an apparent increase of metal impurities with the time of steam treatment. This has been previously observed, and can be due to the fact that the steam treatment starts being more efficient in the oxidation of the other carbon species rather than graphitic catalyst coatings.[63] Since TGA cannot discern between iron and the presence of other inorganic impurities, SQUID was next employed to determine the iron content, because it has been reported as an ultrasensitive method for the determination of metal impurities in samples of carbon nanotubes.[217] As it can be seen in Figure 16B (solid black squares), SQUID data also reveals the decrease of iron impurities after the steam and acid treatment with respect to the as-received carbon nanotubes. This is in agreement with TGA. Interestingly though, the amount of metal content remains practically constant, within experimental error, after 3 h of steam. Therefore, the continuous increase of inorganic solid residue at 4, 5 and 6 hours observed in the TGA might indicate the presence of other inorganic materials employed during the synthesis or purification of the samples, such as alumina or silica that have been previously observed in other samples of CVD grown CNTs.[211, 215]

With the aim of further reducing the amount of metal content present in the samples, a double treatment was tested, by repeating both the steam and acid treatments twice (Fig. 16B, 3 hours step, solid red dots). This lead to a larger decrease in catalyst content compared to the direct steam purification for the same total period of time. This suggests a more efficient removal of catalyst by repeating the purification steps multiple times. Therefore, the steam treatment was further fractioned. The total amount of time that the sample of carbon nanotubes was exposed to steam was kept constant (up to 6 hours), but the sample was removed from the purification system (i) every hour in a set of experiments (solid green triangles facing down, Fig. 16B) or (ii) every

two hours in another set of experiments (solid blue triangles facing up, Fig. 16B). The samples were treated with HCl and placed again in the furnace until a total amount of 6 hours were employed for the steam purification. The amount of catalyst content was monitored by SQUID. Interestingly, the higher the number of fractions employed, the lower the amount of catalyst present in the samples. This is easily visible in the samples that have been exposed to steam for a total amount of 6 hours (6 hours points in Fig. 16B). The iron content can be decreased by about 40 %, from around 0.5 wt.% of Fe after a 6 hours continuous steam treatment, down to around 0.2 wt.% of Fe after six treatments of 1 hour each. As mentioned, an HCl treatment is always performed after removing the sample from the steam purification system. This proves an increased efficacy of multiple treatments: the more times the treatment is repeated with shorter steam treatments, the lower the catalyst content becomes.

As mentioned, the dissolution of the iron catalyst in HCl leads to a yellow color. This is due to the formation of hexaaquairon(III) chloride which can be detected by UV-Vis. Therefore, we next explored the possibility of using UV-Vis for the determination of the iron content present in the purified samples as an alternative to TGA and SQUID.

The calibration curve was prepared by dissolving iron(III) oxide in HCl at five different concentrations. The measured UV-Vis spectra are presented in Figure 17 along with the corresponding calibration curves. As it can be seen, three peaks are clearly visible at 243 nm, 315 nm and 360 nm. The peak at 243 nm has the highest sensitivity:

y_{243}=0.0836x + 0.0336, R^2=0.9993;

when compared to the other two peaks:

y_{312}=0.0549x + 0.0182, R^2=0.9992;

y_{360}=0.056x + 0.0186, R^2=0.9990;

and was therefore used for the quantification of iron in the samples.

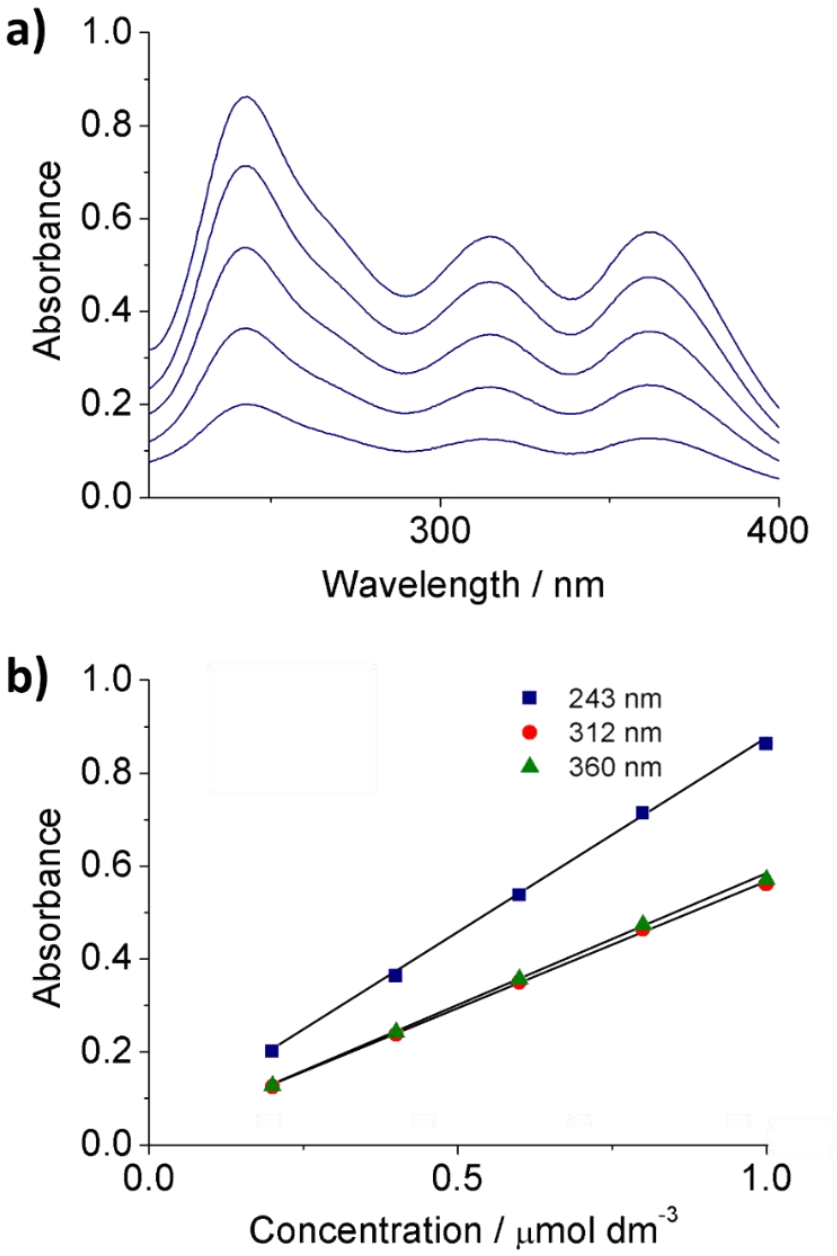

Figure 17. UV-Vis spectra of the prepared iron(III) oxide standards prepared by dissolving Fe_2O_3 in HCl (a) and the corresponding calibration curves (b) constructed from the intensity of the peaks at 243 nm, 312 nm and 360 nm.

To compare the sensitivity of UV-Vis for the detection and quantification of the iron content, all the purified samples after 6 hours of steam treatment in total, including multiple treated samples (six times 1 hour, three times 2 hours, two times 3 hours and one time 6 hours) were analyzed by UV-Vis. To do this, the solid residue after the TGA was collected and dissolved in HCl in an analytical manner. The resulting solution was then measured by UV-Vis. Figure 18 and Table 1 summarize the iron content determined by the different employed techniques, namely TGA, SQUID and UV-Vis.

Table 1. Iron content determined by TGA, SQUID and UV-Vis and I_D/I_G Raman ratio of purified carbon nanotubes after 6 hours of direct or multiple steam purifications (the SQUID data corresponds to the 6 hours point from Fig. 16B) with an HCl wash after each steam treatment.

Sample	*wt% Fe (TGA)*	*wt% Fe (SQUID)*	*wt% Fe (UV-Vis)*	*I_D/I_G (Raman)*
1 x 6 h	1.62	0.51	0.64	0.11 ± 0.04
2 x 3 h	1.34	0.39	0.43	0.14 ± 0.04
3 x 2 h	1.28	0.28	0.39	0.14 ± 0.01
6 x 1 h	1.05	0.21	0.21	0.17 ± 0.07

The content of iron determined by SQUID is in a very good agreement with the results obtained by UV-Vis (Fig. 18, Table 1). However, the iron content determined by TGA is higher, which, as mentioned earlier, might be due to the presence of other inorganic material in the sample, such as alumina or silica, introduced during the synthesis or purification methods, leading to an increase of total inorganic residue after the TGA analysis. However, it is worth noting that by dissolving the solid residue remaining after TGA, a complete dissolution of the residue has been observed. Nevertheless, even if these other inorganic impurities were present, only iron is dissolved by the HCl treatment, and the quantitative determination performed by UV-Vis is directly related to this element, like in the case of the SQUID analysis. Therefore, the

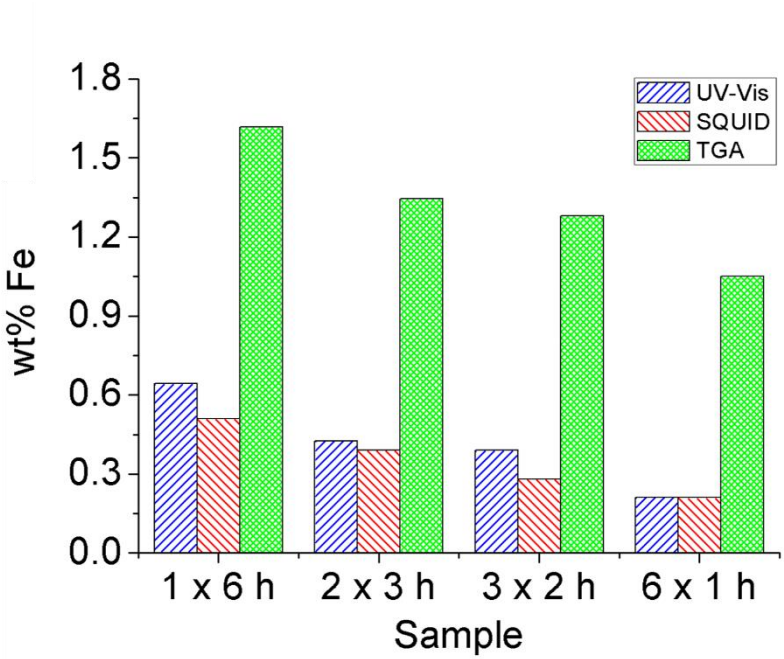

Figure 18. Iron content determined by the proposed UV-Vis analysis, SQUID and TGA of purified carbon nanotubes; All analyses have been performed after a total amount of 6 hours of steam treatment, using a direct (1x6h) or multiple steam purifications (2 x 3h, 3 x 2h, 6 x 1h). An HCl wash has been performed after each steam treatment.

presented UV-Vis methodology for the quantification of iron impurities in samples of carbon nanotubes arises as a fast and economic alternative to SQUID and TGA.

To complete the study, the same group of samples (6 hours) were analyzed by Raman spectroscopy and the D to G band ratios, which are commonly employed to assess the amount of structural defects, are included in Table 1. As it can be seen this ratio remains practically unaltered, with differences that lie within the statistical error.

3.1.2.4. Conclusion

Steam treatment is a valuable asset in the purification of carbon nanotubes, as it removes carbonaceous impurities and exposes the catalyst allowing its further removal with an HCl treatment. When low catalyst amounts are required, we suggest employing multiple purification treatments for single-walled carbon nanotubes, as the catalyst content can be lowered to about 0.2 wt% of iron.

UV-Vis analysis of the dissolved solid residue in HCl obtained after the complete combustion of the sample gives a reliable quantification of the catalyst content, in agreement with the determination from the SQUID data. Compared to SQUID or ICP-MS, UV-Vis is a faster and more affordable technique that also provides reliable results.

3.2. Filled Carbon Nanotubes with Metal Halides

3.2.1. Synthesis of Dry $SmCl_3$ from Sm_2O_3 Revisited. Implications for the Encapsulation of Samarium Compounds into Carbon Nanotubes

This work has been published in *Polyhedron*[218], and the article has been approved by the UAB Commission as part of this Thesis. The original manuscript is included in Chapter 6.

There are three main approaches to fill carbon nanotubes: solution, vapor and melt filling. Solution filling consists in stirring the previously prepared opened-ended nanotubes in a liquid containing the material to be encapsulated. The CNTs are then collected by filtration and dried. The other most commonly used approach consists of mixing the material to be filled with carbon nanotubes in solid state and subsequently annealing them at a temperature above the melting point of the selected payload. The annealing has to be performed in an oxygen-free atmosphere as oxygen can chemically alter the salt or even oxidize carbon during the filling experiment. The melt filling is a versatile approach for the confinement of inorganic materials that results in high filling yields.

Samarium is an excellent candidate for filling in carbon nanotubes for future applications in biomedicine in its ^{153}Sm form, thanks to its radioactive properties that are beneficial for diagnosis, imaging and therapy. In view of the fact that filling samarium(III) oxide inside carbon nanotubes is not straightforward because of its high melting point, which exceeds 2000 °C, we have developed a protocol by which we can

efficiently convert samarium(III) oxide to an anhydrous samarium(III) chloride form that can then easily be filled into carbon nanotubes. This protocol has been developed and optimized using non-radioactive (cold) samarium(III) oxide, but the same protocol can be translated to the radioactive material (hot) as both cold and hot materials have the same chemical behavior. When performing melt filling, different properties of samarium salts need to align for the successful encapsulation of these compounds into carbon nanotubes. These properties include chemically stability above 700 °C, as there is a spontaneous closure of the ends of carbon nanotubes after annealing at this temperature, and the salts must be water-free to avoid possible oxidation of the carbon nanotubes and/or the metal halides themselves. The latter is a key aspect to be taken into account when developing the protocol for the synthesis of $SmCl_3$ from Sm_2O_3 and its posterior encapsulation into SWCNTs, because samarium halides are highly hygroscopic compounds that attract water from air easily. The next problem arises from the radioactive point of view, where rapidity is a must.

Like discussed above, the idea of confinement of radioactivity within carbon nanotubes allows both therapeutic and diagnostical implementation of the material, allowing specific targeting of the nanoplatform, especially for cancer treatment purposes.

3.2.2. Quantitative Monitoring of the Removal of Non-Encapsulated Material External to Filled Carbon Nanotube Samples

This work has been published in *Physical Chemistry Chemical Physics*[219], and the article has been approved by the UAB Commission as part of this Thesis. The original manuscript is included in Chapter 6.

Almost all applications of carbon nanotubes require clean samples, free of non-nanotube material. As discussed, catalyst content can be minimized by the purification process to negligible amounts. Otherwise, the presence of catalyst will be noticeable depending on the application – it can induce toxicity in biological systems or even interfere in their electronical response.[220-221] The same assumption can be made for external non-encapsulated material outside filled carbon nanotubes – it can be detached from nanotube bundles and circulate in the body, induce toxicity or electrical response which is not expected with filled carbon nanotubes clean of impurities. Therefore, an efficient removal has to be developed in order to remove the external non-encapsulated material from the prepared filled carbon nanotube samples. The removal of the external material without affecting the encapsulated compounds of the same nature, is in general only possible when the ends of nanotubes are closed, otherwise, the removal of the internal encapsulated material can be expected, unless there is a strong interaction of the filler and the inner CNT walls.

Most reports on filled carbon nanotubes assess the quality of the samples, i.e. degree of filling and amount of external material, by means of electron microscopy techniques. With the present study, we wanted to develop a fast and simple protocol that would allow monitoring the removal of non-encapsulated material from samples of filled CNTs. Encouraged by the sensitivity that UV-Vis offers for the determination of catalytic impurities in samples of carbon nanotubes (section 3.1.2.), we also wanted to explore the possibility of assessing the amount of

metal halides that was removed after each washing step on samples of filled CNTs. In contrast to the analyzed iron from section 3.1.2., that gave a yellow color to the solution, dissolved Sm(III) is colorless in the studied range of concentrations. Therefore, we created a samarium complex by adding CPC/CAS to the filtrate collected after the washing steps. The resulting complex can be easily detected by means of UV-Vis spectroscopy.[222] Therefore, a simple colorimetric UV-Vis analysis of the metal complex created after the complexation of the metal from the filtered water can be used in tracking the removal of external metal from samples of filled CNTs in a straightforward way allowing the evaluation of the metal content. This is a fast, cheap and reliable method that can be used to assess the efficacy of different protocols for the removal of non-encapsulated material in samples of filled CNTs.

The washing of filled carbon nanotubes can be performed in different ways, with the goal of removing the non-encapsulated material. The most obvious course of action is to try to dissolve the material in a suitable solvent, allowing the physical separation between filled carbon nanotubes and the dissolved material. Naturally, a proper solvent is required, in which the material is readily soluble and which will not affect the overall structure of carbon nanotubes. For instance, oxidizing solutions may result in the creation of defects and even attachment of functional groups onto the outer wall of the nanotubes and even opening their ends. Both the creation of structural defects and end-opening are undesired, since they could result in the release of the encapsulated material from the interior of carbon nanotubes. Once this criterion is met, the washing can be designed in different ways, bearing in mind that the material in combination with carbon nanotubes is harder to remove than the isolated material by itself, probably due to electrostatic forces gluing the material to the outer walls or “external encapsulation” between bundles of nanotubes.

Just to give an example of the use of UV-Vis as a monitoring tool, 50 mL of pre-heated water at 100 °C or cold water at room temperature was passed through a sample of $SmCl_3$-filled carbon nanotubes with a large amount of external material (whose preparation is discussed in the published paper that constitutes this section, Chapter 6). The sample was placed on top of a filter membrane, Milipore, type JHWP with pore size 0.45 µm (for hot water, due to high temperature resistance) or Milipore polycarbonate membrane with pore size 0.2 µm (for room temperature water). The filtrate was collected for analysis, and, without moving the sample from the membrane, additional water was passed through for 4 more times. The collected filtrates were analyzed by UV-Vis spectroscopy after adding CPC/CAS in order to quantify the amount of Sm present (Fig. 19). As it can be seen in the presented data, a similar

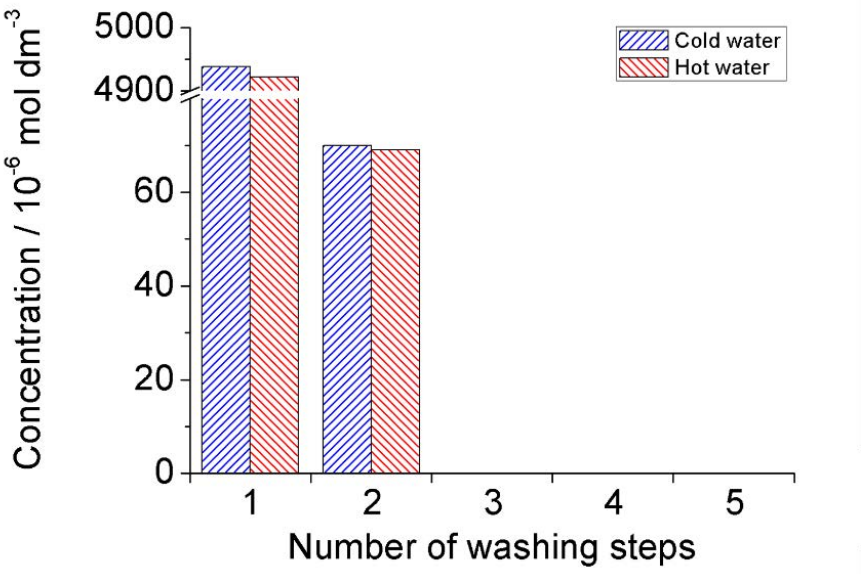

Figure 19. UV-Vis profile of the concentration of samarium(III) chloride in the aliquots collected after washing the sample of $SmCl_3$-filled carbon nanotubes with either cold (room temperature) or hot (100 °C) water.

behavior in the removal of the external material was observed with either hot or cold water. The third filtrate did not show the presence of samarium regardless of the temperature of water employed. This led us

to believe that a more efficient cleaning method can be achieved by changing different parameters, including not only temperature, but also the volume of water employed, the time of contact of the sample with water and ultimately sonication and/or stirring.

3.2.3. Closing the Ends of Filled Multi-Walled Carbon Nanotubes

3.2.3.1. Introduction

Closing the ends of carbon nanotubes is interesting for the development of novel hybrid materials based on filled carbon nanotubes. Having closed ends not only prevents the escape, or leakage, of the material from the interior, but also confers stability to the system which can be beneficial in tuning the properties of the nanotubes in a stable manner, making permanent the newly acquired property. As opposed to that, having opened ends in samples of filled carbon nanotubes can lead to leakage of the inner payload resulting in the fluctuation of the properties of the hybrid, making the whole system unreliable. Furthermore, in the biological context, the leakage of material can lead to undesired side effects, depending on the material employed, which questions the benefit of using carbon nanotubes as nano-carriers.

Spontaneous closure of the ends of single-walled carbon nanotubes by thermal annealing has already been observed[76] and different hybrid materials have been prepared in this way[185, 223], resulting in the formation of closed-ended filled single-walled carbon nanotubes that were coined as “carbon nanocapsules”.[75] It has been demonstrated that pore shrinkage on graphene sheets can be induced by heat under electron beam irradiation.[224] The same has been observed with a multi-walled nanotube tip under a focused electron beam[225], suggesting the possibility of closing the ends of multi-walled nanotubes. The effect of annealing on the structural integrity of multi-walled carbon nanotubes at temperatures up to 2800 °C has already been reported elsewhere.[226-227] Annealing of MWCNTs modified their structural features by eliminating impurities and defects. A radical structural enhancement

occurs at temperatures above 1800 °C. However, since raw MWCNTs with closed ends were used in these studies, the effect of annealing on opened tips was not investigated. When it comes to closing the ends of previously filled MWCNTs, a method using a benzene stream together with argon and hydrogen at elevated temperature has been reported[228], which leads to the formation of a carbon layer coating the entire surface of the MWCNTs.

The surface area of different materials can be measured by using the Brunauer-Emmett-Taller (BET) model developed back in 1938, based on nitrogen gas adsorption and desorption at the boiling point of the adsorbate, i.e. 77 K.[229] The BET equation takes into account different parameters:

$$\frac{n}{n_m} = \frac{CP}{(P - P_0)\left[1 + (C - 1)(\frac{P}{P_0})\right]}$$

where n corresponds to the measured amount of gas adsorbed, P is the measured pressure, P_0, the vapor pressure of the adsorbate, n_m the monolayer coverage and C are fitting parameters. Nitrogen, being the most used adsorbate for surface area measurements, has also been previously used for carbon nanotubes, although different gasses, including argon, helium, hydrogen or carbon dioxide can be employed. On the other hand, nitrogen has a permanent quadrupole that prevents adsorption on some substrate structures and can have an effect on low microporosity systems, such as single-walled carbon nanotubes, ending up with the miscalculation of the surface area.[230-231] To avoid this, other gases can be used, such as argon or helium, with an increased precision in the analysis of the gas. Bundling, aggregation and defects present in carbon nanotube samples can have an impact on the surface area of the material.[232] Purification of carbon nanotubes resulting in opened-ends can be monitored by BET. In a similar way, BET analysis is also a useful tool in evaluating the closure of the nanotube ends by thermal annealing, as it has been shown for single-walled carbon nanotubes.[233]

Filled carbon nanotubes can find application in different smart-designed systems[234-236], with special emphasis in nanomedicine for diagnosis, imaging and therapy.[31] When discharge of the material is not desired, such as for biomedical imaging, using X-ray contrast agents or when employing radionuclides for either diagnosis or therapeutic purposes, having closed ends have clear benefits compared to opened-ended CNTs, as discussed earlier, since they prevent leakage of the material from the inner cavity of the nanotubes and thus avoid any potential toxicity of the encapsulated payload. On the other hand, opened ends are required when, for instance, drug release is necessary to induce a desired response at the targeted site. In this sense (as discussed in dection 1.4.1.), the development of removable corks is of great interest.

Multi-walled carbon nanotubes possess some advantageous properties compared to their single-walled counterparts. These properties include: a bigger cavity that enables more material to be filled in, ease of functionalization and individualization (lower bundling rate) leading to a better dispersability, improved biocompatibility, lower catalyst content, or even the availability of catalyst free nanotubes. Here we present a fast one-step preparation method that allows the preparation of closed-ended filled MWCNTs. The main asset of the developed protocol is its simplicity in filling and blocking inorganic materials within the cavities of multi-walled carbon nanotubes.

3.2.3.2. Experimental

CVD synthesized multi-walled carbon nanotubes were provided by Thomas Swan Co. Ltd. MWCNTs were grinded for a short amount of time, to avoid the creation of structural defects.[237] Purification of nanotubes was performed by employing three different protocols. The first protocol consists in a direct high temperature annealing in a tubular furnace in a mild-oxidizing steam + argon flow for two hours.[211]

This treatment removes amorphous carbon and graphitic particles which can in turn be coating metal catalyst, allowing further removal of the exposed iron catalyst by using a subsequent acid treatment (reflux in 6M hydrochloric acid, Panreac, at 110 °C), which does not oxidize CNTs. At the same time, during the steam purification, carbon nanotubes are shortened and the ends are opened allowing their subsequent filling with selected materials. The second protocol consist in acid cutting, by using a mixture of concentrated nitric and sulphuric acid (Panreac) in a 1:3 ratio with carbon nanotubes (1 mg/mL concentration) and sonication of the mixture for 24 hours. This treatment cuts the carbon nanotubes and at the same time exposes (oxidizes the graphitic coating) and dissolves some catalyst particles, as described elsewhere.[238] The samples were quenched in water, filtered to remove acid, and neutralized with water. The acid treatment is then followed by an argon + steam treatment in a tubular furnace in order to remove the created carboxylated carbonaceous fragments (CCFs)[239] and further expose catalyst particles that can be removed by means of a hydrochloric acid treatment. The third protocol is a combination of the previous two, that combines an initial steam treatment, followed by HCl, acid cutting performed for 24 hours, and a final steam and HCl treatment.

Due to their hygroscopic properties, inorganic salts, namely samarium(III) chloride, potassium iodide, sodium iodide, gadolinium(III) chloride and barium iodide (Sigma Aldrich), were handled inside a Labconco glove box with an inert argon atmosphere, with below 1 ppm of oxygen and 5 ppm of water. To fill CNTs with the given metal halide, purified carbon nanotubes were mixed with the chosen inorganic salt by grinding them together inside the glovebox. The mixture was then placed into a silica tube, which was sealed by using a vacuum pump, lowered the pressure to around 0.05 mbar inside the silica tube. The resulting ampule was annealed at temperatures in the range between 700 - 1300 °C inside a tubular furnace for 12 hours. The program used for annealing the samples consisted of a heating ramp at 300 °C/h up to

the desired temperature, namely 700, 1000, 1100, 1200 or 1300 °C, keeping this temperature for 12 hours, and cooling down at a set rate of 300 °C/h until room temperature. After cooling the samples, silica tubes were cut, and the collected material was placed into a round bottom flask with 200 mL of water, with an addition of around 10 mL of concentrated hydrochloric acid. The solution was refluxed for about 48 hours, changing the solvent every 24 hours, in order to remove the non-encapsulated external salts from the samples. The sample was collected by filtration, rinsed with water and dried in an oven at about 85 °C.

Thermogravimetric analysis was performed using a TA instrument TGA Q5000-IR in the facilities of MATGAS. The combustion of samples was done in air by using around 5 mg of filled or empty carbon nanotubes in a high temperature 100 µL platinum pan, using a gas flow of 25 mL/min and a heating rate of 10 °C/min.

Inductively coupled plasma (ICP) analysis consisted of two steps, namely the sample combustion and analysis. The combustion was achieved by microwave digestion (Milestone Ethos Plus) of about 5 mg of nanotube sample in a mixture of concentrated nitric acid and hydrogen peroxide at 220 °C. The acquired liquid was diluted with deionized water, and sample duplicates were analyzed. The analysis was performed on Agilent 7500ce Perkin Elmer Elan 6000 ICP-MS or on a Perkin Elmer Optima 3200RL ICP-OES.

Elemental analysis (EA) of carbon nanotubes was performed always on two replicas (around 1 mg per analysis), using an elemental analyzer EA 1108 Instrument by adding vanadium(V) oxide and tin to ease the combustion, and using sulfanilamide as a pattern.

Brunauer-Emmett-Teller (BET) analysis was performed on about 2 mg of empty MWCNTs. These nanotubes were annealed at different temperatures, 900, 1000, 1100, 1200 or 1300 °C under vacuum in a silica tube. After opening of the silica tubes, the nanotubes underwent a treatment of adsorbed gas removal at 300 °C for 15 hours. This was

followed by nitrogen adsorption/desorption in cryo-environment, using liquid nitrogen as adsorbent.

Electron microscopy was performed using a FEI Magellan 400L XHR SEM at 20 keV in transmitted electrons mode using a high angle annular dark field (HAADF) STEM detector and a specially adapted holder was used for sample visualization. Energy dispersive X-Ray (EDX) spectra were acquired using a FEI Tecnai G2 F20 operated at 200 keV and equipped with an EDAX super ultra-thin window (SUTW) X-ray detector. The samples were deposited onto a copper grid coated with a lacey carbon film (Agar Scientific) from a dispersed CNT solution in hexane or o-dichlorobenzene (Sigma Aldrich).

Superconducting Quantum Interference Device (SQUID) measurements, using Quantum design MPMS XL-7T, were performed on carbon nanotubes using 10 K (in liquid nitrogen) under an external DC magnetic field. Hysteresis loops were taken in the range between -50 000 to +50 000 Oe to monitor the catalyst content. CNTs were placed into a gelatin capsule (about 5 mg) and fixed with non-magnetic glass wool to avoid sample movement during the measurement.

3.2.3.3. Results and Discussion

Several purification protocols have been employed on as-received (raw) MWCNTs, with the aim of reducing the amount of catalyst present in the sample. Both the raw starting material of multi-walled carbon nanotubes and the purified samples have been characterized by SQUID and TGA, and the selected ones also with ICP-MS and EA. All the purification processes employed have been proven to be effective in decreasing the catalyst content in carbon nanotube samples (Table 2). The removal of catalyst in samples of single-walled carbon nanotubes by employing similar purification processes (chapter 3.1.) turned out not to be as effective as for multi-walled samples. The catalyst content

is important from the point of view of future applications of the material, since it can dominate the behavior of the sample, such as the electrochemical response[240], or it can also induce oxidative stress or toxicity to cells when employed in the biomedical field.[124-125, 241]

Table 2. Catalyst content in multi-walled carbon nanotube samples determined by SQUID, TGA, ICP-MS and carbon content determined by EA after employing different purification protocols. Steam purification refers to a combined steam + HCl treatment.

Material	*Purification process*	*SQUID/ wt% Fe*	*TGA/ wt% Fe*	*ICP-MS/ ppm Fe*	*EA/ %C*
Raw MWCNTs	None	1.542	2.471	N/A	95.19
Purified MWCNTs (1)	Steam purification	0.002	0.151	179	96.74
Purified MWCNTs (2)	Acid cut + steam purification	0.130	0.788	N/A	N/A
Purified MWCNTs (3)	Steam purification + acid cutting + steam purification	0.002	0.069	265	N/A

The three protocols will lead to samples of opened-ended MWCNTs. The main difference between the purification approaches is in the length of the resulting carbon nanotube materials and catalyst content. Although the length of the different samples has not been determined in the present study, according to previous reports, 24 hours of nitric/sulphuric acid treatment leads to samples of shorter MWCNTs[238] than a 2 hours steam treatment.[211] Note that, since HCl has not been reported to alter the structure of CNTs, no changes are expected in the length distribution of MWCNTs by applying this treatment. Therefore, protocol (1) will result in longer carbon nanotubes, but lower catalyst content compared to protocol (2), while the combination of the two approaches, protocol (3), results in similar catalyst content to protocol (1) and nanotube length more similar to protocol (2) (Table 2). Although the latter approach will lead to samples of short MWCNTs with a very

low amount of catalyst content, it is also the most time consuming of the three investigated protocols.

In order to investigate the role of temperature on the degree of closed-ended MWCNTs, the purified nanotubes prepared by protocol (1) have been annealed at different temperatures, namely 900, 1000, 1100, 1200 and 1300 ˚C. It is known that single-walled carbon nanotubes spontaneously close upon being annealed at temperatures above 700-900 °C.[76] Therefore, the annealing treatment might provide the necessary energy needed to close the ends of multi-walled carbon nanotubes to a certain extent. To assess whether the annealing of MWCNTs at these temperatures had any effect on the closing of their ends, BET analysis was performed on raw and annealed samples (Fig. 20), because opened-ended carbon nanotubes should have a higher surface area compared to their closed-ended analogues due to gas

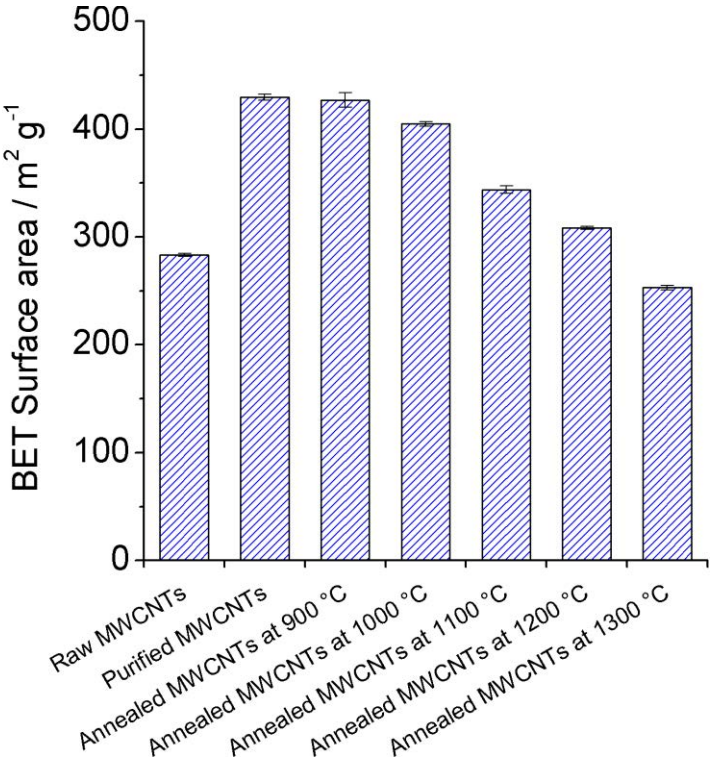

Figure 20. BET surface area determination of raw and steam and HCl purified MWCNTs after being annealed at different temperatures (between 900 - 1300 °C).

adsorption in the inner cavity of the carbon nanotubes. We observed a type IV adsorption isotherm indicating microporous (inner nanotube cavities) and mesoporous (exterior of nanotubes) systems present (Fig. 21). Indeed, pristine raw material comes with mostly closed ends, while the purification has been proven as an efficient method in opening of their extremities.[211] This has also been observed by BET where almost a double-fold increase in the surface area of purified nanotubes was observed, indicating the successful removal of the CNT tips with the employed protocol.

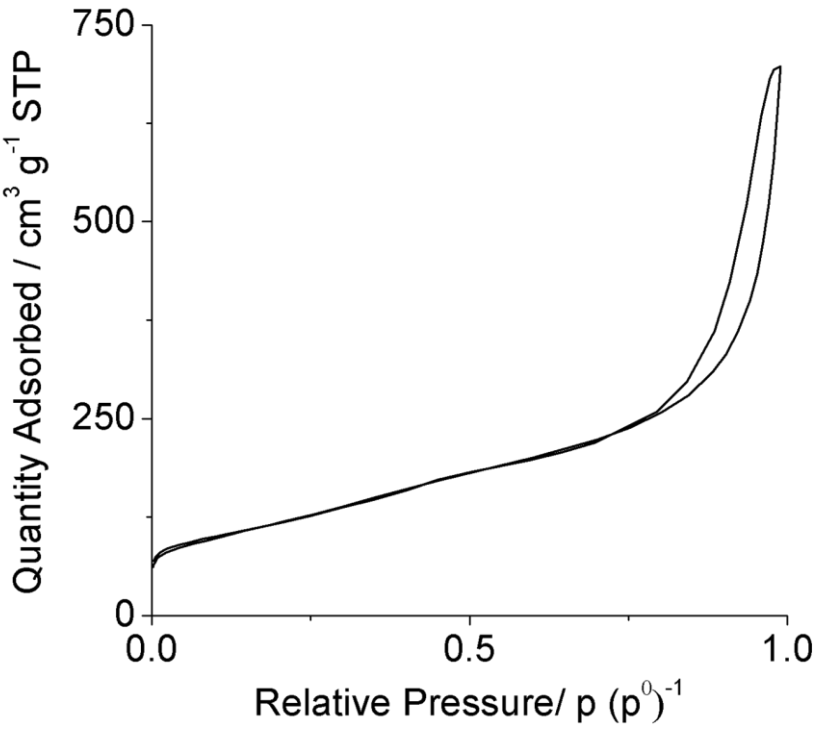

Figure 21. Isotherm curve of steam and HCl purified multi-walled carbon nanotubes.

Discrete Fourier Transformation (DFT) of the collected data reveals the presence of micropores between 3 and 10 nm approximately, corresponding to the CNT inner diameters (Fig. 22). It also indicates the presence of opened-ended MWCNTs already in the as-received material. This pore size allows the quantitative one-layered nitrogen adsorption inside the cavities. The distribution of diameters is being preserved after the purification, but diameters around 1.5 nm are also observed suggesting that the purification treatment is opening some small nanotubes, possibly single-walled carbon nanotubes present as impurities in the sample, that are not present in the open form in the starting pristine material (Fig. 22). The differential pore volume of diameters around 3 nm increases after the purification treatment, suggesting the possible opening of nanotubes that are present in a closed form in the starting material. By annealing the purified material at 900 °C, the fraction of CNTs of about 1.5 nm is no longer detected by DFT, while the observed distribution of diameters between 3 and 10 nm remains unaltered. Probably the 900 °C treatment that is usually used

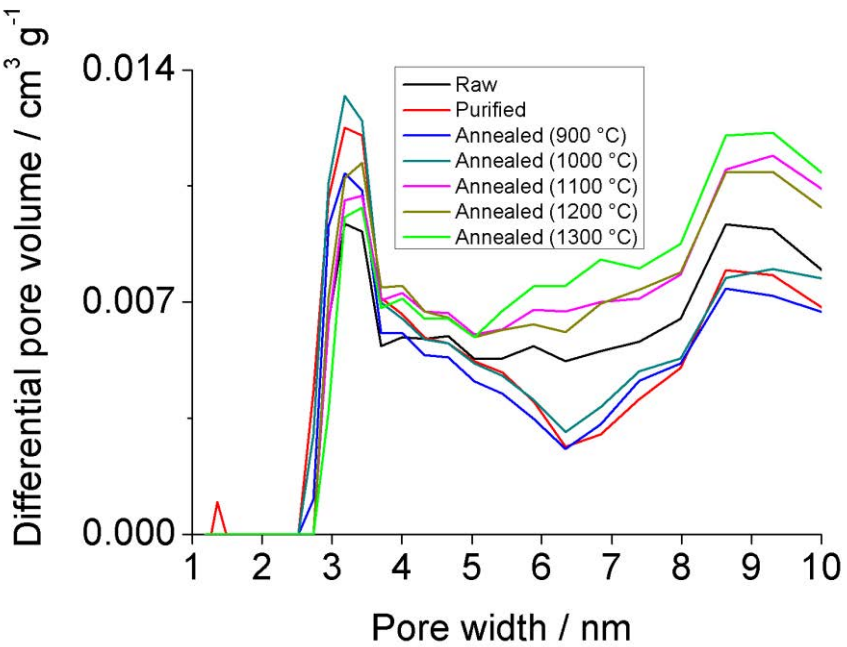

Figure 22. DFT analysis of the obtained BET data; statistical analysis of raw, purified and annealed (previously purified) multi-walled carbon nanotubes at 900, 1000, 1100, 1200 or 1300 °C.

for closing the ends of single-walled carbon nanotubes[76] is sufficient to close nanotubes with small diameters, but has no effect on MWCNTs with inner diameters above 3 nm. By increasing the temperature of the treatment, we observe a continuous decrease in the surface area of the sample, reaching a similar value at 1300 °C like the raw material and with a similar differential pore volume relationship between 3 and 10 nm. A decrease in the surface area is a result of the spontaneous closure of the nanotube ends upon cooling the material that leads to closed-ended multi-walled carbon nanotubes.

Next, we investigated the potential of annealing samples of multi-walled carbon nanotubes at high temperatures to permanently seal materials in their interior. Purified opened-ended MWCNTs were filled with a variety of metal halides by melt filling. Initially both MWCNTs and the selected metal halide were ground together and placed inside a silica tube that was sealed under vacuum in a similar manner that has been employed for the annealing studies performed so far in this section. The mixture was annealed in the range of 1000 °C to 1300 °C since these temperatures have been proven to close the ends of MWCNTs to different degrees. All the investigated metal halides are molten at these temperatures, thus allowing both filling and end-closing of MWCNTs in a single step. Table 3 summarizes the filling experiments that have been performed. To directly visualize the ends of MWCNTs by electron microscopy, nitric/sulphuric acid cut MWCNTs (protocols (2) or (3)) were also employed in this study. After filling the different materials inside multi-walled carbon nanotubes, the resulting samples were properly washed to remove the external, non-encapsulated compounds.

Initially we confirmed that with opened ends present, the material would leak out from the nanotubes during the washing step, leaving them empty. A sample of steam purified opened-ended MWCNTs was filled with NaI at 700 °C. According to the analysis performed so far, at this temperature the ends of the MWCNTs should remain opened. Figure 23 presents T/SEM images of the sample after being filled with

NaI (NaI@MWCNTs). In this imaging modality, the contrast observed is proportional to the atomic number of the elements present; therefore, NaI appears brighter than carbon. As it can be seen in the images a brighter contrast is observed in the inner cavities of the MWCNTs indicating the presence of NaI (Fig. 23A). After extensively washing the opened-ended NaI filled MWCNTs, empty cavities are observed (Fig. 23B). In agreement with BET data, the presence of closed tips could be observed after filling NaI in the cavities of MWCNTs at 1100 °C (Fig. 23C). This suggests the necessity of having closed ends at the tips of filled carbon nanotubes.

Table 3. Filling content of different metal halides in multi-walled carbon nanotubes; after adequate removal of the non-encapsulated material; FY = filling yield.

Filled material	*Temperature of annealing / °C*	*TGA/ wt% FY*	*ICP/ wt% FY*	*EA/ wt% FY*	*Purification process*
KI	1000	13.35	N/A	N/A	(1)
NaI	1100	N/A	N/A	N/A	(1)
$SmCl_3$	1100	15.96	N/A	N/A	(1)
$SmCl_3$	1200	17.51	20.15	18.73	(2)
BaI_2	1200	N/A	N/A	7.53	(2)
$GdCl_3$	1200	28.81	N/A	23.2	(2)
$SmCl_3$	1100	11.33	N/A	N/A	(3)
$SmCl_3$	1200	23.52	N/A	N/A	(3)
$SmCl_3$	1300	N/A	N/A	N/A	(3)

Thereafter, we investigated the role of temperature by filling samarium(III) chloride into MWCNTs ($SmCl_3$@MWCNTs) at 1100, 1200 and 1300 °C for 12 hours. After a subsequent proper washing of the non-encapsulated material, all the samples show the presence of filling inside their cavities by T/SEM analysis (Fig. 24A, B and C respectively). Interestingly, TGA under flowing air shows that the material annealed at 1100 °C has a lower filling yield compared to the sample annealed at

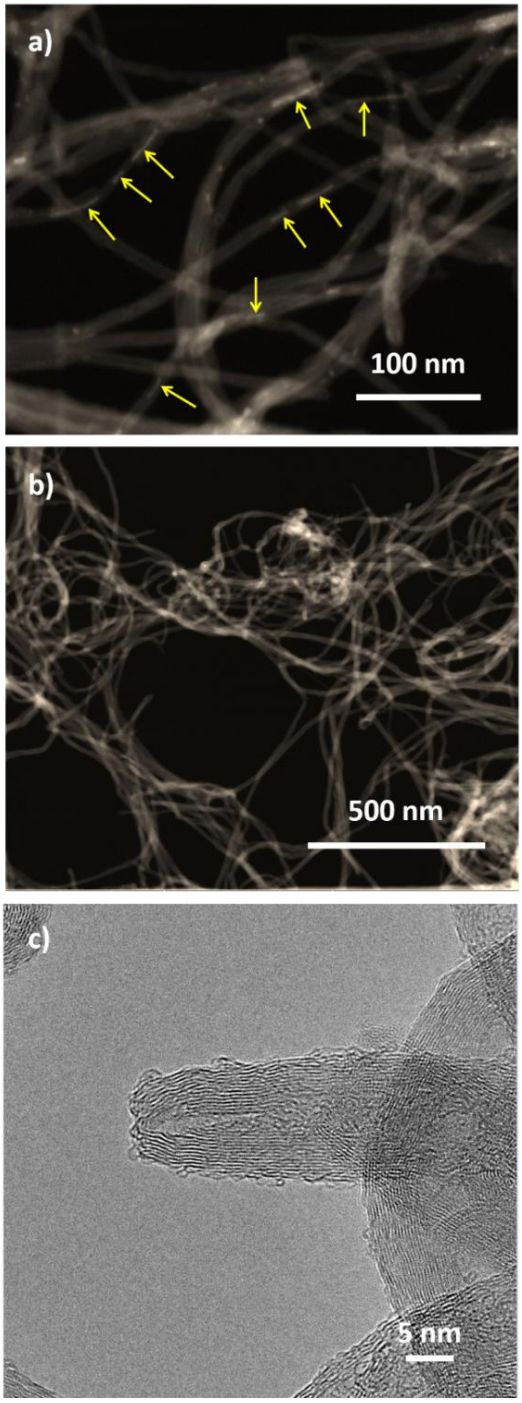

Figure 23. T/SEM images of NaI@MWCNTs; sample annealed at 700 °C showing the presence of filling (a) and the same sample after washing was employed showing empty nanotubes (b); TEM image of NaI@MWCNTs annealed at 1100 °C showing a closed tip (c).

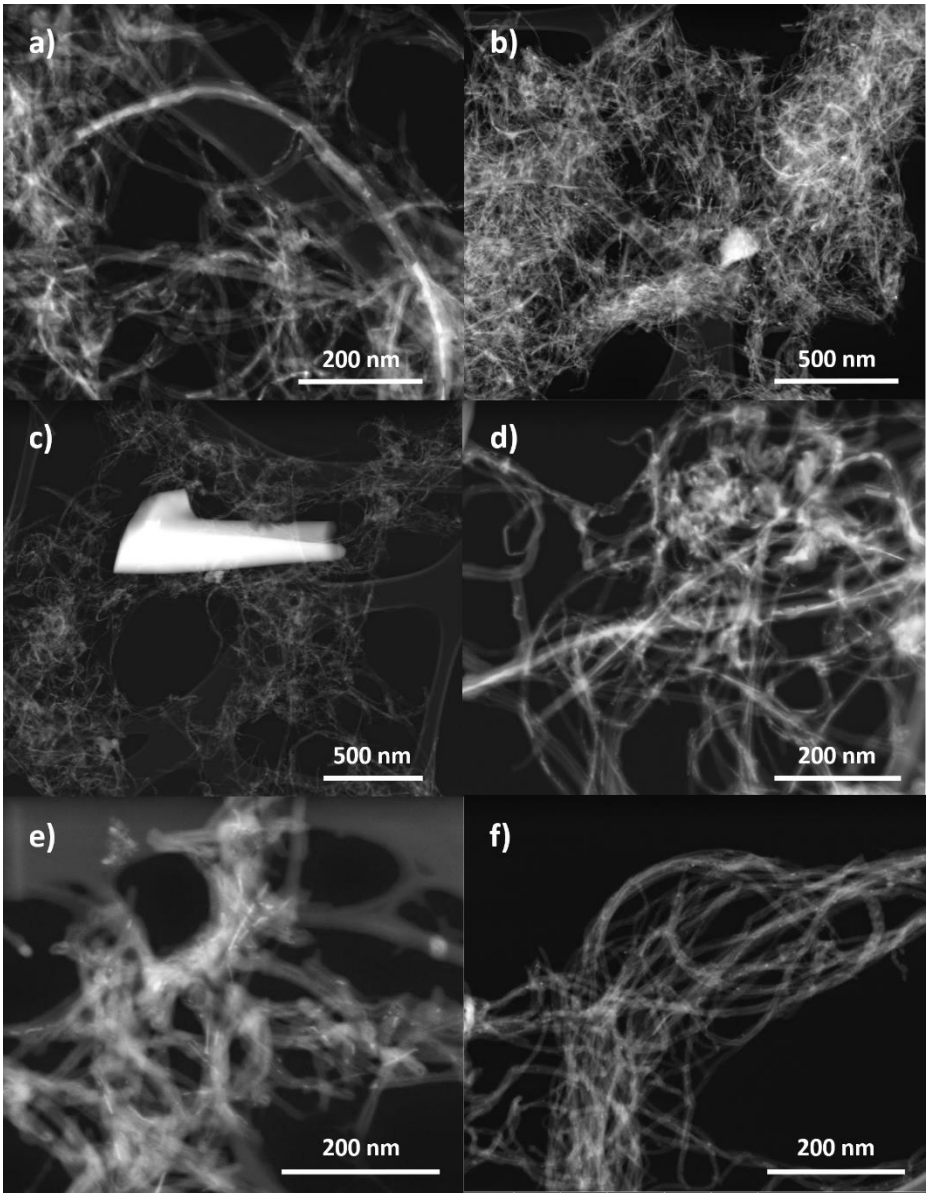

Figure 24. T/SEM images of different filled multi-walled carbon nanotubes; $SmCl_3$@MWCNTs samples prepared by annealing at 1100 ºC(a), 1200 ºC(b) and 1300 ºC (c) and $GdCl_3$@MWCNTs at 1200 ºC (d), BaI_2@MWCNTs at 1200 ºC (e) and NaI@MWCNTs at 1100 ºC (f) showing the presence of filled material after washing of the sample.

1200 °C (11.3 wt.% vs 23.5 wt.%). This is in agreement with BET data that reveals a higher degree of closed ends at 1200 °C than at 1100 °C. Even if the amount of filled tubes was the same at both temperatures, more material would be removed from the inner cavities of opened-ended nanotubes by washing the sample annealed at 1100 °C. The filling yield was determined from by TGA using a previously reported equation developed for filled single-walled carbon nanotubes.[242]

Important to notice is the presence of silica particles, or even chunks in the sample annealed at 1300 °C (Fig. 24C), probably due to the recrystallization of silica upon cooling that might result in the introduction of silica impurities, from the inner wall of the ampoule, into the sample. Actually, the silica ampoule loses its transparency and becomes white after annealing at 1300 °C. Therefore, this sample has not been analyzed by TGA since the resulting residue after the complete oxidation of the sample would include a false positive portion coming from silica particles. From the filling experiments performed so far it becomes clear that the range of 1000 °C - 1200 °C is the most interesting to achieve samples of closed-ended MWCNTs with inner cavities of 3 to 10 nm.

To show the versatility of the one step filling-closing protocol, apart from NaI and $SmCl_3$, additional materials (KI, BaI_2 $GdCl_3$), were also filled in this range of temperatures, with special emphasis on 1200 °C. As mentioned, a summary of the prepared samples is presented in Table 3. After the annealing step, each of the samples was washed to remove the material external to the carbon nanotube walls. Important to notice is that, in contrast to single-walled carbon nanotubes (section 3.2.2.) only few washing steps were necessary to remove the non-encapsulated material from samples of multi-walled carbon nanotubes. This implies that the synthesis process to achieve clean samples of filled carbon nanotubes is faster for multi-walled than for their single-walled counterparts. Samples were characterized by T/SEM to confirm the successful encapsulation of the chosen compounds, and by TGA to determine the filling yield. Alternatively, the filling yield can also be

quantified by ICP analysis, and indirectly by EA assuming that the non-carbon portion arises from the filled material and iron catalyst (content known in the purified samples).

Scanning electron microscopy (SEM) in transmission mode (T/SEM) reveals the presence of the filled material inside the cavities of the carbon nanotubes and absence of external salts (Fig. 24D, E, F). Different degrees of filling can be observed in the images, related to the material and temperature employed for the synthesis.

Samarium(III) chloride filled multi-walled carbon nanotubes annealed at 1200 °C were analyzed by high-resolution transmission electron microscopy to determine whether the tips of the CNTs were opened or closed. Figure 25A is shows an individual nanotube with both ends being closed and the presence of material confined inside the cavity. This is a direct proof of the closure of both ends after annealing, which will prevent the release of the encapsulated compound during the washing protocol. Remarkably, we also observed the creation of smaller carbon compartments within the inner cavities of the nanotube. Figure 25C shows an individual nanotube with material confined in two different compartments separated by carbon layers, which structure resembles the bamboo type carbon nanotubes. We argue that thermal annealing can lead to not only the closure of the tips, but also to the coalescence of the inner walls within the nanotube due to the presence of structural defects in their interior. This is interesting since we can envisage for instance the confinement of two or more different materials within the same carbon nanotube.

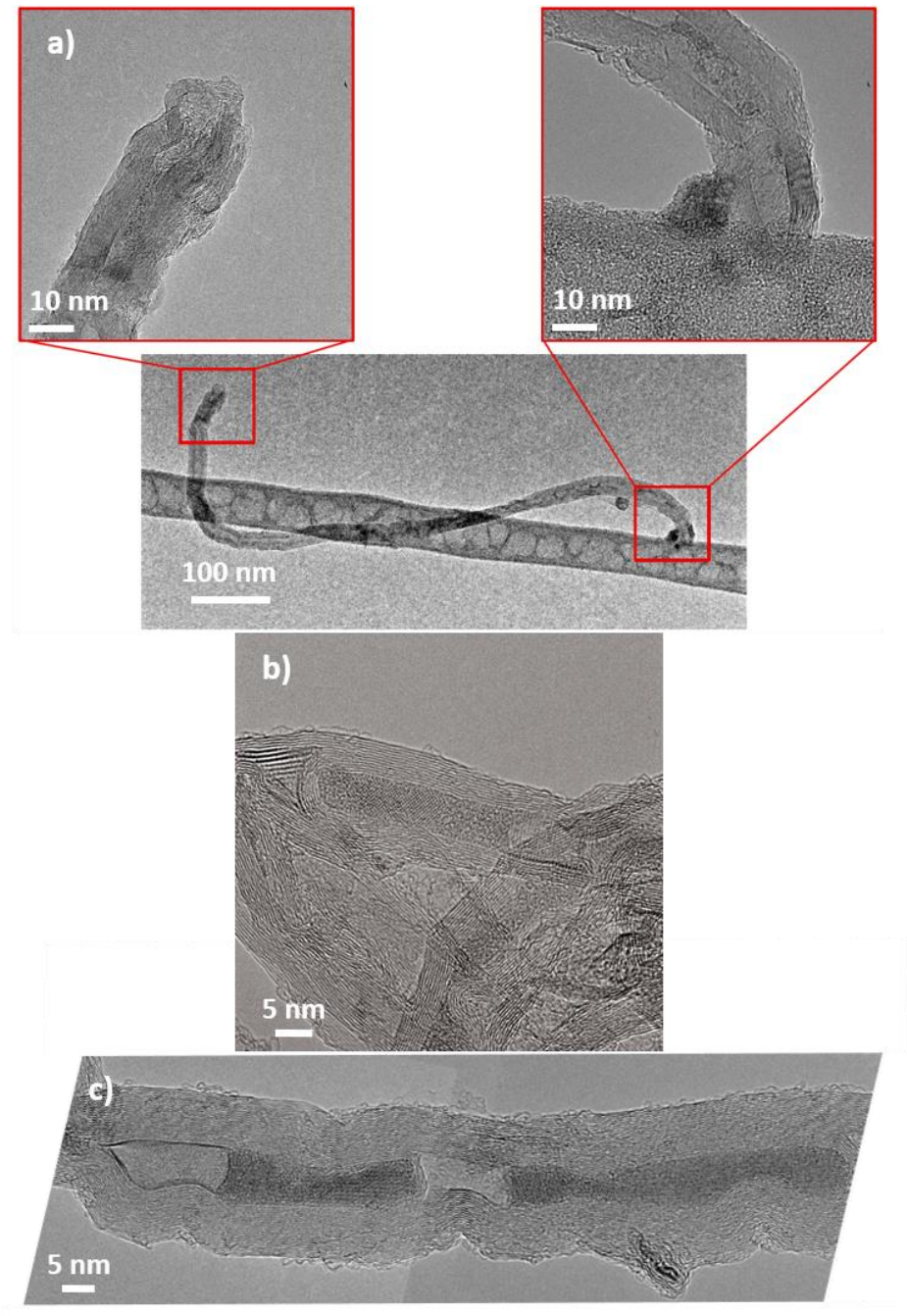

Figure 25. TEM images of $SmCl_3$ filled multi-walled carbon nanotubes ($SmCl_3$@MWCNTs); annealed at 1200 ºC showing the filling and both ends being closed (a), a closed tip (b) and filling in different compartments (c).

To complete the study, we measured the amount of filled and empty carbon nanotubes present in a sample of $SmCl_3$@MWCNTs prepared at 1200 °C with respect to their diameter. This study was performed by Elzbieta Pach from the Catalan Institute of Nanoscience and Nanotechnology (ICN2). From about 200 nanotubes that were analyzed, 50% of them turned out to be filled, while the other 50% remained empty. The diameter distribution determined by TEM is consistent with the BET data, showing the major fraction of both filled and empty nanotubes between 4 and 7 nm (Fig. 26). It is worth noting that the amount of filled MWCNTs is slightly higher than the empty ones for small diameters (2-5 nm). With the increase of the inner cavity of MWCNTs (6 nm and above), this trend is inversed and the fraction of empty tubes becomes slightly higher than the filled ones. This suggests that bigger nanotubes are not closed enough to confine the material in their interior that gets removed during the washing step. Therefore, more energy would be needed to increase the amount of closed MWCNTs with large diameters.

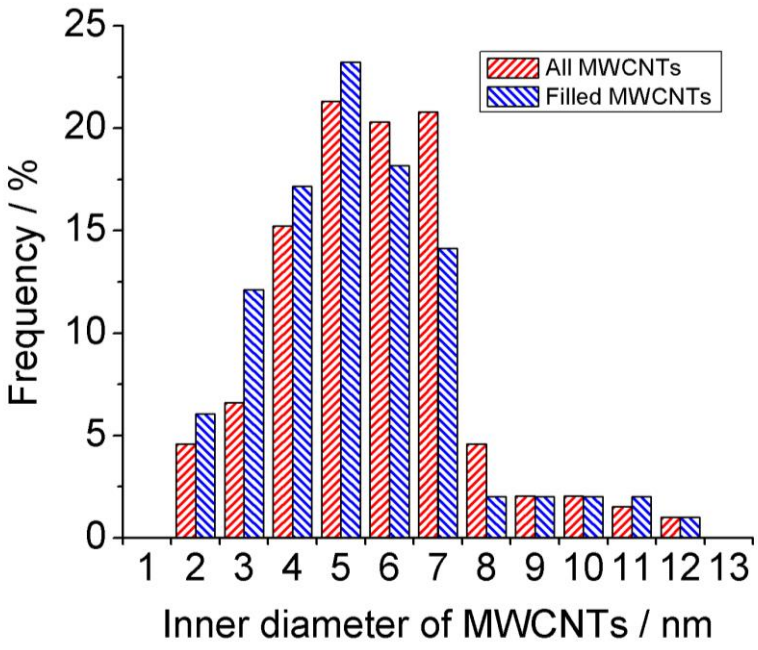

Figure 26. Frequency of filled and both filled and empty (all) multi-walled carbon nanotubes in a sample of $SmCl_3$@MWCNTs prepared at 1200 °C with respect to the nanotube inner diameter measured from TEM images.

3.2.3.4. Conclusion

Thermal post-synthetic closure of the extremities of MWCNTs leads to the creation of multi-walled carbon nanocapsules that can contain a wide variety of materials in their interior. BET, SEM and TEM analyses of the prepared materials suggest a spontaneous closure of the tips of MWCNTs to a certain extent after being annealed at or above 1000 °C. Filling MWCNTs at 1200 °C turned out to be the most suitable temperature in preparing samples of closed-ended filled carbon nanotubes clean from external, non-encapsulated material. Once the MWCNTs are filled, the non-encapsulated compounds can easily be removed in a faster manner than what has been reported for samples of SWCNTs. The present one-step filling and end-closing protocol is highly versatile, provided that the material to be encapsulated is stable in the molten state at this range of temperatures (1000 - 1200 °C), and does not react with the carbon nanotubes.

3.2.4. Biomedical Study of Filled Multi-Walled Carbon Nanotubes In-Vitro

3.2.4.1. Introduction

The most promising application of filled carbon nanotubes is in the biomedical field. Nanotubes filled with many different drug molecules have been proven to be more effective in different therapeutic applications compared to free drugs alone.[31] Of course, targeting and on-demand release of the drug can also be achieved using carbon nanotubes, something that is usually not possible with free drugs. Apart from that, filled nanotubes have been successfully used as contrast agents in biomedical diagnostics. The biggest obstacle in the application of nanotubes in nanomedicine is their toxicity. Toxicity of carbon nanotubes in the biological media has been reported. However, this can be overcome by using functionalized and shortened carbon nanotubes, ensuring the bio-friendliness of the material. It is necessary to study the behavior of each and every synthesized nanomaterial in the biological milieu in order to assess its toxicological behavior. For sure, many successful functionalized systems based on CNTs have already been developed.[31, 243-245] However, the full potential of carbon nanotubes that were both exohedrally and endohedrally functionalized was presented back in 2010 for single-walled carbon nanotubes.[185] In that initial study, radioactive sodium iodide was used for imaging purposes in-vivo. This led us to believe that multi-walled nanotubes could be used for the same purpose which as mentioned can accommodate even more material in their cavities, and can more easily be dispersed. To date, there are only a few papers dealing with filled MWCNTs with salts for in-vitro and in-vivo studies.[246-247]

In this work, empty and filled multi-walled carbon nanotubes with non-radioactive material were used for in-vitro studies on the cytotoxicity of

the conjugate on cancer or immortalized cells, keeping in mind that free salts could be potentially hazardous to biological material.[248] Different gadolinium-containing nanotube systems have been already developed[31, 249], as gadolinium is one of the best contrast agents for magnetic resonance imaging (MRI). Therefore, the focus of the present study is on gadolinium and iodide filled multi-walled carbon nanotubes, allowing room for future use of the system with radioactive material and in-vivo studies.

This work has been performed during a three months long research stay at the University of Manchester, Faculty of Medical and Human Sciences, in the Nanomedicine lab of Prof. Kostas Kostarelos, under the close supervision of Dr. Sandra Vranić.

3.2.3.2. Experimental

Empty multi-walled carbon nanotubes, provided by Thomas Swan Co. Ltd., were grinded with a pestle in an agate mortar, and acid cut following the purification protocol from section 3.2.3., consisting of a combined acid and steam treatment. Briefly, as-received MWCNTs were initially treated using a mixture of nitric and sulphuric acid in a 1:3 ratio, with a concentration of 1 mg/mL of CNTs in the acid mixture. The mixture was sonicated for 24 hours, quenched with water and the acid was removed by filtration. An additional argon/steam treatment was used to remove the newly formed functional groups by the acid treatment, and to further remove the graphitic particles that coat the iron catalyst, which was then removed by an HCl treatment. Gadolinium(III) chloride filled multi-walled nanotubes were prepared by mixing and grinding the mixture of nanotubes with the salt until a homogeneous mixture was achieved inside an Ar filled glovebox. The material was vacuum sealed in a silica tube and annealed at high

temperature in an oven, at 1200 °C for 12 hours, as established in the previous section, to achieve samples of closed-ended filled MWCNTs. The content of the silica tube was placed in water and properly washed, with the addition of about 10 mL of concentrated hydrochloric acid to 200 mL of water. The mixture was refluxed for about 48 hours, changing the used solvent every 24 hours, in order to remove the non-encapsulated external material from the sample. The sample was dried in a drying oven at about 85 °C. The same filling protocol was employed for sodium iodide, but the sample was annealed at 1000 °C for 12 hours. A lower temperature was employed because NaI is a highly volatile material.

Human epithelial bronchial immortalized cells (BEAS-2B, ATCC, CRL-9609) were maintained in an RPMI 1640 media containing glutamine (Sigma Aldrich) supplemented with 10% fetal bovine serum (FBS, Thermo Scientific), 50 µg/mL Penicillin, 50 µg/mL Streptomycin (Sigma Aldrich) at 37°C in 5% CO_2. Similarly, human epithelial breast cancer cells (MCF-7, ATCC, HTB-22) were maintained in an EMEM media (Sigma Aldrich) supplemented with 10 % FBS, 50 µg/mL Penicillin, 50 µg/mL Streptomycin at 37 °C in 5% CO_2. Both BEAS-2B and MCF-7 cells were passaged twice a week using Trypsin-EDTA 0.05%, at 80% confluence, whose activity was stopped using 10 % FBS.

Cells were seeded in 96 for LDH (lactate dehydrogenase) release studies, 12 for FACS (fluorescence-activated cell sorting, flow cytometry) analysis or 6 for ImageStream studies well-plates, and treated at about 80 % confluence. The treatments were carried out in the cell culture medium without FBS, while a 10 % FBS solution was added to each well 4 hours after the treatment. The treatment engaged the usage of empty multi-walled nanotubes, sodium iodide or gadolinium(III) chloride filled multi-walled nanotubes that were dispersed in the cell culture media, depending on the cell line, up to 0.5 mg/mL. The sonication of the material in the cell culture media ensured the suitable dispersion for the study after 5 minutes of sonication. The sonicated material was then diluted with the cell culture media of

interest and cells were exposed for 24 hours to different concentrations of the material, ranging from 12.5 and 100 µg/mL.

LDH assays are used for cytotoxicity studies. However, due to the possible interactions between carbonaceous material with the assay itself, the test was modified, and we measured cell survival rate in contrast to cell death.[250] The media was removed and cells were treated with 100 µL of lysis buffer for 45 min at 37 °C. This resulted in cell lysates formation, which were then centrifuged at 4000 rpm for 20 min with the aim of separation of the material. 50 µL of the supernatant was mixed with 50 µL of LDH substrate mix (Promega) in a new 96-well plate and incubated for 15 min at room temperature, followed by the addition of 50 µL stop solution. This was followed by a colorimetric analysis by reading the absorbance of every plate at 490 nm. The percentage of survival can be estimated as follows:

$$Survival\% = \left(\frac{A_{490} treated\ cells}{A_{490} untreated\ cells}\right) \times 100$$

After treating cells for 24 h with the nanomaterial, supernatants were removed and cells washed three times with PBS containing Ca^{2+} and Mg^{2+} ions (Sigma Aldrich). Cells were then treated with Trypsin-EDTA 0.05% for 5 minutes to detach them from the plates, merged with the corresponding supernatants and centrifuged for 5 min at 1500 rpm. This was followed by the re-suspension in 100 µL Annexin binding buffer (Thermo Fisher Scientific) and staining of the cells with 2 µL Annexin V-Alexa Fluor®488 conjugate for 20 min at 15–25 °C. Propidium iodide (1 mg/mL, Sigma) was added shortly before the analysis to the final concentration of 1.5 µg/mL. The analyses of these cells were performed by Dr. Vranić, on a BD FACSVerseTM flow cytometer (488 nm excitation) focusing on Annexin V and PI detection at 515 and/or 615 nm. 10000 cells were used per measurement and the material without cells was used to set up the gates for the analysis.

Imagestream analysis was used to verify the uptake of nanotubes inside the cells and was also performed by Dr. Vranić. Same as the previous

analysis, after treating cells with the nanomaterial, cells were washed with PBS Ca^{2+}/Mg^{2+} and cells were harvested. The cell suspension was centrifuged for 5 min at 1500 rpm at 4°C and the pellet was re-suspended in 500 µL of 4% para-formaldehyde (PFA, Thermo Fischer). After 20 min of incubation in PFA, cells were rinsed three times with PBS and finally resuspended in 50 µL of PBS. At least 2500 cells were analyzed using Amnis ImageStreamx platform (Amnis ImageStream MKII, Millipore) and InspireTM system software (Amnis). Camera magnification was 60x, 785 nm excitation laser was set at 0.02 mW. Images were acquired with a normal depth of field, providing a cross-sectional image of the cell with a 2.5 µm depth of focus. A mask representing the whole cell was defined by the bright-field image. An internal mask was defined by eroding the whole cell mask for 6 pixels (equivalent to 3 µm, as the size of 1 pixel is 0.5 µm) in order to eliminate the signal coming from the NPs attached to the cell surface. The results were analyzed by IDEAS software (Amnis). Values of the internalization score and mean side scatter intensity were calculated for at least 500 cells per sample.

3.2.4.3. Results and discussion

As discussed earlier, the lack of cytotoxicity of a nanomaterial is the first condition that has to be fulfilled for successful biomedical applications. Therefore, we studied the effect of either empty and filled multi-walled carbon nanotubes on both MCF-7 and BEAS-2B cell lines after 24 hours of exposure. A modified LDH assay was developed to avoid possible interferences of the reagents and carbon nanotubes.[250] No cytotoxic effect of carbon nanotubes on cell survival rate was observed, for all studied concentrations of carbon nanotubes (*N*=6, Fig. 27). FACS was used to verify the results obtained by LDH. Carbon nanotube treated

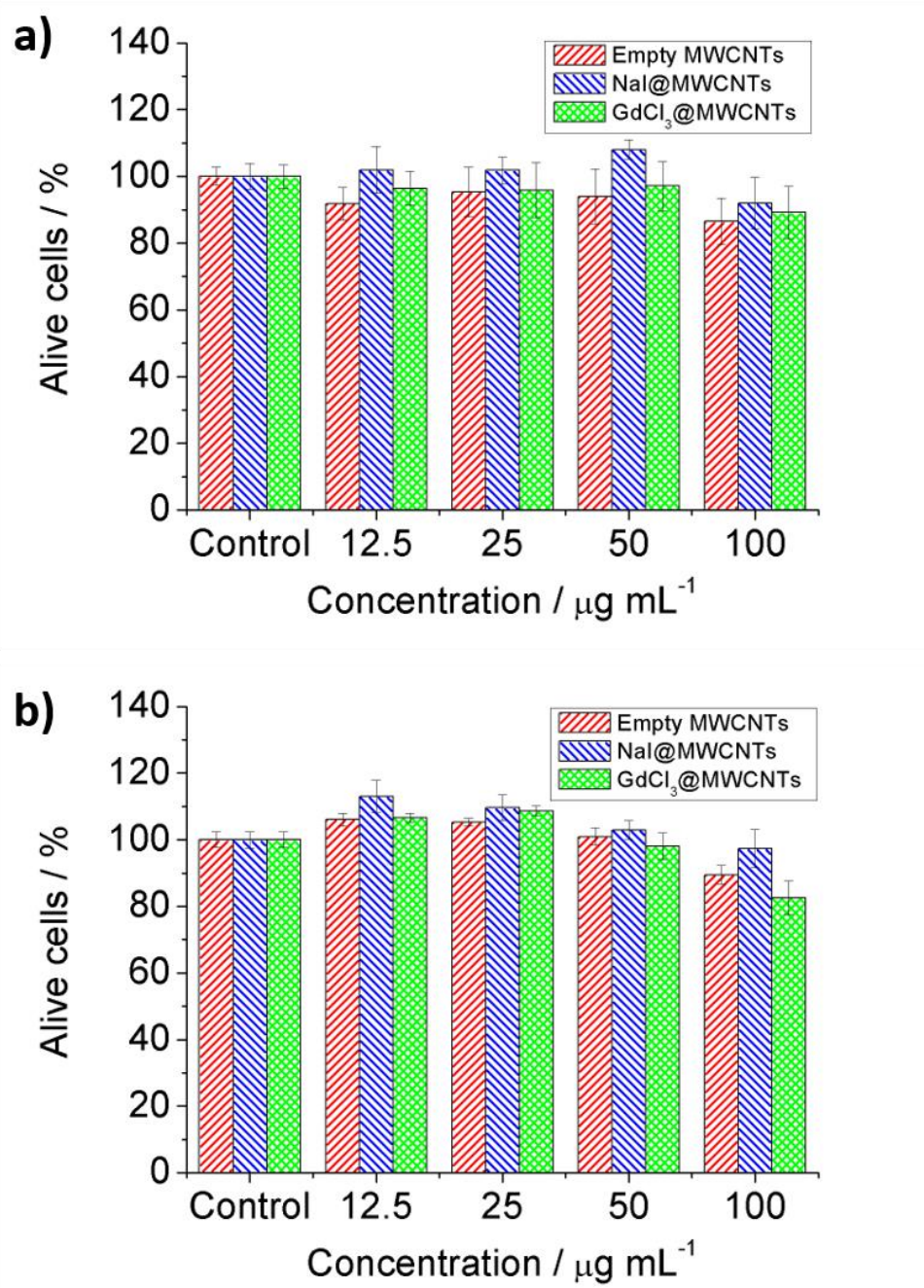

Figure 27. Cytotoxicity studies with the modified LDH assay; analysis for both MCF-7 (a) and BEAS-2B (b) cell lines after 24 hours of exposure to empty multi-walled carbon nanotubes (MWCNTs), sodium iodide filled MWCNTs (NaI@MWCNTs) and gadolinium(III) chloride filled MWCNTs ($GdCl_3$@MWCNTs).

cells were stained with cellular markers for apoptosis and necrosis (Annexin V and propidium iodide respectively). Depending on the response of the cells, we gated healthy (P18), early apoptotic (P19), late apoptotic/necrotic (P17) and necrotic cells (P16). Again, no cytotoxic response was observed, even for cells treated with the highest dose of nanotubes (*N*=3, Fig. 28).

The uptake of carbon nanotubes by cells is another criterion that has to be met if successful applications in the biomedical context are expected. Cellular uptake has been observed for different cell types before[251], as the nanomaterial exhibits needle-like structure that allows both passive penetration and active internalization.[252] Multi-walled nanotubes are more flexible comparing to their single-walled counterparts,[27-28] which makes them more favorable for biomedical applications.

Imaging flow cytometry was used to assess the uptake of carbon nanotubes by MCF-7 cells after 24 hours. Imaging by high-resolution microscopy not only enables the visualization and analysis of cells in the flow, but also of carbon nanotubes as they absorb light and appear as black spots when using the bright-field mode (Fig. 29A). This allows the determination of the location of the carbon nanotubes with respect to cells. We can therefore discern between carbon nanotubes that are found inside or outside the cell membrane. This can be achieved by applying an eroded mask on the image of the whole cell, allowing to evaluate the cellular uptake of the material.[253-256] Mean pixel intensity inside the eroded mask was calculated, by which we determined the cellular uptake of both empty and filled carbon nanotubes (with either NaI or $GdCl_3$) in a dose-dependent manner. With the increase of the concentration of the material, an increase of the mean pixel intensity was observed suggesting a higher cellular uptake of either empty or filled carbon nanotubes (*N*=3, Fig. 29B).

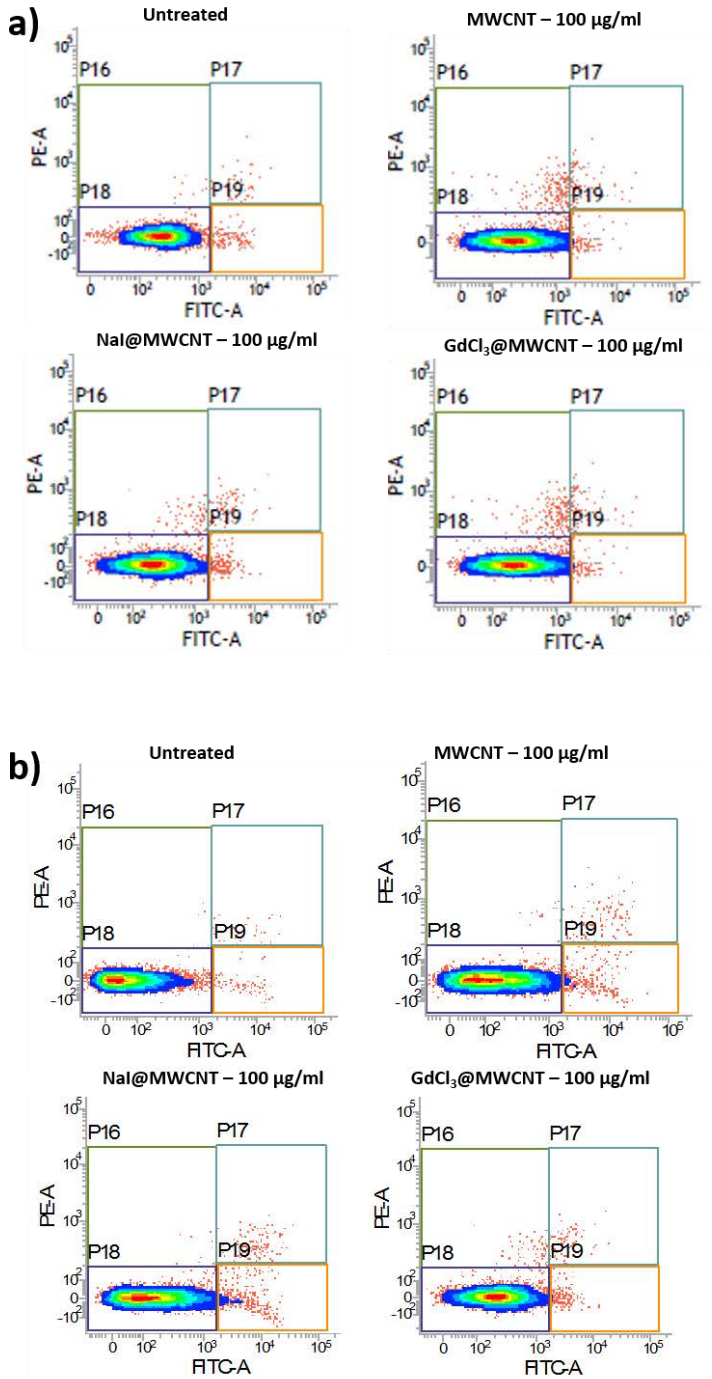

Figure 28. Cytotoxicity studies by flow cytometry; analysis done using Annexin V/PI staining after 24 hours of exposure to the highest concentration of empty and filled (NaI or $GdCl_3$) multi-walled carbon nanotubes, for both MCF-7 (a) and BEAS-2B (b) cell lines. Represented are alive cells (P18), early apoptotic (P19), late apoptotic and/or necrotic (P17) and necrotic cells (P16).

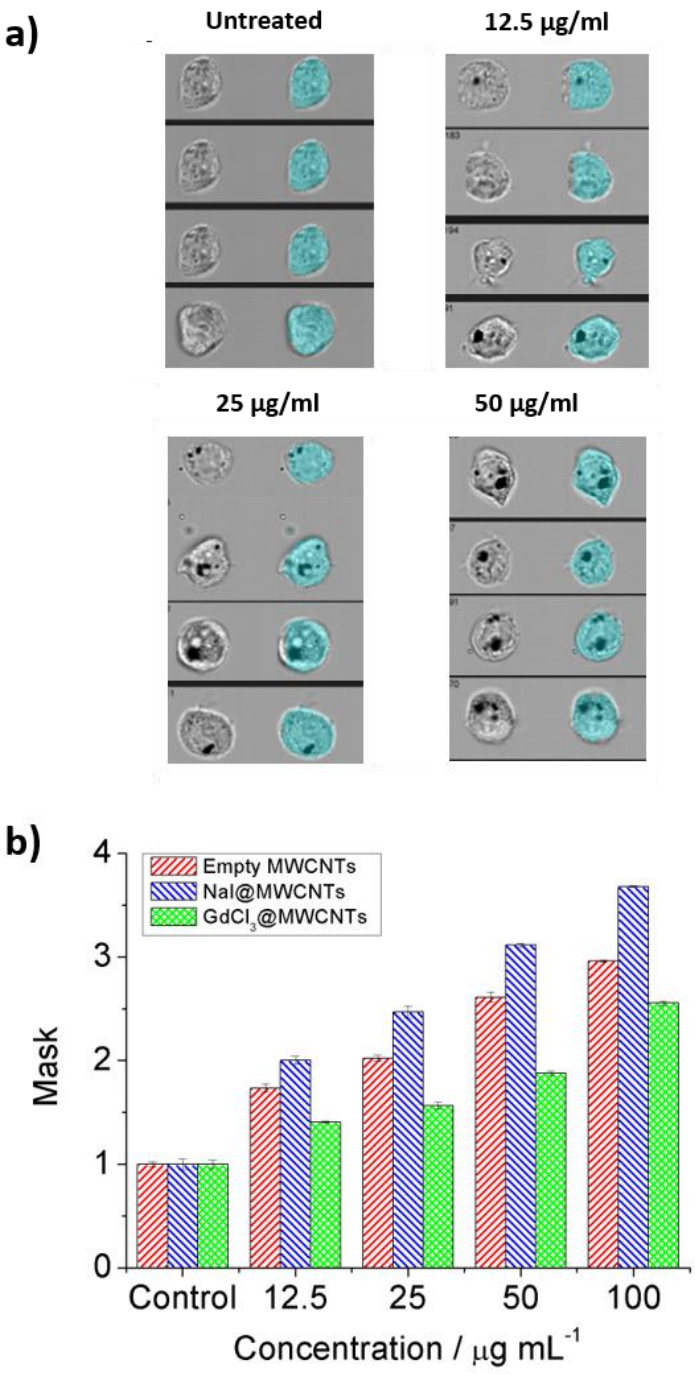

Figure 29. Uptake study of filled (NaI or $GdCl_3$) and empty multi-walled carbon nanotubes; images of MCF-7 cells exposed to carbon nanotubes after 24 hours, where the left column for each employed concentration corresponds to cells in bright-field mode, while the right one corresponds to bright-field merged with the eroded mask (a) and normalized pixel intensity values inside the eroded mask (b).

3.2.4.4. Conclusion

In-vitro studies by both modified LDH assay and FACS have confirmed that empty and filled multi-walled nanotubes, with NaI or $GdCl_3$, did not induce any significant cytotoxic response in MCF-7 human epithelial breast cancer and BEAS-2B human epithelial bronchial cell lines. Keeping in mind the potential hazardous properties of water soluble salts to cells, such as that of gadolinium(III) chloride, it is safe to assume that carbon nanotubes can serve as nano-carriers to isolate biomedically-relevant materials in their interior, thus preventing their interaction with the biological milieu. In this way, any potential cytotoxic effect of the salts is prevented. Overall, the biocompatibility studies performed on both empty and filled carbon nanotubes in-vitro, showed that these nano-construct did not induce cellular death after being internalized by the cells. Therefore, the developed nano-carriers based on filled multi-walled carbon nanotubes hold interest for biomedical diagnosis and therapy.

4. CONCLUSIONS

4.1. Conclusions

We have investigated the role of different parameters employed for the thermogravimetric analysis of carbon nanotubes. Variations on the gas flow rate turned out to have a higher influence on the resulting TGA curve compared to sample mass and heating rate. The combustion temperature for the analyzed single-walled carbon nanotubes falls in the range between 480 and 770 °C, depending on the parameters employed for the analysis. Therefore, these employed parameters ought to be standardized, or at least stated in any report. We suggest the use of the following analysis parameters: sample mass between 2 and 10 mg, gas flow rate between 25 and 100 mL/min and heating rate of 10 °C/min for single-walled carbon nanotubes. This will lead to potentially unified results and accuracy when comparing data.

Multiple purification treatments, with a combined steam and hydrochloric acid protocol, proved to be more efficient in the removal of impurities on single-walled carbon nanotubes than an individual treatment for the same total amount of steam purification time. The catalyst content can be lowered down to around 0.2 wt% of iron with the multiple employed purification treatment. We have developed a fast and simple UV-Vis protocol that allows the determination of the iron catalyst content in samples of carbon nanotubes. The developed protocol requires the complete combustion of the sample and dissolution of the remaining solid residue in HCl. Analysis by UV-Vis of the resulting solution provides a more reliable quantification of the catalyst content than TGA, and is in good agreement with SQUID data, which to date has been reported as the best method for the determination of the catalyst content. UV-Vis spectroscopy is a relatively simple, economic and fast technique accessible to most laboratories.

Dry samarium(III) chloride has been synthesized from samarium(III) oxide by a direct controlled annealing method. Analysis of the prepared material by synchrotron X-ray powder diffraction verified the presence of dry samarium(III) chloride and the absence of impurities. The synthesized dry samarium(III) chloride can be filled into carbon nanotubes by the molten phase method in a high yield. This is important for future radioactive-based carbon nanotube theranostic applications, since samarium in its radioactive form is currently being employed in the clinic. The amount of loaded material surpasses the currently reported amounts of radio-labeled nanotubes, which should potentially lead to higher activities of the radioactive-loaded nanotubes.

We have developed a method that allows monitoring the removal of the non-encapsulated material that remains external to filled carbon nanotubes after the filling experiment. The amount of external samarium chloride that is removed from samples of $SmCl_3$ filled single-walled nanotubes can be determined by UV-Vis analysis of the filtrate collected after each washing step (after forming a complex with CPC and CAS which is added to the filtrate). This has allowed to determine the optimal parameters for a fast and efficient removal of the non-encapsulated material from a sample of 150 mg, namely 1 hour of stirring at 80 °C in 50 mL of water, with 5 minutes of sonication between each washing step. This is important not only for radioactive-based carbon nanotube composites, where reduction of time is a must, but also for the development of other carbon nanotube systems with different payloads that will not necessarily require the complexation of the payload for its assessment.

Analyses of thermally annealed open-ended multi-walled carbon nanotubes by BET, SEM and TEM, suggests the spontaneous closure of the extremities in the range of 1000 °C - 1300 °C (under vacuum), probably upon cooling down of the sample. Molten phase filling proved to be successful for different materials in this range of temperatures, making this a versatile protocol for the synthesis of closed-ended filled multi-walled carbon nanotubes. Since multi-walled carbon nanotubes

have bigger cavities compared to their single-walled counterparts, they arise as ideal candidates for biomedical studies as more active material can fit inside their cavities.

Empty and filled multi-walled carbon nanotubes, with either sodium iodide or gadolinium(III) chloride, were used to assess their cytotoxicity and intake by human epithelial bronchial immortalized cells (BEAS-2B) and human epithelial breast cancer cells (MCF-7). Both LDH and FACS confirmed that the nanomaterial did not induce any significant cytotoxic response in both cell lines. Furthermore, the intake of the material by MCF-7 cells, studied by Imagestream, was confirmed. Altogether, this suggests the internalization of the material with no cellular death, making the developed constructs interesting in further in-vivo tests.

Overall, purification, filling and washing processes of carbon nanotubes, have been optimized, using 'cold' non-radioactive payloads as model compounds for their radioactive analogues. The prepared materials have shown no cytotoxicity and cellular uptake. These studies pave the way for an optimal production of 'hot' radioactive-filled carbon nanotubes for biomedical diagnosis and therapy.

5. REFERENCES

5.1. References

1. Novoselov, K. S.; Geim, A. K.; Morozov, S. V.; Jiang, D.; Zhang, Y.; Dubonos, S. V.; Grigorieva, I. V.; Firsov, A. A., *Science* **2004**, *306*, 666-9.
2. Geim, A. K.; Novoselov, K. S., *Nature Materials* **2007**, *6*, 183-191.
3. Lee, C.; Wei, X.; Kysar, J. W.; Hone, J., *Science* **2008**, *321*, 385.
4. Chen, S.; Wu, Q.; Mishra, C.; Kang, J.; Zhang, H.; Cho, K.; Cai, W.; Balandin, A. A.; Ruoff, R. S., *Nature Matererials* **2012**, *11*, 203-207.
5. Cai, W.; Moore, A. L.; Zhu, Y.; Li, X.; Chen, S.; Shi, L.; Ruoff, R. S., *Nano Letters* **2010**, *10*, 1645-1651.
6. Kroto, H. W.; Heath, J. R.; O'Brien, S. C.; Curl, R. F.; Smalley, R. E., *Nature* **1985**, *318*, 162-163.
7. Foldvari, M.; Bagonluri, M., *Nanomedicine* **2008**, *4*, 183-200.
8. Catherine, J.; Matthieu, P.; Vincent, J., *Nanotechnology* **2012**, *23*, 142001.
9. Hou, P.-X.; Liu, C.; Cheng, H.-M., *Carbon* **2008**, *46*, 2003-2025.
10. Iijima, S., *Nature* **1991**, *354*, 56-58.
11. Iijima, S.; Ichihashi, T., *Nature* **1993**, *363*, 603-605.
12. Bacon, R.; Bowman, J., *Bulletin of the American Physical Society* **1957**, *2*, 131.
13. Monthioux, M.; Kuznetsov, V. L., *Carbon* **2006**, *44*, 1621-1623.
14. Radushkevich, L. V.; Lukyanovich, V. M., *Zum Fisic Chim* **1952**, *26*, 88-95.
15. Hillert, M.; Lange, N., *Zeitschrift für Kristallographie* **1958**, *111*, 24-34.
16. Boehm, H. P., *Carbon* **1973**, *11*, 583-590.
17. Bollmann, W.; Spreadborough, J., *Nature* **1960**, *186*, 29-30.
18. Lieberman, M. L.; Hills, C. R.; Miglionico, C. J., *Carbon* **1971**, *9*, 633-635.
19. Oberlin, A.; Endo, M.; Koyama, T., *Journal of Crystal Growth* **1976**, *32*, 335-349.
20. Esquivel, E. V.; Murr, L. E., *Materials Characterization* **2004**, *52*, 15-25.
21. Bang, J. J.; Guerrero, P. A.; Lopez, D. A.; Murr, L. E.; Esquivel, E. V., *Journal of Nanoscience and Nanotechnology* **2004**, *4*, 716-718.

22. Murr, L. E.; Bang, J. J.; Lopez, D. A.; Guerrero, P. A.; Esquivel, E. V.; Choudhuri, A. R.; Subramanya, M.; Morandi, M.; Holian, A., *Journal of Materials Science* **2004**, *39*, 2199-2204.
23. Lam, C.; James, J.; McCluskey, R., *Critical Reviews in Toxicology* **2016**, *36*, 189-217.
24. Reibold, M.; Paufler, P.; Levin, A. A.; Kochmann, W.; Patzke, N.; Meyer, D. C., *Nature* **2006**, *444*, 286-286.
25. Wu, M. X.; Gordon, R. E.; Herbert, R.; Padilla, M.; Moline, J.; Mendelson, D.; Litle, V.; Travis, W. D.; Gil, J., *Environmental Health Perspectives* **2010**, *118*, 499-504.
26. Robertson, D. H.; Brenner, D. W.; Mintmire, J. W., *Physical Review B* **1992**, *45*, 12592-12595.
27. Treacy, M. M. J.; Ebbesen, T. W.; Gibson, J. M., *Nature* **1996**, *381*, 678-680.
28. Krishnan, A.; Dujardin, E.; Ebbesen, T. W.; Yianilos, P. N.; Treacy, M. M. J., *Physical Review B* **1998**, *58*, 14013-14019.
29. Coleman, J. N.; Khan, U.; Blau, W. J.; Gun'ko, Y. K., *Carbon* **2006**, *44*, 1624-1652.
30. Liu, Z.; Tabakman, S.; Welsher, K.; Dai, H., *Nano Research* **2009**, *2*, 85-120.
31. Martincic, M.; Tobias, G., *Expert Opinion on Drug Delivery* **2015**, *12*, 563-581.
32. Chen, J.; Perebeinos, V.; Freitag, M.; Tsang, J.; Fu, Q.; Liu, J.; Avouris, P., *Science* **2005**, *310*, 1171.
33. Itkis, M. E.; Perea, D. E.; Jung, R.; Niyogi, S.; Haddon, R. C., *Journal of the American Chemical Society* **2005**, *127*, 3439-3448.
34. Rao, A. M.; Richter, E.; Bandow, S.; Chase, B.; Eklund, P. C.; Williams, K. A.; Fang, S.; Subbaswamy, K. R.; Menon, M.; Thess, A.; Smalley, R. E.; Dresselhaus, G.; Dresselhaus, M. S., *Science* **1997**, *275*, 187-191.
35. Fantini, C.; Jorio, A.; Souza, M.; Strano, M. S.; Dresselhaus, M. S.; Pimenta, M. A., *Physical Review Letters* **2004**, *93*, 147406.
36. Eklund, P. C.; Holden, J. M.; Jishi, R. A., *Carbon* **1995**, *33*, 959-972.
37. Kim, P.; Shi, L.; Majumdar, A.; McEuen, P. L., *Physical Review Letters* **2001**, *87*, 215502.
38. Martel, R.; Schmidt, T.; Shea, H. R.; Hertel, T.; Avouris, P., *Applied Physics Letters* **1998**, *73*, 2447-2449.
39. Yao, Z.; Kane, C. L.; Dekker, C., *Physical Review Letters* **2000**, *84*, 2941-2944.
40. Dresselhaus, M. S.; Dresselhaus, G.; Saito, R., *Carbon* **1995**, *33*, 883-891.

41. Hwang, J.-Y.; Shin, U. S.; Jang, W.-C.; Hyun, J. K.; Wall, I. B.; Kim, H.-W., *Nanoscale* **2013**, *5*, 487-497.
42. Nanot, S.; Hároz, E. H.; Kim, J.-H.; Hauge, R. H.; Kono, J., *Advanced Materials* **2012**, *24*, 4977-4994.
43. Takahashi, T.; Takei, K.; Gillies, A. G.; Fearing, R. S.; Javey, A., *Nano Letters* **2011**, *11*, 5408-5413.
44. Wang, C.; Takei, K.; Takahashi, T.; Javey, A., *Chemical Society Reviews* **2013**, *42*, 2592-2609.
45. Jeon, I.-Y.; Chang, D. W.; Kumar, N. A.; Baek, J.-B., *Functionalization of Carbon Nanotubes*, 2011.
46. Wu, H.-C.; Chang, X.; Liu, L.; Zhao, F.; Zhao, Y., *Journal of Materials Chemistry* **2010**, *20*, 1036-1052.
47. Hu, C.-Y.; Xu, Y.-J.; Duo, S.-W.; Zhang, R.-F.; Li, M.-S., *Journal of the Chinese Chemical Society* **2009**, *56*, 234-239.
48. Lee, G. K. C.; Sach, C.; Green, M. L. H.; Wong, L.-l.; Salzmann, C. G., *Chemical Communications* **2010**, *46*, 7013-7015.
49. Peng, X.; Chen, J.; Misewich, J. A.; Wong, S. S., *Chemical Society Reviews* **2009**, *38*, 1076-1098.
50. Salzmann, C. G.; Lee, G. K. C.; Ward, M. A. H.; Chu, B. T. T.; Green, M. L. H., *Journal of Materials Chemistry* **2008**, *18*, 1977-1983.
51. Ugarte, D.; Stöckli, T.; Bonard, J. M.; Châtelain, A.; de Heer, W. A., *Applied Physics A* **1998**, *67*, 101-105.
52. Smith, B. W.; Monthioux, M.; Luzzi, D. E., *Nature* **1998**, *396*, 323-324.
53. Bera, D.; Kuiry, S. C.; McCutchen, M.; Kruize, A.; Heinrich, H.; Meyyappan, M.; Seal, S., *Chemical Physics Letters* **2004**, *386*, 364-368.
54. Costa, S.; Borowiak-Palen, E.; Bachmatiuk, A.; Rümmeli, M. H.; Gemming, T.; Kalenczuk, R. J., *Energy Conversion and Management* **2008**, *49*, 2483-2486.
55. Smith, B. W.; Luzzi, D. E., *Chemical Physics Letters* **2000**, *321*, 169-174.
56. Tsang, S. C.; Chen, Y. K.; Harris, P. J. F.; Green, M. L. H., *Nature* **1994**, *372*, 159-162.
57. Sloan, J.; Hammer, J.; Zwiefka-Sibley, M.; Green, M. L. H., *Chemical Communications* **1998**, 347-348.
58. Saito, Y.; Yoshikawa, T.; Okuda, M.; Fujimoto, N.; Sumiyama, K.; Suzuki, K.; Kasuya, A.; Nishina, Y., *Journal of Physics and Chemistry of Solids* **1993**, *54*, 1849-1860.
59. Saito, Y.; Yoshikawa, T., *Journal of Crystal Growth* **1993**, *134*, 154-156.
60. Reich, S.; Li, L.; Robertson, J., *Physical Review B* **2005**, *72*, 165423.

61. Aqel, A.; El-Nour, K. M. M. A.; Ammar, R. A. A.; Al-Warthan, A., *Arabian Journal of Chemistry* **2012**, *5*, 1-23.
62. Poland, C. A.; Duffin, R.; Kinloch, I.; Maynard, A.; Wallace, W. A. H.; Seaton, A.; Stone, V.; Brown, S.; MacNee, W.; Donaldson, K., *Nature Nanotechnology* **2008**, *3*, 423-428.
63. Ballesteros, B.; Tobias, G.; Shao, L.; Pellicer, E.; Nogués, J.; Mendoza, E.; Green, M. L. H., *Small* **2008**, *4*, 1501-1506.
64. Tobias, G.; Shao, L.; Salzmann, C. G.; Huh, Y.; Green, M. L. H., *The Journal of Physical Chemistry B* **2006**, *110*, 22318-22322.
65. Gao, X. P.; Zhang, Y.; Chen, X.; Pan, G. L.; Yan, J.; Wu, F.; Yuan, H. T.; Song, D. Y., *Carbon* **2004**, *42*, 47-52.
66. Yanagi, K.; Miyata, Y.; Kataura, H., *Advanced Materials* **2006**, *18*, 437-441.
67. Stercel, F.; Nemes, N. M.; Fischer, J. E.; Luzzi, D. E. In *Single Wall Carbon Nanotubes Filled with Metallocenes: A First Example of Non-Fullerene Peapods*, Materials Research Society Symposium - Proceedings, 2002; pp 245-250.
68. Dillon, A. C.; Jones, K. M.; Bekkedahl, T. A.; Kiang, C. H.; Bethune, D. S.; Heben, M. J., *Nature* **1997**, *386*, 377-379.
69. Nakamura, Y.; Ohno, T., *Chemical Physics Letters* **2012**, *539*, 123-127.
70. Botka, B.; Füstös, M. E.; Tõháti, H. M.; Németh, K.; Klupp, G.; Szekrényes, Z.; Kocsis, D.; Utczás, M.; Székely, E.; Váczi, T.; Tarczay, G.; Hackl, R.; Chamberlain, T. W.; Khlobystov, A. N.; Kamarás, K., *Small* **2014**, *10*, 1369-1378.
71. Pederson, M. R.; Broughton, J. Q., *Physical Review Letters* **1992**, *69*, 2689-2692.
72. Dujardin, E.; Ebbesen, T. W.; Hiura, H.; Tanigaki, K., *Science* **1994**, *265*, 1850-2.
73. Fu, Q.; Gisela, W.; Su, D.-s., *New Carbon Materials* **2008**, *23*, 17-20.
74. Nie, C.; Galibert, A.-M.; Soula, B.; Flahaut, E.; Sloan, J.; Monthioux, M., *Carbon* **2016**, *110*, 48-50.
75. Tobias, G.; Ballesteros, B.; Green, M. L. H., *Physica Status Solidi C* **2010**, *7*, 2739-2742.
76. Shao, L.; Tobias, G.; Huh, Y.; Green, M. L. H., *Carbon* **2006**, *44*, 2855-2858.
77. Wang, Q.; Arash, B., *Computational Materials Science* **2014**, *82*, 350-360.
78. Zhang, Q.; Huang, J.-Q.; Qian, W.-Z.; Zhang, Y.-Y.; Wei, F., *Small* **2013**, *9*, 1237-1265.
79. Sholl, D. S.; Johnson, J. K., *Science* **2006**, *312*, 1003.

80. Skoulidas, A. I.; Sholl, D. S.; Johnson, J. K., *The Journal of Chemical Physics* **2006**, *124*, 054708.
81. Kim, S.; Jinschek, J. R.; Chen, H.; Sholl, D. S.; Marand, E., *Nano Letters* **2007**, *7*, 2806-2811.
82. Holt, J. K.; Park, H. G.; Wang, Y.; Stadermann, M.; Artyukhin, A. B.; Grigoropoulos, C. P.; Noy, A.; Bakajin, O., *Science* **2006**, *312*, 1034-7.
83. Sun, L.; Crooks, R. M., *Journal of the American Chemical Society* **2000**, *122*, 12340-12345.
84. Hinds, B. J.; Chopra, N.; Rantell, T.; Andrews, R.; Gavalas, V.; Bachas, L. G., *Science* **2004**, *303*, 62.
85. Corry, B., *The Journal of Physical Chemistry B* **2008**, *112*, 1427-1434.
86. Majumder, M.; Chopra, N.; Andrews, R.; Hinds, B. J., *Nature* **2005**, *438*, 44-44.
87. Carter, R.; Sloan, J.; Kirkland, A. I.; Meyer, R. R.; Lindan, P. J. D.; Lin, G.; Green, M. L. H.; Vlandas, A.; Hutchison, J. L.; Harding, J., *Physical Review Letters* **2006**, *96*, 215501.
88. Flahaut, E.; Sloan, J.; Friedrichs, S.; Kirkland, A. I.; Coleman, K. S.; Williams, V. C.; Hanson, N.; Hutchison, J. L.; Green, M. L. H., *Chemistry of Materials* **2006**, *18*, 2059-2069.
89. Philp, E.; Sloan, J.; Kirkland, A. I.; Meyer, R. R.; Friedrichs, S.; Hutchison, J. L.; Green, M. L. H., *Nature Materials* **2003**, *2*, 788-791.
90. Sloan, J.; Grosvenor, S. J.; Friedrichs, S.; Kirkland, A. I.; Hutchison, J. L.; Green, M. L., *Angewandte Chemie International Edition* **2002**, *41*, 1156-9.
91. Mittal, J.; Monthioux, M.; Allouche, H.; Stephan, O., *Chemical Physics Letters* **2001**, *339*, 311-318.
92. Kuramochi, H.; Uzumaki, T.; Yasutake, M.; Tanaka, A.; Akinaga, H.; Yokoyama, H., *Nanotechnology* **2005**, *16*, 24.
93. Deng, Z.; Yenilmez, E.; Leu, J.; Hoffman, J. E.; Straver, E. W. J.; Dai, H.; Moler, K. A., *Applied Physics Letters* **2004**, *85*, 6263-6265.
94. Arie, T.; Nishijima, H.; Akita, S.; Nakayama, Y., *Journal of Vacuum Science & Technology B: Microelectronics and Nanometer Structures Processing, Measurement, and Phenomena* **2000**, *18*, 104-106.
95. Yoshida, N.; Arie, T.; Akita, S.; Nakayama, Y., *Physica B: Condensed Matter* **2002**, *323*, 149-150.
96. Cui, H.; Kalinin, S. V.; Yang, X.; Lowndes, D. H., *Nano Letters* **2004**, *4*, 2157-2161.

97. Franziska, W.; Uhland, W.; Thomas, M.; Matthias, U. L.; Christian, M.; Albrecht, L.; Bernd, B., *Journal of Physics: Conference Series* **2010**, *200*, 112011.
98. Winkler, A.; Mühl, T.; Menzel, S.; Kozhuharova-Koseva, R.; Hampel, S.; Leonhardt, A.; Büchner, B., *Journal of Applied Physics* **2006**, *99*, 104905.
99. Pan, X.; Fan, Z.; Chen, W.; Ding, Y.; Luo, H.; Bao, X., *Nature Materials* **2007**, *6*, 507-511.
100. Che, G.; Lakshmi, B. B.; Martin, C. R.; Fisher, E. R., *Langmuir* **1999**, *15*, 750-758.
101. Miners, S. A.; Rance, G. A.; Khlobystov, A. N., *Chemical Communications* **2013**, *49*, 5586-5588.
102. Lota, G.; Frackowiak, E.; Mittal, J.; Monthioux, M., *Chemical Physics Letters* **2007**, *483*, 73-77.
103. Yu, W.-J.; Hou, P.-X.; Zhang, L.-L.; Li, F.; Liu, C.; Cheng, H.-M., *Chemical Communications* **2010**, *46*, 8576-8578.
104. Giusca, C. E.; Stolojan, V.; Sloan, J.; Börrnert, F.; Shiozawa, H.; Sader, K.; Rümmeli, M. H.; Büchner, B.; Silva, S. R. P., *Nano Letters* **2013**, *13*, 4020-4027.
105. Li, Y. F.; Kaneko, T.; Hatakeyama, R., *Applied Physics Letters* **2008**, *92*, 183115.
106. Lee, J.; Kim, H.; Kahng, S. J.; Kim, G.; Son, Y. W.; Ihm, J.; Kato, H.; Wang, Z. W.; Okazaki, T.; Shinohara, H.; Kuk, Y., *Nature* **2002**, *415*, 1005-1008.
107. Shimada, T.; Okazaki, T.; Taniguchi, R.; Sugai, T.; Shinohara, H.; Suenaga, K.; Ohno, Y.; Mizuno, S.; Kishimoto, S.; Mizutani, T., *Applied Physics Letters* **2002**, *81*, 4067-4069.
108. Yu, H. Y.; Lee, D. S.; Lee, S. H.; Kim, S. S.; Lee, S. W.; Park, Y. W.; Dettlaff-Weglikowskaand, U.; Roth, S., *Applied Physics Letters* **2005**, *87*, 163118.
109. He, S.-L.; Shen, J.-Q., *Chinese Physics Letters* **2006**, *23*, 211.
110. Lu, D.; Li, Y.; Rotkin, S. V.; Ravaioli, U.; Schulten, K., *Nano Letters* **2004**, *4*, 2383-2387.
111. Corzilius, B.; Gembus, A.; Weiden, N.; Dinse, K. P.; Hata, K., *Physica Status Solidi B* **2006**, *243*, 3273-3276.
112. Simon, C. B.; Arzhang, A.; Briggs, G. A. D.; David, A. B.; Daniel, G.; John, J.; Mark, A. G. J.; David, F. L.; Brendon, W. L.; Andrei, N. K.; Lyon, S. A.; John, J. L. M.; Kyriakos, P.; Mark, R. S.; Alexei, M. T., *Journal of Physics: Condensed Matter* **2006**, *18*, S867.
113. Chuang, I. L.; Vandersypen, L. M. K.; Zhou, X.; Leung, D. W.; Lloyd, S., *Nature* **1998**, *393*, 143-146.
114. Harneit, W., *Physical Review A* **2002**, *65*, 032322.

115. Almeida Murphy, T.; Pawlik, T.; Weidinger, A.; Hohne, M.; Alcala, R.; Spaeth, J., *Physical Review Letters* **1996**, *77*, 1075-1078.
116. Mehring, M.; Scherer, W.; Weidinger, A., *Physical Review Letters* **2004**, *93*, 206603.
117. Kwon, Y.-K.; Tománek, D.; Iijima, S., *Physical Review Letters* **1999**, *82*, 1470-1473.
118. Won Kang, J.; Jung Hwang, H., *Journal of the Physical Society of Japan* **2004**, *73*, 1077-1081.
119. Simon, F.; Fülöp, F.; Rockenbauer, A.; Korecz, L.; Kuzmany, H., *Chemical Physics Letters* **2005**, *404*, 85-89.
120. Hummelen, J. C.; Bellavia-Lund, C.; Wudl, F., *Heterofullerenes*; Springer: Berlin, Heidelberg, 1999; Vol. 199.
121. Bianco, A.; Kostarelos, K.; Prato, M., *Chemical Communications* **2011**, *47*, 10182-10188.
122. Ali-Boucetta, H.; Nunes, A.; Sainz, R.; Herrero, M. A.; Tian, B.; Prato, M.; Bianco, A.; Kostarelos, K., *Angewandte Chemie International Edition* **2013**, *52*, 2274-2278.
123. Kostarelos, K., *Nature Biotechnology* **2008**, *26*, 774-776.
124. Shvedova, A.; Castranova, V.; Kisin, E.; Schwegler-Berry, D.; Murray, A.; Gandelsman, V.; Maynard, A.; Baron, P., *Journal of Toxicology and Environmental Health, Part A* **2003**, *66*, 1909-1926.
125. Pulskamp, K.; Diabaté, S.; Krug, H. F., *Toxicology Letters* **2007**, *168*, 58-74.
126. Wong, B. S.; Yoong, S. L.; Jagusiak, A.; Panczyk, T.; Ho, H. K.; Ang, W. H.; Pastorin, G., *Advanced Drug Delivery Reviews* **2013**, *65*, 1964-2015.
127. Zhang, W. X.; Zhang, Z. Z.; Zhang, Y. G., *Nanoscale Research Letters* **2011**, *6*.
128. Scheinberg, D. A.; McDevitt, M. R.; Dao, T.; Mulvey, J. J.; Feinberg, E.; Alidori, S., *Advanced Drug Delivery Reviews* **2013**, *65*, 2016-2022.
129. Battigelli, A.; Ménard-Moyon, C.; Da Ros, T.; Prato, M.; Bianco, A., *Advanced Drug Delivery Reviews* **2013**, *65*, 1899-1920.
130. Costa, P.; Golberg, D.; Mitome, M.; Hampel, S.; Leonhardt, A.; Buchner, B.; Bando, Y., *Nano Letters* **2008**, *8*, 3120-3125.
131. Costa, P.; Gautam, U. K.; Bando, Y.; Golberg, D., *Carbon* **2011**, *49*, 342-346.
132. Costa, P.; Gautam, U. K.; Bando, Y.; Golberg, D., *Carbon* **2011**, *49*, 3747-3754.
133. Shao, L. D.; Lin, T. W.; Tobias, G.; Green, M. L. H., *Chemical Communications* **2008**, 2164-2166.

134. Luksirikul, P.; Ballesteros, B.; Tobias, G.; Moloney, M. G.; Green, M. L. H., *Carbon* **2010**, *48*, 1912-1917.
135. Ren, Y. P.; Pastorin, G., *Advanced Materials* **2008**, *20*, 2031-+.
136. Fan, J.; Yudasaka, M.; Yuge, R.; Futaba, D. N.; Hata, K.; Iijima, S., *Carbon* **2007**, *45*, 722-726.
137. Simon, F.; Peterlik, H.; Pfeiffer, R.; Bernardi, J.; Kuzmany, H., *Chemical Physics Letters* **2007**, *445*, 288-292.
138. Chen, X. C.; Chen, H. M.; Tripisciano, C.; Jedrzejewska, A.; Rummeli, M. H.; Klingeler, R.; Kalenczuk, R. J.; Chu, P. K.; Borowiak-Palen, E., *Chemistry-a European Journal* **2011**, *17*, 4454-4459.
139. Raoof, M.; Cisneros, B. T.; Guven, A.; Phounsavath, S.; Corr, S. J.; Wilson, L. J.; Curley, S. A., *Biomaterials* **2013**, *34*, 1862-1869.
140. Luo, X. L.; Matranga, C.; Tan, S. S.; Alba, N.; Cui, X. Y. T., *Biomaterials* **2011**, *32*, 6316-6323.
141. Wu, C. H.; Cao, C.; Kim, J. H.; Hsu, C. H.; Wanebo, H. J.; Bowen, W. D.; Xu, J.; Marshall, J., *Nano Letters* **2012**, *12*, 5475-5480.
142. Tripisciano, C.; Rummeli, M. H.; Chen, X. C.; Borowiak-Palen, E., *Physica Status Solidi B-Basic Solid State Physics* **2010**, *247*, 2673-2677.
143. Chaban, V. V.; Savchenko, T. I.; Kovalenko, S. M.; Prezhdo, O. V., *Journal of Physical Chemistry B* **2010**, *114*, 13481-13486.
144. Su, Z. D.; Zhu, S. H.; Donkor, A. D.; Tzoganakis, C.; Honek, J. F., *Journal of the American Chemical Society* **2011**, *133*, 6874-6877.
145. Yeh, I. C.; Hummer, G., *Proceedings of the National Academy of Sciences of the United States of America* **2004**, *101*, 12177-12182.
146. Gao, H. J.; Kong, Y.; Cui, D. X.; Ozkan, C. S., *Nano Letters* **2003**, *3*, 471-473.
147. Xue, Q. Z.; Jing, N. N.; Chu, L. Y.; Ling, C. C.; Zhang, H. X., *RSC Advances* **2012**, *2*, 6913-6920.
148. Cui, D.; Ozkan, C. S.; Ravindran, S.; Kong, Y.; Gao, H., *Mechanics and Chemistry of Biosystems* **2004**, *1*, 113-21.
149. Kaneko, T.; Okada, T.; Hatakeyama, R., *Contributions to Plasma Physics* **2007**, *47*, 57-63.
150. Chen, B.-D.; Yang, C.-L.; Yang, J.-S.; Wang, M.-S.; Ma, X.-G., *Computational and Theoretical Chemistry* **2012**, *991*, 93-97.
151. Tsang, S. C.; Davis, J. J.; Green, M. L. H.; Hill, H. A. O.; Leung, Y. C.; Sadler, P. J., *Journal of the Chemical Society, Chemical Communications* **1995**, 1803-1804.
152. Xu, J.; Tian, Y.-S.; Peng, R.-H.; Xiong, A.-S.; Zhu, B.; Hou, X.-L.; Yao, Q.-H., *Molecular Biology Reports* **2010**, *37*, 1105-1110.
153. Chen, B.-D.; Yang, C.-L.; Yang, J.-S.; Wang, M.-S.; Ma, X.-G., *Current Applied Physics* **2013**, *13*, 1001-1007.

154. Chen, B. D.; Yang, C. L.; Wang, M. S.; Ma, X. G., *Chinese Physics B* **2012**, *21*.
155. Chen, Q.; Wang, Q.; Liu, Y. C.; Wu, T.; Kang, Y.; Moore, J. D.; Gubbins, K. E., *Journal of Chemical Physics* **2009**, *131*.
156. Hilder, T. A.; Hill, J. M., *Nanotechnology* **2007**, *18*.
157. Panczyk, T.; Jagusiak, A.; Pastorin, G.; Ang, W. H.; Narkiewicz-Michalek, J., *Journal of Physical Chemistry C* **2013**, *117*, 17327-17336.
158. Hosni, Z.; Bessrour, R.; Tangour, B., *Journal of Computational and Theoretical Nanoscience* **2014**, *11*, 318-323.
159. Tripisciano, C.; Costa, S.; Kalenczuk, R. J.; Borowiak-Palen, E., *European Physical Journal B* **2010**, *75*, 141-146.
160. Tripisciano, C.; Kraemer, K.; Taylor, A.; Borowiak-Palen, E., *Chemical Physics Letters* **2009**, *478*, 200-205.
161. Guven, A.; Rusakova, I. A.; Lewis, M. T.; Wilson, L. J., *Biomaterials* **2012**, *33*, 1455-1461.
162. Li, J.; Yap, S. Q.; Yoong, S. L.; Nayak, T. R.; Chandra, G. W.; Ang, W. H.; Panczyk, T.; Ramaprabhu, S.; Vashist, S. K.; Sheu, F. S.; Tan, A.; Pastorin, G., *Carbon* **2012**, *50*, 1625-1634.
163. Li, J.; Pant, A.; Chin, C. F.; Ang, W. H.; Ménard-Moyon, C.; Nayak, T. R.; Gibson, D.; Ramaprabhu, S.; Panczyk, T.; Bianco, A.; Pastorin, G., *Nanomedicine: Nanotechnology, Biology and Medicine* **2014**, *10*, 1465-1475.
164. Hampel, S.; Kunze, D.; Haase, D.; Kramer, K.; Rauschenbach, M.; Ritscbel, M.; Leonbardt, A.; Thomas, J.; Oswald, S.; Hoffmann, V.; Buechner, B., *Nanomedicine* **2008**, *3*, 175-182.
165. Wu, L. L.; Man, C. J.; Wang, H.; Lu, X. H.; Ma, Q. H.; Cai, Y.; Ma, W. S., *Pharmaceutical Research* **2013**, *30*, 412-423.
166. Li, J.; Yap, S. Q.; Chin, C. F.; Tian, Q.; Yoong, S. L.; Pastorin, G.; Ang, W. H., *Chemical Science* **2012**, *3*, 2083-2087.
167. Yoong, S. L.; Wong, B. S.; Zhou, Q. L.; Chin, C. F.; Li, J.; Venkatesan, T.; Ho, H. K.; Yu, V.; Ang, W. H.; Pastorin, G., *Biomaterials* **2014**, *35*, 748-59.
168. Mollaamin, F.; Najafi, F.; Khaleghian, M.; Hadad, B. K.; Monajjemi, M., *Fullerenes, Nanotubes and Carbon Nanostructures* **2011**, *19*, 653-667.
169. Mousavi, S. Z.; Amjad-Iranagh, S.; Nademi, Y.; Modarress, H., *The Journal of Membrane Biology* **2013**, *246*, 697-704.
170. Hilder, T. A.; Hill, J. M., *Micro & Nano Letters* **2008**, *3*, 41-49.
171. Sornmee, P.; Rungrotmongkol, T.; Saengsawang, O.; Arsawang, U.; Remsungnen, T.; Hannongbua, S., *Journal of Computational and Theoretical Nanoscience* **2011**, *8*, 1385-1391.

172. Arsawang, U.; Saengsawang, O.; Rungrotmongkol, T.; Sornmee, P.; Wittayanarakul, K.; Remsungnen, T.; Hannongbua, S., *Journal of Molecular Graphics and Modelling* **2011**, *29*, 591-596.
173. Rungnim, C.; Arsawang, U.; Rungrotmongkol, T.; Hannongbua, S., *Chemical Physics Letters* **2012**, *550*, 99-103.
174. Rungnim, C.; Rungrotmongkol, T.; Hannongbua, S.; Okumura, H., *Journal of Molecular Graphics and Modelling* **2013**, *39*, 183-192.
175. Singh, R.; Mehra, N. K.; Jain, V.; Jain, N. K., *J Drug Target* **2013**, *21*, 581-92.
176. Belmiloud, Y.; Ouraghi, M.; Brahimi, M.; Benaboura, A.; Charqaoui, D.; Tangour, B., *Journal of Computational and Theoretical Nanoscience* **2012**, *9*, 1101-1108.
177. Rezvani, M.; Darvish Ganji, M.; Faghihnasiri, M., *Physica E* **2013**, *52*, 27-33.
178. Hicks, E.; Desgranges, C.; Delhommelle, J., *Molecular Simulation* **2014**, *40*, 656-663.
179. Saikia, N.; Jha, A. N.; Deka, R. C., *The Journal of Physical Chemistry Letters* **2013**, *4*, 4126-4132.
180. Li, Y. T.; Wang, T. Y.; Wang, J.; Jiang, T. Y.; Cheng, G.; Wang, S. L., *Applied Surface Science* **2011**, *257*, 5663-5670.
181. Sanz, V.; Tilmacîu, C.; Soula, B.; Flahaut, E.; Coley, H. M.; Silva, S. R. P.; McFadden, J., *Carbon* **2011**, *49*, 5348-5358.
182. Marega, R.; De Leo, F.; Pineux, F.; Sgrignani, J.; Magistrato, A.; Naik, A. D.; Garcia, Y.; Flamant, L.; Michiels, C.; Bonifazi, D., *Advanced Functional Materials* **2013**, *23*, 3173-3184.
183. Ashcroft, J. M.; Hartman, K. B.; Kissell, K. R.; Mackeyev, Y.; Pheasant, S.; Young, S.; Van der Heide, P. A. W.; Mikos, A. G.; Wilson, L. J., *Advanced Materials* **2007**, *19*, 573-576.
184. Mackeyev, Y. A.; Marks, J. W.; Rosenblum, M. G.; Wilson, L. J., *Journal of Physical Chemistry B* **2005**, *109*, 5482-5484.
185. Hong, S. Y.; Tobias, G.; Al-Jamal, K. T.; Ballesteros, B.; Ali-Boucetta, H.; Lozano-Perez, S.; Nellist, P. D.; Sim, R. B.; Finucane, C.; Mather, S. J.; Green, M. L. H.; Kostarelos, K.; Davis, B. G., *Nature Materials* **2010**, *9*, 485-490.
186. Hartman, K. B.; Hamlin, D. K.; Wilbur, D. S.; Wilson, L. J., *Small* **2007**, *3*, 1496-1499.
187. Rivera, E. J.; Tran, L. A.; Hernandez-Rivera, M.; Yoon, D.; Mikos, A. G.; Rusakova, I. A.; Cheong, B. Y.; Cabreira-Hansen, M. d. G.; Willerson, J. T.; Perin, E. C.; Wilson, L. J., *Journal of Materials Chemistry B* **2013**, *1*, 4792-4800.

188. Rivera, E. J.; Sethi, R.; Qu, F. F.; Krishnamurthy, R.; Muthupillai, R.; Alford, M.; Swanson, M. A.; Eaton, S. S.; Eaton, G. R.; Wilson, L. J., *Advanced Functional Materials* **2012**, *22*, 3691-3698.
189. Hashimoto, A.; Yorimitsu, H.; Ajima, K.; Suenaga, K.; Isobe, H.; Miyawaki, A.; Yudasaka, M.; Iijima, S.; Nakamura, E., *Proceedings of the National Academy of Sciences of the United States of America* **2004**, *101*, 8527-8530.
190. Sethi, R.; Mackeyev, Y.; Wilson, L. J., *Inorganica Chimica Acta* **2012**, *393*, 165-172.
191. Sitharaman, B.; Kissell, K. R.; Hartman, K. B.; Tran, L. A.; Baikalov, A.; Rusakova, I.; Sun, Y.; Khant, H. A.; Ludtke, S. J.; Chiu, W.; Laus, S.; Toth, E.; Helm, L.; Merbach, A. E.; Wilson, L. J., *Chemical Communications* **2005**, 3915-3917.
192. Ma, Q.; Jebb, M.; Tweedle, M. F.; Wilson, L. J., *Journal of Materials Chemistry B* **2013**, *1*, 5791-5797.
193. Law, J. J.; Guven, A.; Wilson, L. J., *Contrast Media and Molecular Imaging* **2014**, 409-412.
194. Tran, L. A.; Hernandez-Rivera, M.; Berlin, A. N.; Zheng, Y.; Sampaio, L.; Bovee, C.; Cabreira-Hansen, M. D.; Willerson, J. T.; Perin, E. C.; Wilson, L. J., *Biomaterials* **2014**, *35*, 720-726.
195. Tang, A. M.; Ananta, J. S.; Zhao, H.; Cisneros, B. T.; Lam, E. Y.; Wong, S. T.; Wilson, L. J.; Wong, K. K., *Contrast Media and Molecular Imaging* **2011**, *6*, 93-99.
196. Sitharaman, B.; Van Der Zande, M.; Ananta, J. S.; Shi, X. F.; Veltien, A.; Walboomers, X. F.; Wilson, L. J.; Mikos, A. G.; Heerschap, A.; Jansen, J. A., *Journal of Biomedical Materials Research Part A* **2010**, *93A*, 1454-1462.
197. van der Zande, M.; Sitharaman, B.; Walboomers, X. F.; Tran, L.; Ananta, J. S.; Veltien, A.; Wilson, L. J.; Alava, J. I.; Heerschap, A.; Mikos, A. G.; Jansen, J. A., *Tissue Engineering Part C: Methods* **2011**, *17*, 19-26.
198. Cisneros, B. T.; Law, J. J.; Matson, M. L.; Azhdarinia, A.; Sevick-Muraca, E. M.; Wilson, L. J., *Nanomedicine* **2014**, 1-11.
199. Weissker, U.; Hampel, S.; Leonhardt, A.; Büchner, B., *Materials* **2010**, *3*, 4387.
200. Lu, C.; Sandoval, S.; Puig, T.; Obradors, X.; Tobias, G.; Ros, J.; Ricart, S., *RSC Advances* **2017**, *7*, 24690-24697.
201. Monch, I.; Leonhardt, A.; Meye, A.; Hampel, S.; Kozhuharova-Koseva, R.; Elefant, D.; Wirth, M. P.; Buchner, B., Synthesis and Characteristics of Fe-Filled Multi-Walled Carbon Nanotubes for Biomedical Application. In *Proceedings of the International Conference on Nanoscience and Technology*, Meyer, E.; Hegner, M.; Gerber, C.;

Guntherodt, H. J., Eds. Iop Publishing Ltd: Bristol, 2007; Vol. 61, pp 820-824.
202. Ding, X.; Singh, R.; Burke, A.; Hatcher, H.; Olson, J.; Kraft, R. A.; Schmid, M.; Carroll, D.; Bourland, J. D.; Akman, S.; Torti, F. M.; Torti, S. V., *Nanomedicine* **2011**, *6*, 1341-1352.
203. Mönch, I.; Meye, A.; Leonhardt, A.; Krämer, K.; Kozhuharova, R.; Gemming, T.; Wirth, M. P.; Büchner, B., *Journal of Magnetism and Magnetic Materials* **2005**, *290–291, Part 1*, 276-278.
204. Chen, M. L.; He, Y. J.; Chen, X. W.; Wang, J. H., *Langmuir* **2012**, *28*, 16469-16476.
205. Serpell, C. J.; Rutte, R. N.; Geraki, K.; Pach, E.; Martincic, M.; Kierkowicz, M.; De Munari, S.; Wals, K.; Raj, R.; Ballesteros, B.; Tobias, G.; Anthony, D. C.; Davis, B. G., *Nature Communications* **2016**, *7*, 13118.
206. Pang, L. S. K.; Saxby, J. D.; Chatfield, S. P., *Journal of Physical Chemistry* **1993**, *97*, 6941-6942.
207. Syrgiannis, Z.; La Parola, V.; Hadad, C.; Lucio, M.; Vazquez, E.; Giacalone, F.; Prato, M., *Angewandte Chemie-International Edition* **2013**, *52*, 6480-6483.
208. Tobón, J. I.; Paya, J.; Borrachero, M. V.; Soriano, L.; Restrepo, O. J., *Journal of Thermal Analysis and Calorimetry* **2012**, *107*, 233-239.
209. Archer, P., Jr.; Ming, D.; Sutter, B., *Planetary Science* **2013**, *2*, 1-21.
210. Shao, L.; Tobias, G.; Salzmann, C. G.; Ballesteros, B.; Hong, S. Y.; Crossley, A.; Davis, B. G.; Green, M. L. H., *Chemical Communications* **2007**, 5090-5092.
211. Cabana, L.; Ke, X.; Kepić, D.; Oro-Solé, J.; Tobías-Rossell, E.; Van Tendeloo, G.; Tobias, G., *Carbon* **2015**, *93*, 1059-1067.
212. Dresselhaus, M. S.; Jorio, A.; Hofmann, M.; Dresselhaus, G.; Saito, R., *Nano Letters* **2010**, *10*, 751-758.
213. González-Guerrero, A. B.; Lechuga, L. M.; Mendoza Gómez, E.; Nogués, J.; Pellicer, E., *Carbon* **2009**, *47*, 758-763.
214. Park, T.-J.; Banerjee, S.; Hemraj-Benny, T.; Wong, S. S., *Journal of Materials Chemistry* **2006**, *16*, 141-154.
215. Kierkowicz, M.; Pach, E.; Santidrián, A.; Tobías-Rossell, E.; Kalbáč, M.; Ballesteros, B.; Tobias, G., *ChemNanoMat* **2016**, *2*, 108-116.
216. Agustina, E.; Goak, J.; Lee, S.; Seo, Y.; Park, J.-Y.; Lee, N., *ChemistryOpen* **2015**, *4*, 613-619.
217. Kolodiazhnyi, T.; Pumera, M., *Small* **2008**, *4*, 1476-1484.
218. Martincic, M.; Frontera, C.; Pach, E.; Ballesteros, B.; Tobias, G., *Polyhedron* **2016**, *116*, 116-121.

219. Martincic, M.; Pach, E.; Ballesteros, B.; Tobias, G., *Physical Chemistry Chemical Physics* **2015**, *17*, 31662-31669.
220. Wang, L.; Pumera, M., *Chemical Communications* **2014**, *50*, 12662-12664.
221. Pumera, M., *Chemistry – A European Journal* **2009**, *15*, 4970-4978.
222. Soylak, M.; Turkoglu, O., *Talanta* **2000**, *53*, 125-9.
223. Monthioux, M., *Carbon* **2002**, *40*, 1809-1823.
224. Lu, N.; Wang, J.; Floresca, H. C.; Kim, M. J., *Carbon* **2012**, *50*, 2961-2965.
225. de Jonge, N.; Doytcheva, M.; Allioux, M.; Kaiser, M.; Mentink, S. A. M.; Teo, K. B. K.; Lacerda, R. G.; Milne, W. I., *Advanced Materials* **2005**, *17*, 451-455.
226. Chen, J.; Shan, J. Y.; Tsukada, T.; Munekane, F.; Kuno, A.; Matsuo, M.; Hayashi, T.; Kim, Y. A.; Endo, M., *Carbon* **2007**, *45*, 274-280.
227. Castillejos, E.; Bachiller-Baeza, B.; Pérez-Cadenas, M.; Gallegos-Suarez, E.; Rodríguez-Ramos, I.; Guerrero-Ruiz, A.; Tamargo-Martinez, K.; Martinez-Alonso, A.; Tascón, J. M. D., *Journal of Alloys and Compounds* **2012**, *536, Supplement 1*, S460-S463.
228. Satishkumar, B. C.; Govindaraj, A.; Mofokeng, J.; Subbanna, G. N.; Rao, C. N. R., *Journal of Physics B: Atomic, Molecular and Optical Physics* **1996**, *29*, 4925.
229. Brunauer, S.; Emmett, P. H.; Teller, E., *Journal of the American Chemical Society* **1938**, *60*, 309-319.
230. Müller, E. A., *The Journal of Physical Chemistry B* **2008**, *112*, 8999-9005.
231. Lehman, J. H.; Terrones, M.; Mansfield, E.; Hurst, K. E.; Meunier, V., *Carbon* **2011**, *49*, 2581-2602.
232. Gauden, P.; Terzyk, A.; Furmaniak, S.; Wiśniewski, M.; Kowalczyk, P.; Bielicka, A.; Zieliński, W., *Adsorption* **2013**, *19*, 785-793.
233. Lafi, L.; Cossement, D.; Chahine, R., *Carbon* **2005**, *43*, 1347-1357.
234. Bajpai, A.; Gorantla, S.; Löffler, M.; Hampel, S.; Rümmeli, M. H.; Thomas, J.; Ritschel, M.; Gemming, T.; Büchner, B.; Klingeler, R., *Carbon* **2012**, *50*, 1706-1709.
235. Li, Y. F.; Hatakeyama, R.; Kaneko, T.; Izumida, T.; Okada, T.; Kato, T., *Nanotechnology* **2006**, *17*, 4143.
236. Porter, A. E.; Gass, M.; Muller, K.; Skepper, J. N.; Midgley, P. A.; Welland, M., *Nature Nanotechnology* **2007**, *2*, 713-717.

237. Muller, J.; Huaux, F.; Moreau, N.; Misson, P.; Heilier, J.-F.; Delos, M.; Arras, M.; Fonseca, A.; Nagy, J. B.; Lison, D., *Toxicology and Applied Pharmacology* **2005**, *207*, 221-231.
238. Marshall, M. W.; Popa-Nita, S.; Shapter, J. G., *Carbon* **2006**, *44*, 1137-1141.
239. Salzmann, C. G.; Llewellyn, S. A.; Tobias, G.; Ward, M. A. H.; Huh, Y.; Green, M. L. H., *Advanced Materials* **2007**, *19*, 883-887.
240. Pumera, M.; Miyahara, Y., *Nanoscale* **2009**, *1*, 260-265.
241. Kagan, V. E.; Tyurina, Y. Y.; Tyurin, V. A.; Konduru, N. V.; Potapovich, A. I.; Osipov, A. N.; Kisin, E. R.; Schwegler-Berry, D.; Mercer, R.; Castranova, V.; Shvedova, A. A., *Toxicology Letters* **2006**, *165*, 88-100.
242. Ballesteros, B.; Tobias, G.; Ward, M. A. H.; Green, M. L. H., *The Journal of Physical Chemistry C* **2009**, *113*, 2653-2656.
243. Bianco, A.; Kostarelos, K.; Partidos, C. D.; Prato, M., *Chemical Communications* **2005**, 571-7.
244. Spinato, C.; Perez Ruiz de Garibay, A.; Kierkowicz, M.; Pach, E.; Martincic, M.; Klippstein, R.; Bourgognon, M.; Wang, J. T.-W.; Menard-Moyon, C.; Al-Jamal, K. T.; Ballesteros, B.; Tobias, G.; Bianco, A., *Nanoscale* **2016**, *8*, 12626-12638.
245. Perez Ruiz de Garibay, A.; Spinato, C.; Klippstein, R.; Bourgognon, M.; Martincic, M.; Pach, E.; Ballesteros, B.; Ménard-Moyon, C.; Al-Jamal, K. T.; Tobias, G.; Bianco, A., *Scientific Reports* **2017**, *7*, 42605.
246. Vyalikh, A.; Wolter, A. U.; Hampel, S.; Haase, D.; Ritschel, M.; Leonhardt, A.; Grafe, H. J.; Taylor, A.; Krämer, K.; Büchner, B.; Klingeler, R., *Nanomedicine* **2008**, *3*, 321-7.
247. Wang, J. T.; Rubio, N.; Kafa, H.; Venturelli, E.; Fabbro, C.; Ménard-Moyon, C.; Da Ros, T.; Sosabowski, J. K.; Lawson, A. D.; Robinson, M. K.; Prato, M.; Bianco, A.; Festy, F.; Preston, J. E.; Kostarelos, K.; Al-Jamal, K. T., *Journal of Controlled Release* **2016**, *224*, 22-32.
248. Edward, M.; Quinn, J. A.; Mukherjee, S.; Jensen, M. B.; Jardine, A. G.; Mark, P. B.; Burden, A. D., *The Journal of Pathology* **2008**, *214*, 584-93.
249. Servant, A.; Jacobs, I.; Bussy, C.; Fabbro, C.; da Ros, T.; Pach, E.; Ballesteros, B.; Prato, M.; Nicolay, K.; Kostarelos, K., *Carbon* **2016**, *97*, 126-133.
250. Ali-Boucetta, H.; Al-Jamal, K. T.; Kostarelos, K., *Methods in Molecular Biology* **2011**, *726*, 299-312.

251. Kostarelos, K.; Lacerda, L.; Pastorin, G.; Wu, W.; Wieckowski, S.; Luangsivilay, J.; Godefroy, S.; Pantarotto, D.; Briand, J. P.; Muller, S.; Prato, M.; Bianco, A., *Nature Nanotechnology* **2007**, *2*, 108-13.
252. Pantarotto, D.; Singh, R.; McCarthy, D.; Erhardt, M.; Briand, J. P.; Prato, M.; Kostarelos, K.; Bianco, A., *Angewandte Chemie International Edition in English* **2004**, *43*, 5242-6.
253. Marangon, I.; Boggetto, N.; Ménard-Moyon, C.; Venturelli, E.; Béoutis, M. L.; Péchoux, C.; Luciani, N.; Wilhelm, C.; Bianco, A.; Gazeau, F., *Nano Letters* **2012**, *12*, 4830-7.
254. Marangon, I.; Boggetto, N.; Ménard-Moyon, C.; Luciani, N.; Wilhelm, C.; Bianco, A.; Gazeau, F., *Journal of Visualized Experiments* **2013**, e50566.
255. Vranic, S.; Boggetto, N.; Contremoulins, V.; Mornet, S.; Reinhardt, N.; Marano, F.; Baeza-Squiban, A.; Boland, S., *Particle and Fibre Toxicology* **2013**, *10*, 2.
256. Vranic, S.; Gosens, I.; Jacobsen, N. R.; Jensen, K. A.; Bokkers, B.; Kermanizadeh, A.; Stone, V.; Baeza-Squiban, A.; Cassee, F. R.; Tran, L.; Boland, S., *Archives of Toxicology* **2016**.

6. ACCEPTED PAPERS AS PART OF THIS THESIS

Accepted Papers as Part of this Thesis

Article 1. *Synthesis of Dry $SmCl_3$ from Sm_2O_3. Implications for the Encapsulation of Samarium Compounds into Carbon Nanotubes*, Markus Martincic, Carlos Frontera, Elzbieta Pach, Belen Ballesteros, Gerard Tobias, *Polyhedron*, **2016**, 116, 116.

https://doi.org/10.1016/j.poly.2016.03.045

Article 2. *Quantitative Monitoring of the Removal of Non-Encapsulated Material External to Filled Carbon Nanotube Samples*, Markus Martincic, Elzbieta Pach, Belen Ballesteros, Gerard Tobias, *Phys Chem Chem Phys*, **2015**, 17, 31662.

https://doi.org/10.1039/C5CP04664E

ANNEX I. OTHER CO-AUTHORED ARTICLES

Other Co-Authored Articles

Article 1. *Carbon Nanotubes Allow Capture of Krypton, Barium and Lead for Multichannel Biological X-ray Fluorescence Imaging*, Christopher Serpell, Reida Rutte, Kalotina Geraki, Elzbieta Pach, Markus Martincic, Magdalena Kierkowicz, Sonia De Munari, Kim Wals, Ritu Raj, Belen Ballesteros, Gerard Tobias, Daniel Anthony, Benjamin Davis, *Nat Commun*, **2016**, 7, 13118.

https://doi.org/10.1038/ncomms13118

Article 2. *Design of Antibody-Functionalized Carbon Nanotubes Filled with Radioactivable Metals Towards a Targeted Anticancer Therapy*, Cinzia Spinato, AritzPerez Ruiz de Garibay, Magdalena Kierkowicz, Elzbieta Pach, Markus Martincic, Rebecca Klippstein, Maxime Bourgognon, Julie Tzu-Wen Wang, Cecilia Menard-Moyon, Khuloud T. Al-Jamal, Belen Ballesteros, Gerard Tobias, Alberto Bianco, *Nanoscale*, **2016**, 8, 12626.

https://doi.org/10.1039/C5NR07923C

Article 3. *Evaluation of the Immunological Profile of Antibody-functionalized Metal-Filled Single-walled Carbon Nanocapsules for Targeted Radiotherapy*, Aritz Perez Ruiz de Garibay, Cinzia Spinato, Rebecca Klippstein, Maxime Bourgognon, Markus Martincic, Elzbieta Pach, Belen Ballesteros, Cecilia Menard-Moyon, Khuloud T. Al-Jamal, Gerard Tobias, Alberto Bianco, *Sci Rep*, **2017**, 7, 42605.

https://doi.org/10.1038/srep42605